# Photocatalytic Water Splitting in Sodium Tantalate Suspensions

Von der Naturwissenschaftlichen Fakultät

der Gottfried Wilhelm Leibniz Universität Hannover

zur Erlangung des Grades

## Doktorin der Naturwissenschaften

## Dr. rer. nat.

genehmigte Dissertation

von

## Dipl.-Chem. Irina Ivanova

geboren am 03.06.1984 in Taschkent (Usbekistan)

2014

*Für meine Eltern*

## Danksagung

An dieser Stelle möchte ich mich bei allen bedanken, die mich während meiner Promotion unterstützt und zum Gelingen dieser Arbeit beigetragen haben.

Zuerst möchte mich ganz besonders bei Prof. Dr. Detlef W. Bahnemann für die hervorragende Betreuung meiner Arbeit bedanken. Ich danke für die anregenden Diskussionen, für die Freiheit bei der Gestaltung meiner Konzepte und für das Vertrauen in die eigenständige Durchführung dieser Arbeit.

Prof. Dr. Thomas Scheper danke ich recht herzlich für die Möglichkeit an seinem Institut zu promovieren und für die Übernahme des Koreferats.

Prof. Dr. Thomas Bredow danke ich für eine schöne und produktive Zusammenarbeit in unserem gemeinsamen Projekt „Hycats". Ich danke ganz herzlich für die Übernahme des Drittprüferamtes.

Ein großer Dank gilt Dr. Ralf Dillert für den wertvollen Erfahrungs- und Wissensaustausch, für seine ständige Hilfsbereitschaft und zahlreichen kritischen Diskussionen.

Ich möchte mich bei Dr. Tarek Kandiel für die Betreuung meiner Arbeit im frühen Stadium bedanken. Ich danke für eine sehr schöne aber leider nur kurze Zusammenarbeit im Projekt „Hycats".

Ganz besonders möchte ich mich bei Prof. Dr. Cecilia Mendive bedanken für das Erwecken eines großen Interesses für die „echte" Wissenschaft und für einen intensiven Erfahrungs- und Wissensaustausch während der Betreuung meiner Diplomarbeit. Danke für eine exzellente Vorbereitung für meine Promotion.

Ich danke Prof. Dr. Feldhoff für die TEM Untersuchungen und für eine produktive Zusammenarbeit an einer wissenschaftlichen Veröffentlichung. Frank Steinbach danke ich auch für die TEM Untersuchungen.

Ich danke allen Mitarbeitern der Mechanik- und Elektrowerkstatt für die schnelle Hilfe bei allen Problemen und für die vielen Spezialanfertigungen.

Ich danke allen Mitarbeitern des Arbeitskreises Bahnemann und dem gesamten Insitut für Technische Chemie für die schöne Zeit und Zusammenarbeit. Ich danke auch alle ausländischen Kollegen, insbesondere Juan F. Montoya (Kolumbien),

# Kurzzusammenfassung

Um die globalen Energie- und Umweltprobleme lösen zu können, ist die Entwicklung hoch effizienter Systeme für die Umwandlung und Speicherung der Sonnenenergie notwendig. Eine Möglichkeit der Umwandlung ist die photokatalytische Spaltung von Wasser in molekularen Wasserstoff mit Hilfe von Metalloxid-Halbleitern als Katalysatoren. Da die photokatalytische Wasserspaltung eine wenig verstandene Reaktion darstellt, ist Grundlagenforschung in diesem Gebiet erforderlich.

In dieser Doktorarbeit wird über die photokatalytische Aktivität von reinem und Lanthan dotiertem Natriumtantalat zur Wasserspaltung unter UV-vis-Bestrahlung berichtet. Die Beurteilung der Aktivitäten erfolgt durch die Bestimmung der Quantenausbeuten der photokatalytischen Wasserstoff- und Sauerstoff-Bildung. In reinem Wasser zeigen beide Materialien geringe Aktivitäten bezüglich der $H_2$-Bildung. Jedoch wurde in reinem Wasser kein $O_2$ detektiert.

Die Oberfläche der untersuchten Materialien wurde mit verschiedenen Cokatalysatoren wie z.B. Edelmetalle (Pt, Au und Rh) und Metalloxide (NiO, CuO, CoO, AgO und $RuO_2$) modifiziert, um deren photokatalytische Aktivität zu verbessern. Die Aktivitäten der Photokatalysator-Cokatalysator-Kombinationen wurden in reinem Wasser, in wässriger Methanol-Lösung sowie in wässriger Silbernitrat-Lösung untersucht. Die Ergebnisse zeigen, dass die Cokatalysatoren mit der höchsten Aktivität für die $H_2$-Produktion, z.B. $RuO_2$ oder CuO, gleichzeitig die geringste Aktivität bezüglich der $O_2$-Bildung in wässriger Silbernitrat-Lösung besitzen.

Die unterschiedlichen Aktivitäten der eingesetzten Cokatalysatoren wurden zusätzlich mittels Laser-Flash-Photolyse untersucht. Diese Methode wurde verwendet, um den Zusammenhang zwischen der Lebensdauer der photogenerierten Ladungsträger und der katalytischen Aktivität der Cokatalysatoren zu ermitteln.

Die höchsten Quantenausbeuten von 33 % für die $H_2$-Bildung wurden im Falle des mit Pt beladenem La:$NaTaO_3$ in Gegenwart von Methanol erzielt. Um die Rolle von Methanol in diesem photokatalytischen System zu klären, wurden Langzeitexperimente und Untersuchungen mit Isotopen durchgeführt. Die zugrunde liegenden Mechanismen der Methanol-Oxidation wurden aufgeklärt.

**Stichwörter:** Natriumtantalat, Photokatalyse, Wasserspaltung, Methanol-Oxidation, getrappte Ladungsträger.

# Abstract

In order to solve the global energy and environment issues, highly efficient systems for solar energy conversion and storage are needed. One of them is the photocatalytic conversion of solar energy into the fuel molecular hydrogen *via* the water splitting process utilizing metal-oxide semiconductors as catalysts. Since photocatalytic water splitting is a poorly understood reaction, fundamental research in this field is required.

In this thesis, the photocatalytic activity of pure and lanthanum doped sodium tantalates for water splitting under UV-vis irradiation is reported. The activity of these materials was assessed by the determination of the overall quantum yield of molecular hydrogen and molecular oxygen evolution. In pure water both materials exhibit rather poor activity for the photocatalytic $H_2$ evolution. However, no $O_2$ was detected in pure water.

The surface of the studied materials was modified with various cocatalysts including noble metals (Pt, Au and Rh) and metal oxides (NiO, CuO, CoO, AgO and $RuO_2$) to enhance their photocatalytic activity. Their activity was evaluated in pure water, in aqueous methanol solution, and in aqueous silver nitrate solution. The results reveal that the cocatalysts, *i.e.*, $RuO_2$ or CuO with the highest catalytic activity for $H_2$ evolution from pure water, exhibit, however, the lowest activity for $O_2$ evolution from aqueous silver nitrate solution.

Different catalytic activity of the utilized cocatalysts for $H_2$ and $O_2$ evolution was additionally studied by means of the laser flash photolysis. This technique was performed to investigate the relationship between the lifetime of the photogenerated charge carriers and the catalytic activity of the various cocatalysts.

La-doped $NaTaO_3$ modified with Pt shows the highest quantum yield of 33 % with respect to the $H_2$ evolution in the presence of methanol. To clarify the role of methanol in such a photocatalytic system, long-term investigations and isotopic studies were performed. The underlying mechanisms of methanol oxidation were elucidated.

**Keywords:** sodium tantalate, photocatalysis, water splitting, methanol oxidation, trapped charge carrier.

# Table of Contents

# Abbreviations

| | |
|---|---|
| BET | Specific Surface Area (Brunauer Emmett Teller) |
| XRD | X-ray Diffraction |
| TEM | Transmission Electron Microscopy |
| HRTEM | High-resolution Transmission Electron Microscopy |
| SEM | Scanning Electron Microscopy |
| UV | Ultraviolet |
| Vis | Visible |
| NHE | Normal Hydrogen Electrode |
| ESR | Electron Spin Resonance |
| SPR | Surface Plasmon Resonance |
| QMS | Quadrupole Mass Spectrometer |
| MFC | Mass Flow Controller |
| QE | Quantum Yield |
| SG | Sol-Gel Synthesis |

## Symbols

| | |
|---|---|
| $E_g$ | Band Gap Energy |
| $\alpha$ | Absorption Coefficient |
| $\nu$ | Oscillation Frequency |
| $h$ | Planck's Constant |
| $c$ | Speed of the Light |
| $\lambda$ | Wavelength |
| $\phi$ | Quantum Yield |
| $r$ | Rate of Gas Evolution |
| $N_A$ | Avogardo Constant |
| $A$ | Area |
| $I_0$ | Number of Absorbed Photons |
| $d$ | Diameter |
| $\pi$ | Mathematic Constant |
| $\rho$ | Density |
| $\Delta G^0$ | Gibbs Free Energy |

## Units

| | |
|---|---|
| a.u. | Arbitrary Unit |
| % | Percentage |
| °C | Grad Celsius |
| wt% | Percentage by Weight |
| m | Mass |
| g | Gram |

IV

| | |
|---|---|
| L | Liter |
| M | Molar Mass [mol·l⁻¹] |
| V | Volume |
| s | Second |
| h | Hour |
| W | Watt |
| V | Volt |
| eV | Electron Volt |
| Å | Angstrom |
| cm | Centimeter |
| m | Meter |
| nm | Nanometer |
| J | Joul |

## 1.  Introduction and objectives

The worldwide energy demand due to the inevitable depletion of the world's fossil fuel reserves and at the same time growing environmental concern is driving the search for new, sustainable, and renewable energy sources. At present, approximately 88 % of the world's energy supply is derived from fossil fuels.[1, 2] However, the fossil fuel combustion increases the level of atmospheric $CO_2$, thus significantly contributing to the global warming and the so-called greenhouse effect.

Since the first energy crisis in the early 1970s more attention has been paid to the utilization of solar energy that provides a tremendous amount of free energy and intensity to the earth. Many researchers focused their attention on the development of efficient systems being able to absorb and convert solar light into useful chemical energy resources.

In nature, solar energy is converted into chemical energy by means of photosynthesis and stored in the bonds of glucose, accompanied by a large positive change in the Gibbs free energy: [3]

$$H_2O + CO_2 \xrightarrow{\ h\nu\ } \frac{1}{6}(C_6H_{12}O_6) + O_2 \qquad \Delta G^0 = 480 \text{ kJ} \cdot \text{mol}^{-1} \qquad 1$$
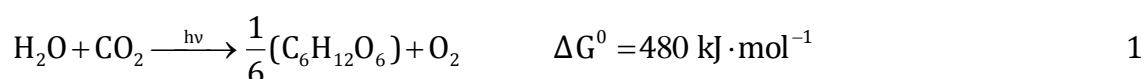
Water decomposition into $H_2$ and $O_2$ by means of sunlight mimics natural photosynthesis providing a new attractive environmental-friendly method to capture available solar energy and to convert it into chemical energy, *i.e.*, molecular hydrogen: [4, 5]

$$H_2O \xrightarrow{\ h\nu\ } H_2 + \frac{1}{2}O_2 \qquad \Delta G^0 = 273 \text{ kJ} \cdot \text{mol}^{-1} \qquad 2$$
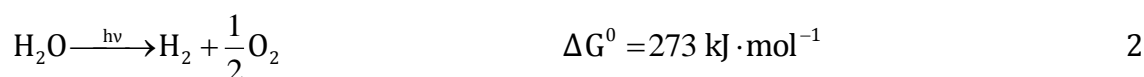
Hydrogen gas produced in this way could be considered as a green energy fuel because the chemical energy stored in the H-H bond is released when it combines with oxygen, *e.g.*, in a fuel cell or upon incineration, yielding only water as byproduct. Moreover, solar hydrogen would significantly contribute to the world's chemical and electricity demand, powering everything from laptops to submarines.[6]

The process of the splitting of water into hydrogen and oxygen was already predicted in 1874 by Jules Verne in his book "Mysterious Island":

> "*Yes, my friends, I believe that water will one day be employed as fuel, that hydrogen and oxygen which constitute it will furnish an inexhaustible source of heat and light. Water will be the coal of the future.*"

The pioneering work of Fujishima and Honda from 1972 demonstrated for the first time that the overall water splitting can be achieved using a photo-electrochemical cell, consisting of a single-crystalline $TiO_2$ (rutile) anode and a Pt cathode under ultraviolet irradiation and an external bias.[7] However, the fabrication of suitable photoelectrode materials with appropriate band gap structures and stability is rather expensive and complicated.[8] Therefore, considerable attention has been paid to photocatalytic systems using semiconductor particles or powders as initially proposed by Bard and co-workers.[9-11] Such systems appear in general to be much simpler and less expensive in use and fabrication with the advantage to employ also materials which are normally not available as single-crystal semiconductor electrodes.[12] Furthermore, from the viewpoint of large-scale hydrogen production the particulate photocatalyst systems exhibit a wide range of potential applications.[13]

In contrast to a photo-electrochemical cell, the spatial separation between oxidative and reductive sites in a particulate system is very low, thus increasing the undesired back reaction, *i.e.*, water formation to a great extent.[11] Lehn *et al.* reported that water splitting took place only at elevated temperatures and/or reduced pressures working on metallised $SrTiO_3$ powders.[14] On the one hand, no water photodecomposition was observed at room temperature and atmospheric pressure employing platinized $TiO_2$ powders as photocatalysts. [15] On the other hand, there are reports claiming the photocatalytic water splitting employing $RuO_2$ and /or Pt modified $TiO_2$ at room temperature and ambient pressure.[16, 17] Hence, more than 30 years after the pioneering work of Bard *et al.*, there are still uncertainties in the reports regarding the stoichiometric overall water splitting into molecular $H_2$ and molecular $O_2$. Therefore, the continuation of fundamental research

on this topic seems to be very important with the overall aim of producing a reproducible and efficient photocatalytic device for overall water splitting.

The vast majority of the current research is focused mainly on the synthesis of a broad spectrum of diverse materials that can be employed as photocatalysts for the overall water splitting reaction. The respective photocatalytic test reactions are usually carried out in classical batch reactors connected to a standard gas chromatograph with a thermal conductivity detector (GC/TCD). Hence, the photocatalytic activity of the newly synthesized materials is mostly evaluated only for hydrogen evolution in the presence of the so-called sacrificial agents. Moreover, the photocatalytic activity for $H_2$ evolution is generally given exclusively as a rate ($\mu mol \cdot h^{-1}$), making the comparison of the photocatalytic activity with other systems almost impossible. The main drawback of such photocatalytic setups is the limitation in the performance of the long term experiments due to the often generated overpressure in the system. In addition, the employment of a standard GC/TCD does not allow performing any mechanististic investigations, *e.g.*, detection of isotopes or other gases like $CO_2$, CO etc. besides $H_2$ and $O_2$.

Therefore, from a technical point of view the objective of this thesis is the development and construction of a novel photocatalytic setup for the investigation of water splitting reactions. Such a new photocatalytic setup should be based on a continuously measurement method allowing both, the quantitative and the qualitative determination of all gaseous reaction products including isotopes. Additionally, the performance of the photocatalytic test reactions over a long period of time (up to one month) should be enabled. A second technical objective of this study is the determination of the absolute quantum yields ($\phi$) in particulate suspensions facilitating a better comparison of the obtained photocatalytic activities for $H_2$ and $O_2$ evolution with those of other systems reported in the literature.

From the scientific point of view the focus of this thesis is not the synthesis of the novel photocatalytic materials but rather the elucidation of the fundamental processes occurring during the water splitting reactions. Based on the previously published work by the research group of Kudo in 2003, sodium tantalate ($NaTaO_3$) has been chosen as the model photocatalyst in the present work.[18] Up to now, lanthanum doped sodium tantalates modified with NiO cocatalysts have

3

demonstrated the highest apparent quantum yield for water splitting of 56% when illuminated at 270 nm. The sodium tantalate materials employed in this work have been synthesized *via* conventional solid state reactions and were kindly provided by H.C. Starck Company (Goslar) within the framework of a joint BMBF Project ("Hycats"). While these materials are not of any great interest for possible future solar energy applications because of their wide band gap (4eV) allowing light absorption only in UV region, due to their high photostability and high photocatalytic activity for water splitting they are considered to be suitable model photocatalysts for basic research.

As the central objective of the present thesis is to investigate photocatalytic water splitting in sodium tantalate suspensions, it is important to clarify the effect of different parameters, *i.e.*, lanthanum doping and in particular cocatalyst loading and employment of the so-called sacrificial agents on photocatalytic formation of molecular hydrogen and molecular oxygen.

The photocatalytic activity for water splitting can usually be improved by the utilization of different cocatalysts loaded onto the host catalyst surface due to suppression of the photogenerated charge carriers recombination and/or due to the creation of active sites, decreasing the activation energy for the gas evolution. The research in this field is focused on measurements of the photocatalytic activity for water splitting of the newly synthesized materials frequently employing noble metals (Pt or Rh) or transition metal oxides (NiO or $RuO_2$). Since noble metal cocatalysts, in particular Pt, are usually very expensive and may also catalyze the undesired backward reaction, *i.e.*, the water formation, more research is needed to identify low-cost cocatalysts exhibiting a notable enhancement of the photocatalytic activity and high stability. Therefore, besides noble metal cocatalysts (Pt, Rh and Au) in particular different low-cost metal oxides, *i.e.*, NiO, CuO, CoO, $RuO_2$ and AgO will be investigated regarding their photocatalytic activity for water splitting. The photocatalytic test reactions will be carried out both in pure water and in the presence of the so-called sacrificial agents, *i.e.*, aqueous methanol and silver nitrate solutions in order to identify the most efficient catalysts for the photocatalytic $H_2$ and/or $O_2$ formation.

It is furthermore aimed to elucidate the mechanisms of the photocatalytic $H_2$ and/or $O_2$ formation particularly for each system employed within this work. For this purpose all materials will be characterized regarding their optical, morphological and structural properties. Moreover, the effect of different cocatalysts loaded on the $NaTaO_3$ surface will be investigated for the first time by means of the laser flash photolysis technique providing essential information concerning the lifetime of the photogenerated charge carriers (electrons and holes).

Different alcohols acting as electron donors have shown different activities for the photocatalytic $H_2$ evolution employing different photocatalysts including $TiO_2$. However, a systematic study of the effect of different alcohols on the photocatalytic activity for $H_2$ evolution employing sodium tantalate materials has not been performed yet. Moreover, only few mechanistic studies have been published (mainly on $TiO_2$) dealing with the fundamental understanding of the photocatalytic processes occurring in the presence of such sacrificial systems. Thus, within this thesis long-term investigations will be carried out for the first time employing $NaTaO_3$ and methanol as a frequently used electron donor for the enhanced photocatalytic $H_2$ evolution. By means of the newly developed photocatalytic setup, it is possible to detect different products of the photocatalytic methanol reforming, *e.g.*, $H_2$, CO, $CO_2$ or $CH_4$ determining the overall mass balance of the oxidation products. Thus, the obtained results can be used to propose mechanisms of such reactions.

Only few studies are known dealing with isotopic labeling experiments for the extended elucidation of the mechanisms of the photocatalytic hydrogen production and the concomitant methanol oxidation. Moreover, all these valuable studies were carried out on the intensively studied $TiO_2$. Within this thesis an isotopic study will be performed for the first time employing $NaTaO_3$ in order to identify the origin of the evolved $H_2$ from the (deuterated) water and (deuterated) methanol mixtures.

## 2. Literature review

### 2.1 Photocatalytic splitting of pure water

In recent years numerous studies have been executed examining the overall water splitting for the production of molecular hydrogen and oxygen using particulate photocatalyst systems. Herein, the electronic structure of the semiconductor plays a key role. Semiconductors have a band structure consisting of a valence and a conduction band, which are separated from each other by a band gap with a suitable width. The band gap defines the wavelength sensitivity of the semiconductor, *i.e.*, which part of the solar spectrum can be employed for the irradiation.

Depending on the electronic structure of a semiconductor it is differentiated between the direct and indirect band-to band transitions (Figure 1). Direct semiconductors, such as cadmium or zinc sulfide, have much higher absorption coefficients than the indirect ones exhibiting a steep onset. In contrast the indirect semiconductors such as titania show an absorption tail and flatter onset.[19]
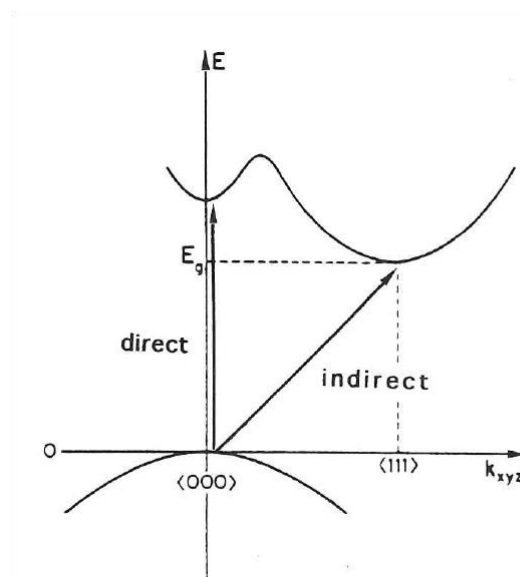


**Figure 1:** Direct and indirect optical transitions in semiconductors.[20]

The general way to determine the kind of the electronic transition, i.e., direct or indirect, is to apply the following equation:[21]

$$\alpha \propto \frac{\left(hv - E_g\right)^n}{hv} \quad or \quad \left(\alpha v\right)^{1/n} \propto hv - E_g \qquad\qquad 3$$

Where $\alpha$ is the absorption coefficient, $h$ is the Planck constant, $v$ is the oscillation frequency, $E_g$ is the optical band gap and $n$ is a constant relating to the mode of transition. The constant $n$ is equal to ½, 3/2 or 2 for allowed direct transitions, forbidden direct transitions or indirect transitions, respectively, whereby the forbidden transitions are often neglected.[21] The transition mode and the optical band gap can be estimated plotting $\left(\alpha v\right)^{1/n}$ against $hv$ using n as ½, 3/2 or 2.

Semiconductors can be excited due to the absorption of photons with an energy which is equal or greater than that of the band gap (Figure 2). In this case the electrons of the valance band will be exited to the conduction band leaving positive charge carriers, the holes, in the valance band.
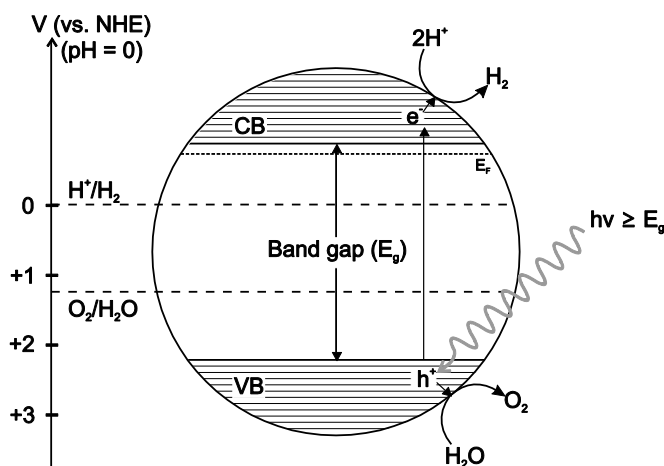


**Figure 2**: Basic principle of the overall water splitting at a heterogeneous particulate photocatalyst

The photo-generated electrons and holes can either recombine, releasing energy in the form of heat or photons (photoluminescence), or they can separate and migrate to the surface of the semiconductor particle. Water molecules adsorbed on the surface of the semiconductor particle can be reduced by the electrons forming hydrogen molecules and can be oxidized by the holes forming oxygen molecules according to the following equations:

$$SC_{(s)} + 2h\nu \rightarrow 2e^{-}_{CB} + 2h^{+}_{VB} \qquad\qquad 4$$

$$2h^{+}_{VB} + H_2O \rightarrow \frac{1}{2}O_2(\uparrow) + 2H^{+}_{(aq)} \qquad\qquad 5$$

$$2e^{-}_{CB} + 2H^{+}_{(aq)} \rightarrow H_2(\uparrow) \qquad\qquad 6$$

$$H_2O + 2h\nu \rightarrow \frac{1}{2}O_2(\uparrow) + H_2(\uparrow) \qquad \Delta G^0 = 237\,kJ \cdot mol^{-1} \qquad 7$$
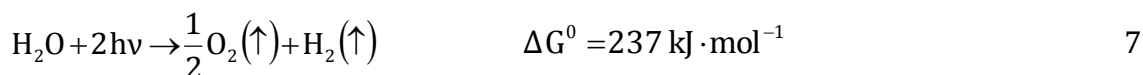
Thermodynamically, the overall water splitting reaction is an uphill reaction with a large positive Gibbs free energy change (Equation 7). An important requirement for the achievement of the overall water splitting is the energetic position of the conduction and valance band. The bottom of the conduction band level has to be located more negatively than the reduction potential of $H^+$ to $H_2$ (0 V *vs*. NHE at pH 0), while the top of the valance band has to be located more positively than the oxidation potential of $H_2O$ to $O_2$ (1.23 V *vs*. NHE at pH 0).

Accordingly, the theoretical minimum of the photon energy thermodynamically required to split water into hydrogen and oxygen is 1.23 eV, corresponding to a wavelength of ca. 1000 nm. This leads to the conclusion that theoretically the entire visible spectral range can be used to achieve the water splitting reaction. However, it is important to consider the thermodynamic and kinetic energy losses in photochemical systems, which affect the band gap energy of a semiconductor that can be used for water splitting. The thermodynamic energy losses have been estimated to be 0.4 eV.[22] The kinetic losses associated mostly with bulk and interfacial charge carrier transport, *i.e.*, with non-radiative recombination, interfacial kinetics (overpotentials), and band bending in the semiconducting materials have also been estimated to be at least 0.4 eV.[23, 24] Therefore, the total contribution to the energy losses has been estimated to be 0.8 eV, which increases the minimum band gap energy from 1.23 eV to 2.03 eV.

A suitable photocatalyst for solar water splitting should meet three requirements: (1) band edge potentials suitable for overall water splitting, (2) bandgap energy smaller than 3 eV, and (3) stability against photocorrosion during the photocatalytic reaction. However, it is still a challenging task to develop such materials.

Figure 3 demonstrates the total energy and the number of photons as a function of wavelength. The solar-to-hydrogen (STH) efficiency can be calculated from the number of photons in the spectrum.[25] Utilizing only UV light ($\lambda \leq 400$ nm), the theoretical maximum STH efficiency is only 3.3 % for a quantum efficiency (QE) of 100 %. The theoretical maximum STH efficiency is increased to 17.8 % using UV and visible region up to 600 nm. For instance, a photocatalyst exhibiting a QE of 30 % at wavelengths between 300-600 nm, an STH efficiency of 5 % can be achieved being economically feasible and competitive with hydrogen production from other energy sources.[25]
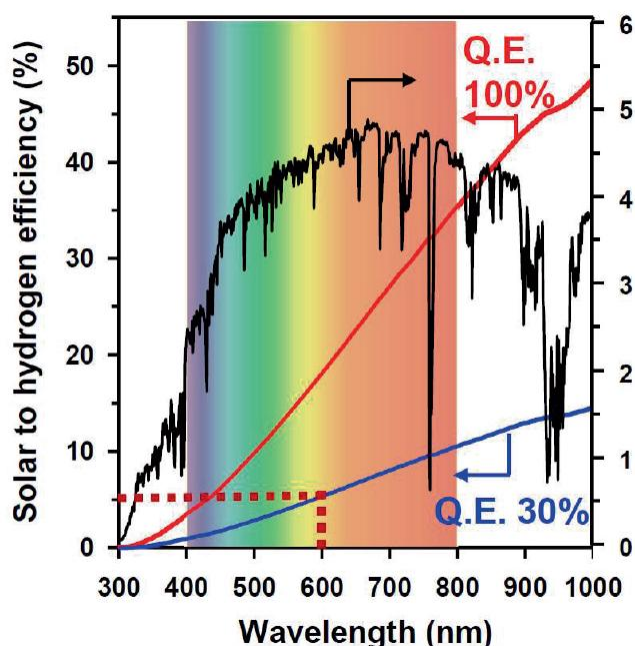


**Figure 3**: Solar spectral irradiance at a global air mass of 1.5 as a function of the wavelength and the maximum theoretical solar-to-hydrogen (STH) conversion efficiency. [25]

Figure 4 presents energy levels of various semiconductors in aqueous media at pH 0 together with the redox potentials of water splitting. Hereby, the metal mixed oxides ($NaTaO_3$, $SrTiO_3$) and metal oxides ($TiO_2$, $ZnO$) possess suitable band structure for water splitting under UV irradiation when they are suitably modified with cocatalysts. Furthermore, they are considered to be the most stable materials for photocatalytic redox reactions, since they do not undergo photocorrosion.
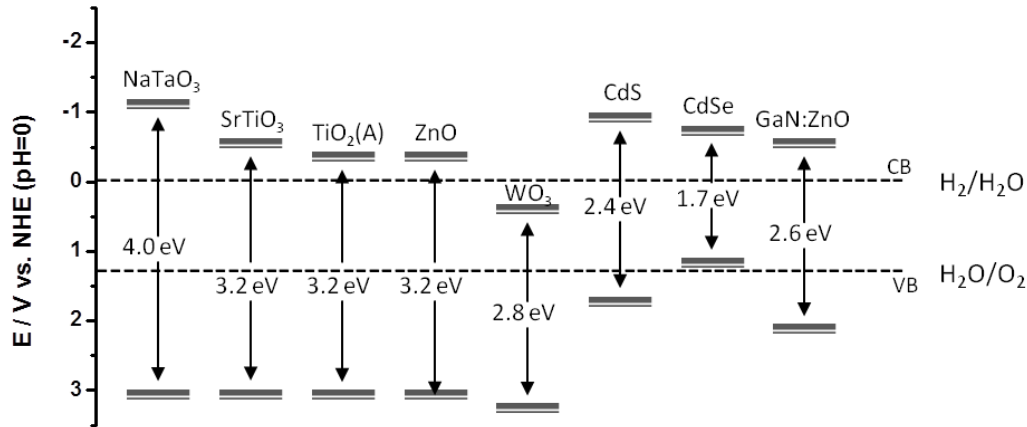
**Figure 4**: Energy-level diagram indicating the energy positions of the conduction and valence bands for various in aqueous media at pH 0.[26]

Although CdS seems to have an ideal band structure and a band gap with the visible light response (2.4 eV), it is not active for water splitting into $H_2$ and $O_2$ since $S^{2-}$ in CdS rather than $H_2O$ is oxidized by the photogenerated holes accompanied with the anodic dissolution of the semiconductor and the formation of $Cd^{2+}$ accor-ding to the following equations:[27]

$$CdS \xrightarrow{h\nu} e_{CB}^{-} + h_{VB}^{+} \qquad\qquad 8$$

$$CdS + 2h_{VB}^{+} \rightarrow Cd^{2+} + S \qquad\qquad 9$$

In the presence of molecular oxygen, the overall process will be:

$$CdS + 2O_2 \rightarrow Cd^{2+} + SO_4^{2-} \qquad\qquad 10$$

$WO_3$ does not have the ability to reduce $H^+$ to $H_2$ due to the fact that the bottom of its conduction band is located at a more positive potential than that of the water reduction. On the other hand, the location of the valence band of CdSe is less posi-tive than it is required for water oxidation. Moreover, similar to CdS also CdSe suffers from the photocorrosion processes.[28] The development of visible light-driven photocatalysts for water splitting has often been attempted through the doping with nitrogen or sulfur.[8] For instance, the GaN:ZnO solid solution $(Ga_{0.88}Zn_{0.12})$-$(N_{0.88}O_{0.12})$ exhibits a narrow bandgap of 2.6 eV, whereby the bandgap energies of both GaN and ZnO are larger than 3 eV.[29, 30] Moreover, the photocatalytic activity of this material for water splitting under visible light

irradiation ($\lambda$ > 420 nm) could significantly be enhanced by loading with $Rh/Cr_2O_3$ core/shell structures.[31]

## 2.2  Surface modification for efficient water splitting reactions

### 2.2.1  Noble metal cocatalysts

Since the simultaneous reduction and oxidation of water is a complex multistep reaction involving four electrons, the process of photocatalytic water splitting is still rather inefficient. One of the most important challenges is the separation of the photogenerated charge carriers and reduction of their recombination. Therefore, the photocatalytic activity for water splitting can usually be improved by the utilization of different cocatalysts loaded onto the catalyst surface.

Noble metals are widely used and well-known as effective cocatalysts for photocatalytic water splitting. Dispersed on the surface of the photocatalyst they play an important role in improving the efficiency of various photocatalytic reactions and, particularly, for hydrogen evolution. [32-35]

It is believed, that in the presence of noble metal deposits on the surface of a semiconductor photocatalyst an efficient charge carrier separation can be achieved by suppressing the electron-hole recombination.[36] In particular, noble metal islands seem to be very effective electron traps due to the formation of a Schottky barrier at the metal-semiconductor contact.[37, 38] Noble metals and, *e.g.*, n-type semiconductors, electrically neutral and isolated from one another, have different Fermi level positions. When those two materials are electrically connected, electrons migrate from the more negatively located conduction band of the semiconductor to the more positively located conduction band of the metal until both Fermi levels become equal (see Figure 5). The surface of the metal becomes rich in electrons while that of the semiconductor becomes poor and depleted. As a result of this excess of negative charges (electrons) at the metal-semiconductor interface (*i.e.*, on the metal side) the semiconductor bands bend upwards towards the interface. This barrier formed at the metal-semiconductor interface is called the Schottky barrier and can serve as an efficient barrier preventing the undesired

electron migration back to the semiconductor.[39] While the electrons are trapped at the cocatalyst (noble metal) surface, the holes remain at the host photocatalyst and migrate to its free surface ensuring an efficient charge separation (see Figure 5, right hand side).[40]
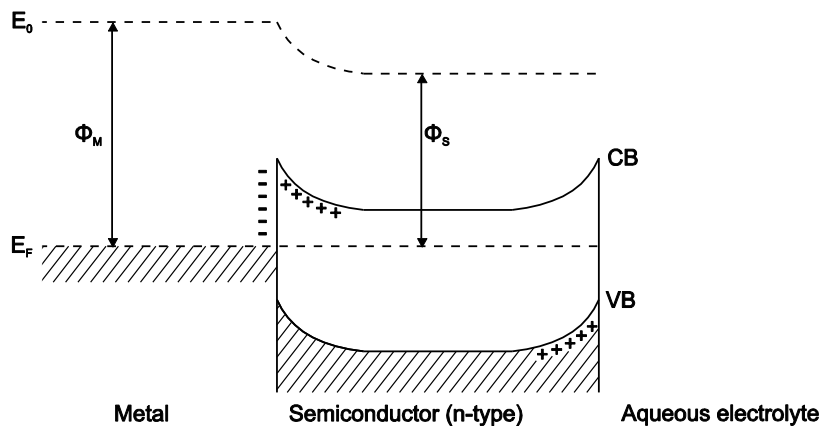


**Figure 5**: Schematic illustration of the Schottky barrier formation at the metal-semiconductor interface in equilibrium. $E_0$: vacuum level; $E_F$: Fermi level; $\Phi_M$: work function of the metal; $\Phi_S$: Schottky barrier height.

Such an efficient charge separation will result in the usually observed acceleration of the surface redox reactions and the simultaneous suppression of the backward reaction. Usually, the formation of a Schottky barrier is suggested for the interfacial contact between a metal electrode (Pt electrode) and a n-type semiconductor. However, in the case of Pt nanoparticles (instead of a Pt-electrode), being in contact with a semiconductor nanoparticles the situation might vary significantly. Hence, it is highly questionable whether in the case of Pt nanoparticles the formation of a Schottky barrier can be taken into consideration. In the latter case, even the exact chemical nature of the interfacial species is often unknown, *i.e.*, it has been reported that besides $Pt^0$ the Pt nanoparticles also contain $Pt^{+2}$ and $Pt^{+4}$ oxidation states.[41]

Selli et al. studied the effect of Pt, Au, and Ag deposition on $TiO_2$ and found Pt ($\Phi$ = 5.65 eV) to be the most effective cocatalyst, followed by gold ($\Phi$ = 5.10 eV) and silver ($\Phi$ = 4.00 eV).[42] The difference in the photocatalytic activity of the three metal cocatalysts was assumed to be related to their work function values ($\Phi$), *i.e.*, the energy required to promote an electron from the Fermi energy level into the

12

vacuum. The higher $\Phi$ the lower is the Fermi energy level and the bigger is the difference between the metal work function and that of the semiconductor.[43] Thus, the Schottky barrier will be increased leading to a more efficient electron trapping by the metal, an efficient charge separation and a higher photocatalytic activity for hydrogen evolution.

However, Pt does not always exhibit the highest activity as compared with other noble metals *e.g.*, Au, Ru, and Rh. This means that there are also other factors that need to be considered that affect the overall efficiency of the $H_2$ gas evolution. Hara *et al.* reported an enhancement of the $H_2$ evolution by Ru deposits on a TaON photocatalyst under visible light irradiation.[44] The loading of TaON with other noble metals such as Pt, Ir, and Rh, on the other hand, did not exhibit any significant hydrogen evolution at all. The authors explained this observation by the fact that the electronic structure of the interface between the Ru particles and TaON actively promotes the electron transfer from TaON to Ru.

The effect of the co-loading of two different noble metals on the photocatalytic activity for hydrogen evolution has also been studied. Liu *et al*. reported an enhancement effect of Pt/ Ru coloading on $LaTaON_2$ for hydrogen evolution as compared with that of either Pt or Ru alone.[45] The observed enhancement in photocatalytic activity for $H_2$ evolution was explained by a more efficient retardation of the electron-hole recombination in the valance band and thus an improvement of the charge separation efficiency. Mizukoshi et al. reported an enhanced photocatalytic activity for $H_2$ evolution from ethanolic aqueous solutions when Au-core/Pd-shell bimetallic nanoparticles were immobilized onto the $TiO_2$ surface.[46] They suggested that both, the structure and the composition of the bimetallic nanoparticles are responsible for the high activity of $H_2$ evolution. Additionally, selective $H_2$ permeability by the Pd-shell might contribute to the selective transfer of photogenerated electrons to protons, resulting in a considerable enhancement of the photocatalytic $H_2$ evolution.[47]

The loading of $TiO_2$ with Au nanoparticles has attained great interest from many researchers because such systems exhibit increasing hydrogen production yields under visible light irradiation.[46, 48] The visible light absorption of gold nanoparticles is mainly attributed to the excitation of their surface plasmon resonance

(SPR), which is due to the collective oscillations of electrons at the surface of these nanoparticles.[49, 50] Thus, an increased local electromagnetic field is generated promoting the selective formation of electron/hole-pairs near the surface of the semiconductor particles (essentially at the semiconductor-liquid interface).[51] The advantage of these charge carriers generated near the surface as compared with those generated in the bulk is that they are readily separated from each other and can more easily reach the active surface sites participating in the photocatalytic reactions. This results in an efficient suppression of the charge carrier recombination rate and therefore a significant enhancement of the water splitting activity.[52]

Fang *et al.* reported that $Au^0/TiO_2$ exhibits more than three times higher $H_2$ evolution rates than $Pt^0/TiO_2$ system upon excitation at $\lambda >400$ nm.[48] The authors claimed that the obtained result can be associated with the tremendous effect of the gold excitation since the small Pt nanoparticles do not exhibit SPR in the visible light region. In this way, the utilization of the Au nanoparticles for $H_2$ evolution in the visible light region may provide a considerable advantage over the use of Pt cocatalysts, since the latter can only be excited by UV light.

Generally, it should be noted, that the metal activity growth does not only correlate with a decrease of the water reduction overvoltage and thus an effective charge carrier separation. Moreover, additional specific factors need to be taken into consideration, such as the affinity of the metal ions to the surface of the photocatalyst, the size and the surface structure of the photodeposited metal nanoparticles as well as the physical characteristics of the contact between the metal and the semiconductor.[53]

### 2.2.2 Transition-metal oxide cocatalysts

The two main roles of an efficient cocatalyst are (a) to extract photogenerated electrons or holes from the photocatalyst bulk and (b) to create reaction sites decreasing the activation energy for gas evolution. A serious disadvantage of the employment of noble metals is that they do not only catalyze the water splitting but also the water formation from $H_2$ and $O_2$, *i.e.*, the undesirable back reaction.[54] Therefore, metal oxide nanoparticles exhibiting metallic behavior (such as $RuO_2$ or

Rh$_2$O$_3$) have been utilized in the past as cocatalysts, in particular, to assist the O$_2$ formation.

Some transition-metal oxides such as RuO$_2$ and NiO are frequently employed as efficient cocatalysts in water splitting systems.[5, 12, 55, 56] Perovskite-like NaTaO$_3$ loaded with NiO cocatalysts exhibits high activity for water splitting under UV irradiation.[57-59] The NiO cocatalyst promotes the transfer of the photo-induced electrons from the conduction band of NaTaO$_3$ and their transfer to H$^+$ thereby enhancing the charge separation, resulting in a high activity of the NiO/NaTaO$_3$ system.[60] Teramura $et$ $al$. reported that the high dispersion of RuO$_2$ nanoclusters on the catalyst surface improves the photocatalytic activity for H$_2$ and O$_2$ evolution in overall water splitting devices under visible light illumination.[61] It was observed that both Ru(IV) species and bulk RuO$_2$ exhibit less activity for overall water splitting as compared with RuO$_2$ nanoclusters which provided a significant enhancement for H$_2$ and O$_2$ evolution as cocatalysts on (Ga$_{1-x}$Zn$_x$)(N$_{1-x}$O$_x$) surface. CoO and IrO$_2$ are well known to oxidize water molecules and to thus catalyze molecular oxygen formation during water splitting.[62-66] Nocera and coworkers reported that Co-based catalysts deposited on an n-type semiconductor electrode can directly use photogenerated holes to form O$_2$ without applying an external bias.[67, 68]

The utilization of the metal oxide cocatalysts often requires an activation treatment, such as a reduction or an oxidation to obtain high activities.[29, 31, 55, 69-71] However, this approach is limited and cannot be applied in the presence of photocatalysts such as oxynitrides as the latter are thermally less stable as compared with the corresponding metal oxides.[72] Therefore, Domen and coworkers suggested a new modification method that provides cocatalysts consisting of a noble metal core (Rh, Ir, Pt) and a nanoparticulate Cr$_2$O$_3$ shell prepared by $in$ $situ$ photodeposition methods.[73]

Cr$_2$O$_3$ is known to be an active catalyst for hydrogen-related reactions such as hydrogenation and dehydrogenation. [74] Moreover, it has been reported that H atoms can adsorb on a hydrogen-activated Cr$_2$O$_3$ surface forming Cr-H bonds.[75] Thus, such a surface nature of Cr$_2$O$_3$ provides a good approach contributing to an enhanced photocatalytic activity for H$_2$ evolution. Maeda $et$ $al$. have shown that

also other noble metals, *e.g.*, Ir and Pt can be employed as a core covered with a $Cr_2O_3$ shell.[73]

Yoshida *et al*. investigated the reaction mechanism of hydrogen evolution on core/shell-structured nanoparticles using electrochemical and in situ spectroscopic measurements employing Pt or Rh electrode plates with electrochemically deposited $Cr_2O_3$.[76] They observed an infrared absorption band which they assigned to a Pt-H stretching and measured proton adsorption/desorption currents for both $Cr_2O_3$-coated and bare electrodes. [77] These results showed that no interference exists between the $Cr_2O_3$ layer and the reduction of $H^+$ into $H_2$ taking place at the $Cr_2O_3$/Pt interface. In contrast, the reduction of oxygen to water was inhibited only in the case of the $Cr_2O_3$-coated samples indicating their impermeability for molecular oxygen. In this way the undesired back reaction, i.e., the water formation can be effectively suppressed.

## 2.3 Sacrificial agents for hydrogen and oxygen evolution

### 2.3.1 Hydrogen evolution from aqueous methanol solution

The photocatalytic formation of hydrogen and oxygen on a photocatalyst is often ineffective because the amount of hydrogen evolved is limited by the rapid back reaction of $H_2$ and $O_2$, resulting in water formation.[78]

Organic compounds, such as alcohols (methanol, ethanol, *etc*.), organic acids (formic acid, acetic acid *etc*.), and aldehydes (formaldehyde, acetaldehyde *etc*.) have therefore been used as efficient hole scavengers, *i.e.*, as electron donors for the photocatalytic $H_2$ formation.[6] As the holes are scavenged by these molecules and no $O_2$ can be evolved, the back reaction of water formation can be successfully suppressed resulting in an increase of the $H_2$ formation yield.

Among different alcohols, methanol is widely used as sacrificial reagent for the photocatalytic $H_2$ production. $CH_3OH$ reacts with the photogenerated valance band holes undergoing relatively rapid and irreversible oxidation reactions.[79] To date there are, however, only few studies dealing with the mechanistic aspects of the photocatalytic methanol oxidation pathway.[80, 81] Some authors even describe the

photocatalytic $H_2$ evolution from aqueous methanol solutions as water splitting[82-84], while others qualify the process as dehydrogenation of methanol to formaldehyde or as the reforming of methanol to carbon dioxide.[85-87]

Other alcohols such as ethanol or 2-propanol have also been shown to act as efficient hole scavengers for the photocatalytic $H_2$ evolution. Tamaki *et al.* reported the following order for the oxidation efficiency of different alcohols by the trapped holes using transient absorption spectroscopy: methanol > ethanol > 2-propanol.[88] However, efficient hole scavenging requires that the transfer process of holes to the alcohols predominates the recombination process. For the case of the photocatalytic oxidation of $SCN^-$ Bowman *et al.* observed a direct competition between the hole reaction and the $e^-/h^+$ recombination.[89] Similar studies for the photocatalytic alcohol oxidation have not been reported yet.

Kawai *et al.* proposed the following overall methanol decomposition reaction mechanism: [79, 81, 85, 90-92]
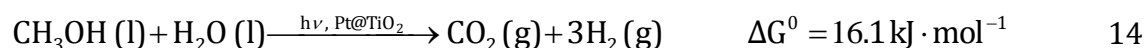
$$CH_3OH\,(l) \xrightarrow{\;h\nu,\;Pt@TiO_2\;} CH_2O\,(g) + H_2\,(g) \qquad \Delta G^0 = 64.1\,kJ \cdot mol^{-1} \qquad 11$$

$$CH_2O\,(g) + H_2O\,(l) \xrightarrow{\;h\nu,\;Pt@TiO_2\;} HCOOH\,(l) + H_2\,(g) \qquad \Delta G^0 = 87.8\,kJ \cdot mol^{-1} \qquad 12$$

$$HCOOH\,(l) \xrightarrow{\;h\nu,\;Pt@TiO_2\;} CO_2\,(g) + H_2\,(g) \qquad \Delta G^0 = -95.8\,kJ \cdot mol^{-1} \qquad 13$$
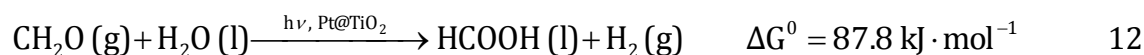
with the overall reaction beeing

$$CH_3OH\,(l) + H_2O\,(l) \xrightarrow{\;h\nu,\;Pt@TiO_2\;} CO_2\,(g) + 3H_2\,(g) \qquad \Delta G^0 = 16.1\,kJ \cdot mol^{-1} \qquad 14$$

The formation of formaldehyde and formic acid is thermodynamically unfavorable at room temperature since both reactions exhibit a positive Gibbs free energy (Equations 11 and 12 ). Thus, the photon energy is required to drive these first steps to the product side. On the other hand, the decomposition of formic acid into $CO_2$ and $H_2$ has a large negative Gibbs free energy providing a barrier for the back reaction and the subsequent $H_2$ consumption (Equation 13). The overall decomposition of methanol results, however, in significantly lower energy (16.1 kJ·mol$^{-1}$) that can be stored as compared with cyclic splitting of pure water (237 kJ·mol$^{-1}$) (Equation 14).
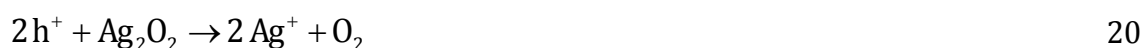
### 2.3.2 Oxygen evolution from aqueous silver nitrate solution

The choice of electron acceptors for sacrificial photocatalytic oxidation of water reported in the literature is rather limited as compared with that of electron donors for the photocatalytic formation of molecular $H_2$. The majority of the research groups working on this topic employ silver cations, $Ag^+$, as electron acceptor for enhanced photocatalytic formation of molecular oxygen.

It is generally assumed that the photocatalytic formation of molecular oxygen is accompanied by the deposition of metallic silver nanocontacts ($Ag_n^0$) on the semiconductor's surface with the involved reactions being proposed as follows: [93-95]

$$4\,h^+ + H_2O \xrightarrow{\ h\nu\ } O_2 + 4\,H_{aq}^+ \qquad\qquad 15$$

$$4\,e^- + 4\,Ag^+ \xrightarrow{\ h\nu\ } 4\,Ag^0 \qquad\qquad 16$$

$$n\,Ag^0 \xrightarrow{\ h\nu\ } Ag_n^0 \qquad\qquad 17$$

However, it is very important to consider also alternative pathway of $O_2$ formation, *i.e.*, through the oxidation reaction of $Ag^+$ ions by the photogenerated holes (Equation 18). The so formed $Ag^{2+}$ can be further oxidized by water resulting in $Ag_2O_2$ formation (Equation 19). The subsequent photocatalytic oxidation of these peroxides is then proposed to result in the observed $O_2$ formation (Equation 20).[96]

$$h^+ + Ag^+ \rightarrow Ag^{2+} \qquad\qquad 18$$

$$2\,Ag^{2+} + 2\,H_2O \rightarrow Ag_2O_2 + 4\,H_{aq}^+ \qquad\qquad 19$$

$$2\,h^+ + Ag_2O_2 \rightarrow 2\,Ag^+ + O_2 \qquad\qquad 20$$

In fact, silver cations ($Ag^+$) can be readily oxidized due to the rather high one-electron oxidation potential of the holes photogenerated in most semiconductors that have been found to exhibit high activities for photocatalytic water oxidation. Accordingly, the role of suitable sacrificial electron acceptors such as $Ag^+$ is highly underestimated. In particular, their possible involvement in the actual water oxidation mechanism has so far not been discussed at all.[96]

## 2.4 Laser flash photolysis

Laser flash photolysis is a powerful tool for investigations of the light induced charge carrier processes on the time scale from picoseconds to milliseconds and within a spectral range covering the entire UV-visible spectrum, thus, providing important mechanistic information of photocatalytic reactions. The fundamental understanding of the processes happening in the bulk of the material as well as its surface is essential for the design of novel efficient photocatalytic devices and their subsequent utilization. Titanium dioxide ($TiO_2$) is one of the most extensively studied materials concerning processes of charge carrier generation, trapping and recombination. Therefore, this chapter presents a short overview of laser flash photolysis studies performed on $TiO_2$.

The initial step of a photocatalytic reaction employing semiconductor particles is the generation of photoinduced charge carriers, *i.e.*, electron-hole pairs according to the following equation:[97]

$$TiO_2 + h\nu \rightarrow TiO_2 \left( e^-_{CB} + h^+_{VB} \right)$$

21

The photogenerated charge carriers can either directly recombine in the bulk or they can separately migrate to the surface where they are subsequently trapped in subsurface and surface states of the semiconductor particle. The trapped electrons and trapped holes exhibit a strong transient optical absorption which can be detected at 650 nm and 430 nm, respectively (see Figure 6).[98, 99] It has been reported that the lifetime of the trapped charge carriers can be very long while the actual trapping process is usually very fast. [100-102] For instance, the trapping of conduction band electrons occurs in less than 20 ps while the trapping of valence band holes is a significant slower process occurring in ns time scale.[103]
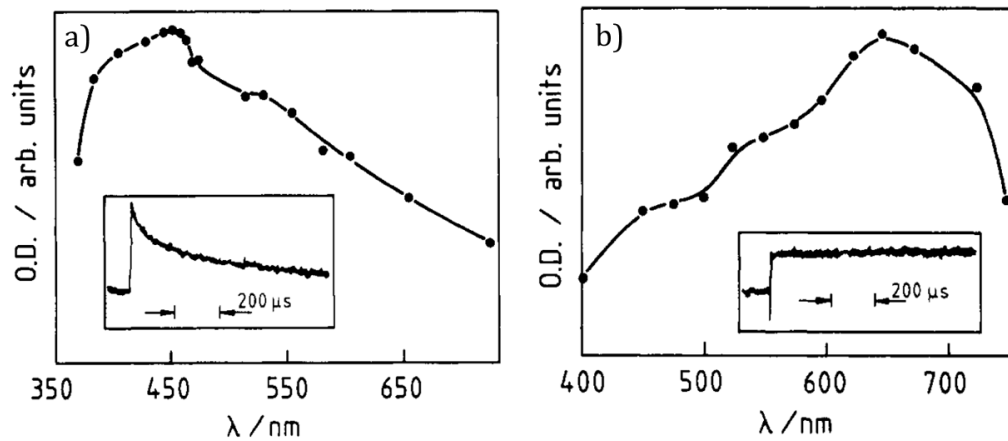
**Figure 6**: a) Optical absorption of a $TiO_2$ sol containing colloidal platinum and the time profile of the absorption at 472 nm (inset). b) Optical absorption of polyvinyl alcohol containing $TiO_2$ sol and the time profile of the absorption at 625 nm (inset).[98]

Generally, it is proposed that the photogenerated electrons can be trapped either at the surface [104, 105] of the titanium dioxide particle or in the bulk [106, 107] as follows:

$$e_{CB}^- + Ti^{4+} - OH \leftrightarrow Ti^{3+} - OH \tag{22}$$

$$e_{CB}^- + Ti^{4+}(bulk) \rightarrow Ti^{3+}(bulk) \tag{23}$$

There are still controversies regarding the trapping sites in $TiO_2$ for the photogenerated holes. Some research groups claim the photogenerated holes are trapped in adsorbed hydroxyl groups yielding weakly adsorbed hydroxyl radicals $Ti^{4+}$-$^\bullet OH$ [108, 109] while ESR investigations confirm a hole trapping at a subsurface oxygen anion of $TiO_2$.[110] Bahnemann *et al.* proposed an extended model with two different types of trapping sites, i.e., energetically deep and shallow traps for the photogenerated holes.[104]

Most of the photogenerated charge carriers recombine, however, directly after their generation in a radiative and nonradiative way. The recombination kinetics of the charge carriers have been studied in detail by many research groups.[103, 111, 112] Most of them reported the mean lifetime of a single electron/hole pair being of around 30 ps following by the second order kinetic recombination law with a recombination constant of $1.8 \pm 0.7 \cdot 10^{-10}$ $cm^3 \cdot s^{-1}$.[111] The charge recombination is mainly affected by trapping, interfacial charge transfer and temperature.[113]

# 3. Materials and experimental methods

## 3.1 Materials

Pure and lanthanum-doped $NaTaO_3$ powders have been provided by H.C. Starck Company (Goslar, Germany). They were synthesized by a conventional solid-state reaction according to the method described elsewhere.[18] In the case of pure $NaTaO_3$ a mixture of wet $Ta(OH)_5$, and $Na_2CO_3$ was employed as starting materials. Lanthanum-doped materials were prepared analogously by adding $La_2(CO_3)_3 \cdot 5H_2O$ into the mixture. The appropriate wet educts were homogeneously mixed and then dried at 105 °C for 16 hours. Afterwards, the dry educts were grinded and subsequently calcinated at 800 °C for 3 hours. Finally, the powder has been thoroughly grinded again. In this way the synthesized $NaTaO_3$ powders contained 0.57, 0.83, and 1.11 wt% lanthanum. The lanthanum content in the samples was preliminary determined by means of a fusion process employing $K_2S_2O_7$. The final determination of lanthanum doping was performed by means of inductively coupled plasma atomic emission spectroscopy (IPC-OES, Ultima 2, Horiba Jobin Yvon) against a cross calibration.

## 3.2 Modification of the materials with cocatalysts

All chemicals were purchased from Sigma Aldrich and were used as received without further purification. All aqueous solutions were prepared with deionized water from a SARTORIUS ARIUM 611 apparatus (resistivity = 18.2 MΩ·cm). All modification methods used in this work were carried out in the same quartz reactor employed for the photocatalytic water splitting reactions.

### 3.2.1 Noble metals

The *in situ* photodeposition of noble metals on the surface of the photocatalyst was performed via an photoreduction reaction from aqueous solutions of $H_2PtCl_6 \cdot 6H_2O$ (≥ 37.50 % Pt basis), $(NH_4)_3RhCl_6$ (99.99 %), and $HAuCl_4 \cdot 3H_2O$ (≥ 49.00 % Au basis). Metal loadings of 0.05-2.5 % (wt.-% of the pure metal) were achieved by the addition of appropriate volumes of the aqueous solution containing the desired

metal ions to the suspension directly before starting the photocatalytic test reaction.

The *ex situ* photodeposition of noble metals was performed via a photoreduction reaction by suspending 2 g of pure or La-doped NaTaO$_3$ in 50 ml aqueous solutions containing the desired concentrations of H$_2$PtCl$_6$·6H$_2$O, (NH$_4$)$_3$RhCl$_6$ or HAuCl$_4$·3H$_2$O to obtain 0.2 wt. % of appropriate metal loading. Additionally, 2 ml methanol was added into the suspension followed by purging with argon for 15-20 min. Subsequently, the reactor was closed and the head space of the reactor was then purged with argon for further 10 min in order to remove all oxygen. Afterwards the suspension was irradiated with a 1000 W Xe arc lamp for 5 h under continuous argon flow of 10 ml·min$^{-1}$. The obtained powder was separated by centrifugation, washed with water three times, and then dried at 110 C for 12 h.

### 3.2.2 Metal oxides

Metal oxide cocatalysts were loaded by an impregnation method employing the corresponding aqueous precursor solutions containing the desired concentrations of Co(NO$_3$)$_2$·6H$_2$O ($\geq$ 98 %), Ni(NO$_3$)$_2$·6H$_2$O ($\geq$ 98.5 %), Cu(NO$_3$)$_2$·3H$_2$O (99-104%), and RuCl$_3$ (99.98 %) to obtain 0.2 wt.% of appropriate metal oxide loading. Pure and La-doped NaTaO$_3$ were thoroughly mixed with the above mentioned precursor solutions of the proper concentration followed by thermal treatment at 266 °C for 1 h in air to form the desired metal oxide cocatalyst. The calcination conditions were chosen according to literature data reported elsewhere.[18]

### 3.2.3 Core-shell structures

Pt-core/Cr$_2$O$_3$-shell cocatalysts were prepared according to a method described elsewhere.[40, 73] First, Pt was deposited via an *in situ* photodeposition method by adding a desired concentration of an aqueous solution of H$_2$PtCl$_6$·6H$_2$O to the La-doped NaTaO$_3$ suspension. After addition of 2 ml methanol, the suspension was purged with argon in a similar way as described in 3.2.1 followed by irradiation for 4 h. The illumination was stopped and a specific volume of the diluted K$_2$CrO$_4$ solution of the desired concentration was added. The wt.-%-ratio of Cr to Pt was adjusted to be 1.5. Subsequently, the illumination was resumed prior to the

de-aeration of the suspension with argon. The $Cr_2O_3$ photodeposition was conducted during further 4 h of irradiation time. The final product was washed three times with water and dried in an oven at 70 °C for 12 h.

## 3.3   Analytical methods

### 3.3.1   X-ray diffraction (XRD)

X-ray diffraction patterns (XRD) were performed at room temperature with Cu Kα radiation on a Bruker D8 Advance instrument in the 2θ range of 10° - 80° in Bragg-Brentano geometry (θ-θ scan). A fixed divergence slit of 0.3 ° was applied. Soller slits of 2.5 ° were applied on both the X-ray tube side and the detector side to minimize scattered radiation. Phase analysis was carried out by the Rietveld method using the TOPAS 4.2 (Bruker AXS) software.

### 3.3.2   Field-emission scanning electron microscopy

Field-emission scanning electron microscopy (FE-SEM) measurements were carried out employing a JEOL JSM-6700F field-emission instrument at an accelerating voltage of 2 kV and using a secondary electron detector (SE). The SEM images of the undoped and the lanthanum doped $NaTaO_3$ powders were taken at 50000 times magnification.

### 3.3.3   High-resolution transmission electron microscopy

Transmission electron microscopy (TEM) was performed at 200 kV on a JEOL JEM-2100F-UHR field-emission instrument, which was operated in bright-field (BF) and selected area electron diffraction (SAED) mode as well as scanning TEM (STEM) to obtain high-angle annular dark-field (HAADF) micrographs. These TEM techniques were applied for the reconstruction of the nanoparticle shape according to a method described elsewhere.[114]

### 3.3.4  Specific surface area measurements (BET)

The BET specific surface area of the investigated materials was determined according to the multi-layer adsorption model by Brunauer, Emmett and Teller .[115] BET surface area measurements were carried out employing a FlowSorb II 2300 instrument (Micromeritics, USA). The gas mixture used for the adsorption and desorption measurements consisted of 30 % $N_2$ and 70 % He. The samples were heated at 120 °C for approximately 1 h prior to the measurements in order to remove water from the particle surface.

### 3.3.5  Diffuse UV-vis spectroscopy

The UV-Vis diffuse reflectance powder spectra of $NaTaO_3$ materials were measured on a Varian Cary 100 Scan UV-vis spectrophotometer in the spectral range from 200 – 800 nm utilizing an Ulbricht sphere. Barium sulfate was used as a reference to provide a nominal 100% reflectance measurement. Reflectance was converted by the instrument software to F(R) values according to the Kubelka-Munk theory. The absorbance of the suspended $NaTaO_3$ and $TiO_2$-P25 materials was directly measured by means of a Varian Cary 1000 UV-vis spectrophotometer by placing the cuvette filled with the appropriate suspension of a proper concentration in the middle of the corresponding integrated Ulbricht sphere.

## 3.4  Photocatalytic tests

### 3.4.1  Photocatalytic setup

The photocatalytic reactions were carried out in a 100 $cm^3$ double jacket quartz glass photoreactor being connected to a quadrupole mass spectrometer (QMS) for gas analysis (Hidden HPR-20). The system is continuously purged with argon as carrier gas; the Ar flow is controlled by a mass flow controller (MFC). This experimental setup shown in Figure 7 allows an in line monitoring of the entire course of the reaction with the advantage of simultaneously detecting several gaseous compounds formed during the photocatalytic reaction.
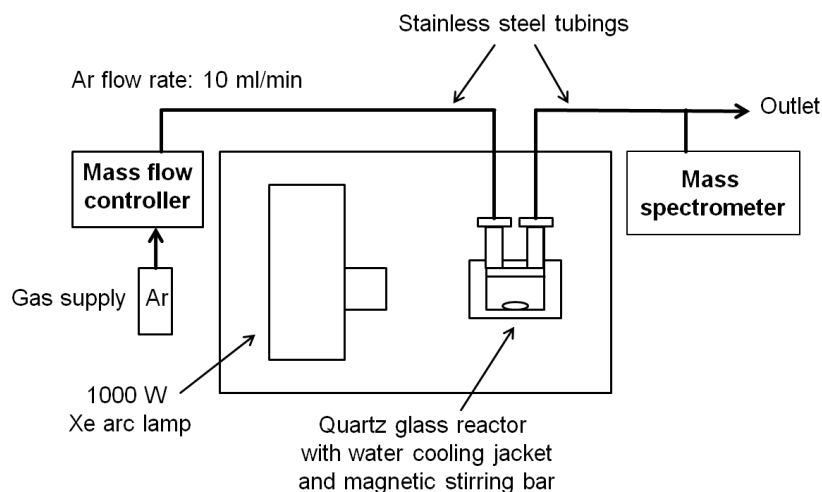
**Figure 7**: Experimental setup for the measurement of the photocatalytic $H_2$ and $O_2$ evolution.

In a typical experimental run, 50 mg of the photocatalyst was suspended in 50 ml of pure water, in 2.5 M aqueous alcoholic solution (methanol ($\geq$ 99.8%), ethanol, isopropanol (99.7%), butanol (99.4%), 2-methyl-2-propanol ($\geq$ 99.7%) or in 0.01 M aqueous solution of silver nitrate ($\geq$ 99.0%) by sonification. All solvents were purged from Sigma Aldrich and used as received without further purification.

The suspension was then transferred into the photoreactor and purged with Ar for 30 min to remove dissolved $O_2$. Afterwards, the reactor was connected to the mass flow controller and the QMS through metal flanges. To remove the air in the headspace of the reactor, an Ar gas stream with a flow rate of 50 cm$^3$ min$^{-1}$ was continuously passed through the reactor before irradiation, until no oxygen or nitrogen was detected by the QMS. The inlet flow rate/gas consumption by the QMS is 1 cm$^3$ min$^{-1}$ and the excess gas is directed towards the exhaust. The sampling rate of the QMS is in the millisecond time range, thus allowing a fast tracking of the reaction. The Ar gas flow rate was subsequently turned down and kept constant at 10 cm$^3$ min$^{-1}$ during the entire reaction. Before starting the irradiation, the system was left for further 40 min in the dark to ensure the stabilization of the system background and to monitor the baseline. Afterwards, the reactor was irradiated for 5-6 hs from the outside using an Osram XBO 1000 W Xe arc lamp in a Müller LAX 1000 lamp housing. During the irradiation time the photocatalytically formed gases were monitored continuously in time intervals of about 30 s.

After 4-5hs of irradiation time the lamp was switched off allowing the system to reach the baseline again. The temperature of the reaction solution was kept constant at 25 °C during the entire experiment employing a thermostatic bath (Julabo Company). For the quantitative analysis of $H_2$ and $O_2$ the QMS was calibrated employing standard dilutions of these gases (a mixture of 2 % of $H_2$ and 1 % of $O_2$ in Ar from Linde Gas Company, Germany).

### 3.4.2 Determination of the quantum yield

The photocatalytic activity of pure and modified La-doped $NaTaO_3$ was assessed by the determination of the quantum yield, $\phi$, of hydrogen and oxygen evolution from pure water, aqueous methanol, and silver nitrate solutions applying the previously reported equations (1-4).[87] Accordingly, the quantum yield $\phi$ is defined as:

$$\phi = r/I_a \tag{24}$$

$$I_a = I_0 \cdot F_s \tag{25}$$

where $r$ is the photocatalytic $H_2$ or $O_2$ evolution rate. $I_a$ and $I_0$ are the absorbed and the incident photon fluxes, respectively. $I_0$ was determined by integration of irradiance of the lamp in the range of 250-400 nm. $F_s$ is the integrated absorption fraction of the semiconductor particles over the range from $\lambda_1 = 250$ to $\lambda_2 = 400$ nm:

$$F_s = \frac{\int_{\lambda 1}^{\lambda 2} I_\lambda T_\lambda^f f_\lambda^s d\lambda}{\int_{\lambda 1}^{\lambda 2} I_\lambda T_\lambda^f d\lambda} \tag{26}$$

where $I_\lambda$ is the irradiance in the wavelength range $d\lambda$, $T_\lambda^f$ is the transmittance of the media between the light source and the reaction suspension. Since no filter was used and the reactor was made from quartz, $T_\lambda^f$ was assumed to be unity.

$$f_\lambda^s = 1 - T_\lambda^s = 1 - 10^{-A_\lambda^s} \tag{27}$$

where $f_\lambda^s$ is the fraction of light absorbed at the wavelength $\lambda$. $T_\lambda^s$ and $A_\lambda^s$ are the transmittance and absorbance, respectively, of the sample at the wavelength $\lambda$.

Figure 8 (left axis) shows the absorbance $A_\lambda^s$ of suspended La-doped NaTaO$_3$ particles in the wavelength range from 250 to 400 nm measured by means of an UV-vis spectrophotometer (Cary 1000) equipped with an integrating sphere. The irradiance $I_\lambda$ of the 1000 W Xe arc lamp (right axis) used for the photocatalytic tests was measured by a radiometer (BW Tek Company) and the obtained spectrum is also shown in Figure 2 (right axis).
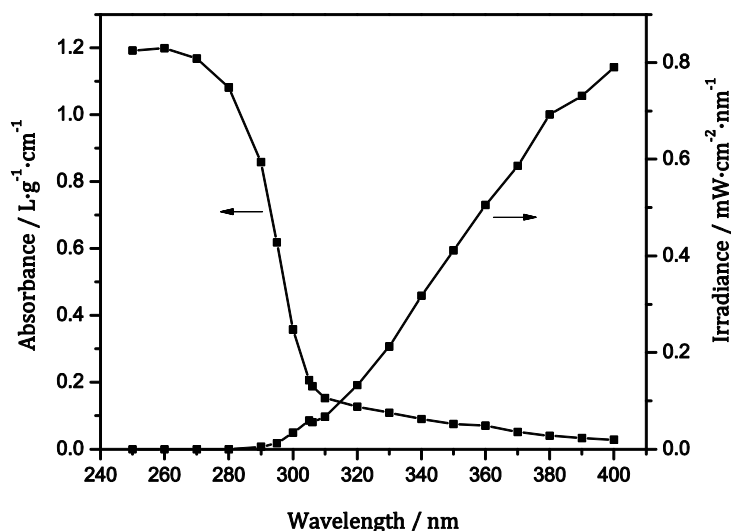


**Figure 8:** Absorption spectrum of suspended La-doped NaTaO$_3$ particles in water (left) and irradiance of a 1000 W Xe arc lamp (right) in the range of 250 to 400 nm.

The absorption property of suspended La-doped NaTaO$_3$ particles was examined in the wavelength range from 250 to 400 nm. For this purpose the absorption of several La-doped NaTaO$_3$ suspensions prepared in different concentrations was measured. The obtained absorption values at appropriate wavelengths were plotted versus the different concentrations of the suspensions. After linear regression the determined slopes of these curves were plotted versus the corresponding wavelengths (Figure 8 left axis). Figure 8 clearly shows that a rather small part of the light provided by the employed xenon lamp can be absorbed by the investigated La-doped NaTaO$_3$ particles.

The absorption property of suspended TiO$_2$-P25 particles as a reference material was examined in the wavelength range from 295 to 450 nm (Figure 9).

The quantum yields were determined by analogy to the La-doped $NaTaO_3$ system in the wavelength range from 295 to 450 nm.
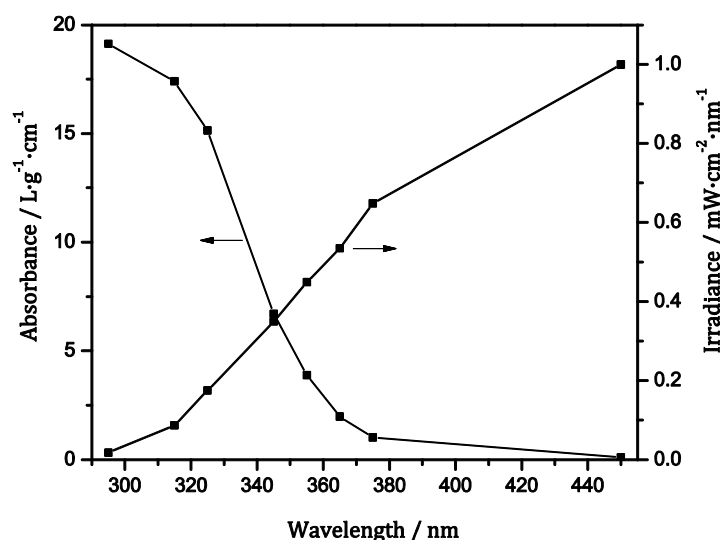


**Figure 9**: Absorption spectrum of suspended $TiO_2$ –P25 particles in water (left) and irradiance of a 1000 W Xe arc lamp (right) in the range of 295 to 450 nm.

### 3.4.3   Determination of hydrogen peroxide

The photocatalytic formation of $H_2O_2$ was determined by s method involving the dimerization of p-hydroxyphenylacetic acid in the presence of $H_2O_2$ and horse-radish peroxidase yielding a detectible fluorescent product, *i.e.*, 5,5-dicarboxymethyl-2,2-dihydroxybiphenyl ($\lambda_{ex}$=312 nm, $\lambda_{em}$=406 nm) which has been described elsewhere[116, 117]. For this purpose aliquots (2 mL) of irradiated La-doped $NaTaO_3$ suspensions were filtered through 0.45 µm filters (Machery-Nagel, Germany) and subsequently added to 0.1 mL of p-hydroxyphenylacetic reagent(8 mg of recrystallized p-hydroxyphenylacetic acid, 2 mg of peroxidase, and 50 mL of 0.1 M pH 8.8 Tris buffer). The calibration was performed by standard additions of $H_2O_2$ to the mixture and was found to be linear in the concentration ranges of interest.

## 3.5   Laser flash photolysis experiments

The time- resolved transient diffuse reflection measurements were performed employing the laser flash photolysis spectrometer LKS 80 (applied photophysics), an excimer laser (LPX 200, Lambda Physik) and a 150 W xenon arc lamp as analysing light (Figure 10). All experiments were carried out at a laser excitation wavelength of $\lambda_{ex}$=248 nm, a laser repetition frequency of 10 Hz, and 15 ns pulse duration. A laser beam energy of 14 mJ was measured with ferrioxalate actinometry.[118] The quantum yield of Fe(II) was taken as 1.28. [119] The samples were employed as dry powders being purged with $N_2$ for one ½ h prior to measurements. The area irradiated on the cuvette's front face was approximately 1 $cm^2$.
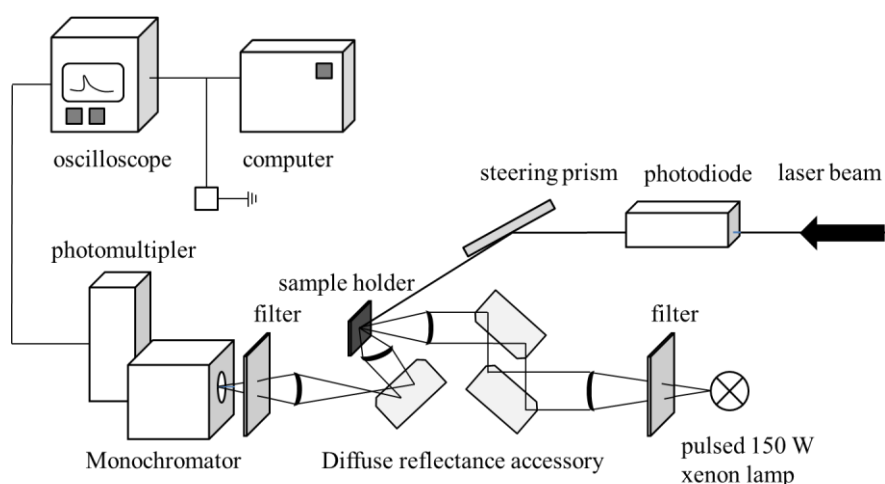


**Figure 10**: Setup used for transient laser flash photolysis measurements.

In the diffuse reflectance experiments the laser beam entered the sample at an oblique angle. The angle of the laser beam path was adjusted by the rotating the Pellin-Broca prism beam steering module. A diffuse reflectance accessory was employed to steer the incoming xenon light beam (via two plane folding mirrors) to the main optical axis. A spectrosil lens focused the optical beam onto the solid sample. The diffuse reflected light from the sample was collected by a second lens. A third folding mirror reflected the converging beam to the monochromator. Subsequently, the monochromator light fell into the photomultiplier detector (Hamamatsu R928 photomultiplier) and produced a current. The photometric light

level falling on the photomultiplier was kept at 100 mV for all measurement by applying high voltages of 550-800 V. The current output from the photomultiplier was terminated by a variable signal terminator (set to 100 Ω) inserted onto the signal input socket of the digital oscilloscope. The transient decay was recorded as voltage changes by an oscilloscope. In order to convert the voltage signal into an absorbance signal, the amplitudes of the reflected analysing light before $A_0$ (in mV) and after $A_t$ (in mV) the laser excitation were calculating according to: $\Delta A = -\log(A_t/A_0)$.

# 4. Results

## 4.1 Characterization of sodium tantalates

### 4.1.1 Optical properties

The absorption of light by a photocatalyst is one of the most crucial steps in photocatalysis enabling to drive a photocatalytic reaction. Thus, it is important to investigate the optical properties of the studied materials prior to investigations of their photocatalytic activity in order to choose the proper experimental conditions, e.g., the suitable irradiation source and the required material for the photoreactor.

The optical properties of pure and lanthanum doped sodium tantalates were examined using the standard technique of UV-Vis diffuse reflectance spectroscopy. The effect of lanthanum doping on the optical properties of pure $NaTaO_3$ was investigated by means of the band gap determination. Figure 11 illustrates the diffuse reflectance spectra of pure and La-doped $NaTaO_3$ containing different amounts of lanthanum, *i.e.*, 0.57, 0.83, and 1.11wt.% La.
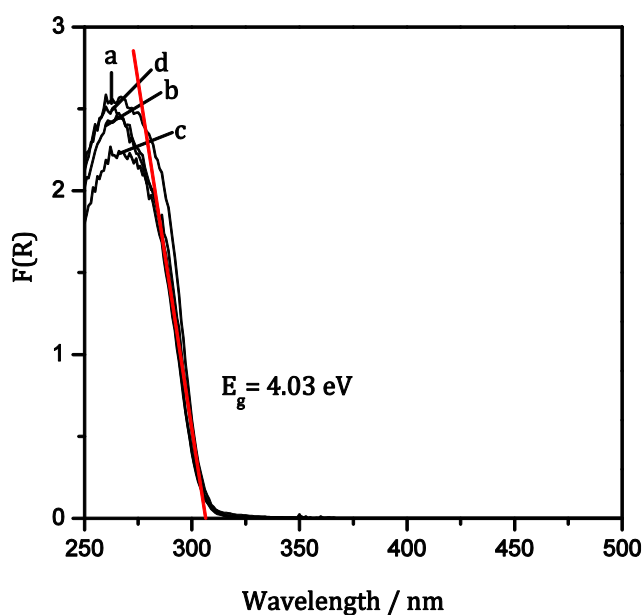


**Figure 11**: Diffuse reflectance spectra of $NaTaO_3$ powders: (a) 0 wt% La, (b) 0.57 wt% La, (c) 0.83 wt% La and (d) 1.11 wt% La.

It is clear from the onset of the absorbance (the Kubelka-Munk function F(R) shown here is equivalent to the absorbance measured in a molecular system) in Figure 11 that the lanthanum doping does not affect the optical properties of pure NaTaO$_3$. The optical band gap of pure and La-doped NaTaO$_3$ was estimated from the onset of the diffuse reflectance spectra at the intercept with the abscissa providing an onset wavelength of 307 nm (see Figure 11). Using the correlation between the photon energy E and the wavelength λ shown in Equation 28, the band gap energy (Eg) of pure and La-doped NaTaO$_3$ was estimated to be of approximately 4.04 eV.

$$E = \frac{hc}{\lambda}$$

28

with $c$ = 299.8·10$^6$ m·s$^{-1}$ being the speed of the light in vacuum and $h$ = 4.136·10$^{-15}$ eV·s the Planck's constant.

## 4.1.2  Structure and morphology

The crystalline structure of pure and La-doped sodium tantalate has been examined by means of powder X-ray diffraction (XRD) measurements. Hereby, the effect of the La doping on the crystallographic structure of sodium tantalate has been investigated in detail. XRD measurements should provide more information for the clarification of the factors being responsible for the enhanced photocatalytic activity of NaTaO$_3$ observed upon lanthanum doping.

   Figure 12 shows X-ray diffraction patterns of pure and La-doped NaTaO$_3$. Both specimens have nearly identical 2-theta positions and all diffraction peaks are assigned to an orthorhombic crystal structure with space group Pnma (N62)[120, 121]. The Rietveld analysis showed lower R factors for the orthorhombic structure (R$_{wp}$ = 9.15) than for the monoclinic structure (R$_{wp}$ = 26.7). The orthorhombic phase is the phase which is expected to be formed according to the chosen synthesis method.[121] In the case of La-doping the peak around 32.5 degree is expected to be slightly shifted to lower angles with increasing of lanthanum content (see highlighted area in red, Figure 12).[18] Figure 13 illustrates an enlarged view of the X-ray diffraction peaks around 32.6 degree of bare and of 0.83wt% La-doped NaTaO$_3$.

In the presence of lanthanum a characteristic small shift to lower angles from 2θ=32.57 to 2θ=32.54 was indeed observed in good agreement with the respective literature reports.[18] Kato *et al.* claimed that this shift can be interpreted as an indication for the homogeneous doping of lanthanum within the $NaTaO_3$ lattice although the majority of lanthanum is more likely localized near the surface of the photocatalyst particles.
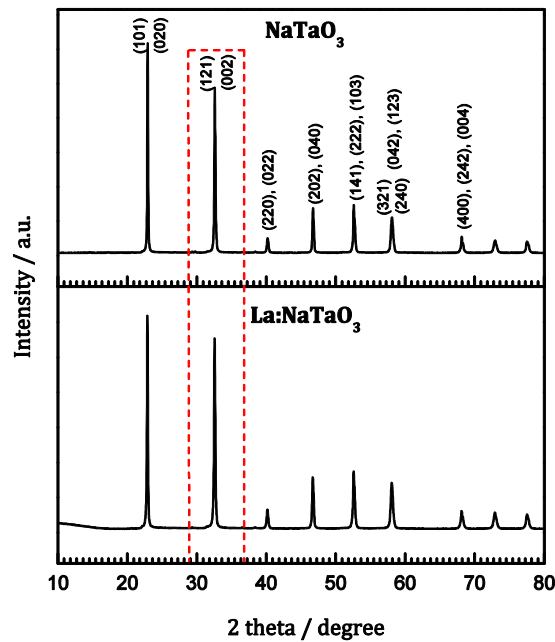


**Figure 12:** X-ray diffraction patterns (XRD) of pure and La-doped $NaTaO_3$ specimens prepared from the solid state method. The crystalline planes labeled on the diffraction peaks correspond to the orthorhombic phase.
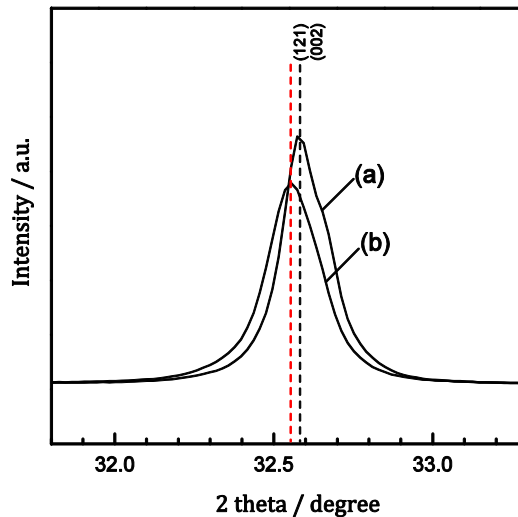
**Figure 13**: Comparison of the X-ray diffraction peaks around 32.6° of (a) nondoped NaTaO₃ and (b) La-doped NaTaO₃ (0.83 wt% La).

The morphology of pure and La-doped $NaTaO_3$ powders (0.57, 0.83 and 1.11 wt% La) was examined by means of scanning electron microscopy (Figure 14). Pure $NaTaO_3$ particles present a mixture of nanoparticles with irregular and rectangular shape with a broad particle size distribution ranging from 100 to 250 nm. It is clearly seen that La-doping remarkably affects both the shape and the particle size of pure $NaTaO_3$ (Figure 14 b-d). Generally, La-doped $NaTaO_3$ particles exhibit a polycrystalline structure. A 0.57 wt% La-doping leads to an increased irregularity of the particles whereby no particles with rectangular shape can be seen anymore. With higher La-doping of 0.83 wt% La the irregularity of the particles rises further. By 1.11 wt% La-doping the irregularity of the particles decreases whereby particles with more defined shape can be observed. It should be noted that La-doped $NaTaO_3$ particles also show a broad particle size distribution with, however, significantly smaller particles ranging from 80-150 nm.
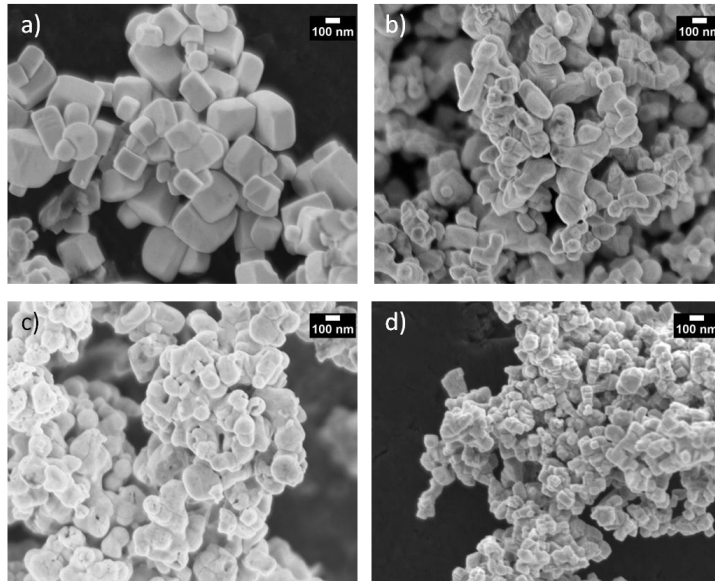
**Figure 14**: Scanning electron micrographs (SEM) of NaTaO$_3$ a) 0 wt% La b) 0.57 wt% La, c) 0.83 wt% La and c) 1.11 wt% La.

The effect of La-doping on the specific surface area (BET) was examined by means of nitrogen absorption measurements. Table 1 summarizes the data obtained for the specific surface area (BET) of investigated materials. With increasing of La-doping up to 0.83 wt% La, the specific surface area increases by a factor of two (from 2.4 to 5.4 m$^2\cdot$g$^{-1}$). However, the further increase of La-doping up to 1.1 wt% La does not significantly affect the specific surface area of NaTaO$_3$ anymore.

**Table 1:** Specific surface area (BET) measurements of pure and La-doped NaTaO$_3$ powders

| NaTaO$_3$ powders | Specific surface area* (BET) / m$^2\cdot$g$^{-1}$ |
|---|---|
| Pure NaTaO$_3$ | 2.4 |
| 0.57 wt% La | 4.1 |
| 0.83 wt% La | 5.4 |
| 1.11 wt% La | 5.6 |

*The relative errors are less than 5% as judged from repeated measurements

Detailed investigations of the photocatalysis processes on the well-studied $TiO_2$ have clearly demonstrated the importance of the knowledge concerning the abundance and the relative surface areas of specific crystal facets since various chemical reactions are preferably (photo-)catalyzed on specific surfaces of the catalyst particles.[114] It is well-known that both the specific structure and the coordination of exposed surface atoms of particulate catalysts are able to affect the mechanisms for bonding to adsorbed molecules to a great extent.[122, 123] The purposeful development of particulate catalysts exhibiting predominantly those specific crystal surfaces that are catalytically most active for specific reactions is therefore highly desirable. Herein, a more detailed shape analysis of $NaTaO_3$ particles was performed for the first time by reconstruction of the shape of the observed particles. For this purpose a newly developed method that combines geometric estimations by TEM and the elucidation of the detailed three-dimensional shapes by a Wulff-type construction has been employed. This type of analysis requires isolated particles with well-defined structure. Therefore, the shape analysis could be carried out only in the case of pure $NaTaO_3$ particles.

According to a method described elsewhere [114] the three-dimensional shape of the $NaTaO_3$ particles was estimated from (S)TEM micrographs as shown in Figure 15. The selected area in Figure 15 b was taken from the 125 nm circular area in the bright-field micrograph of Figure 15 a, and it could be indexed according to a [010] zone axis yielding {100}, {101}, and {001} as prominent bounding facets in addition to {010}. These assignments of bounding facets were applied to the STEM annular dark-field micrograph shown in Figure 15 c to estimate their surface normal in order to reconstruct a polyhedron as shown in Figure 15 d. Here it is worth noting that the TEM-based experiment did not yield the surface normal for the {010} facets, i.e., along the direction of image projection.
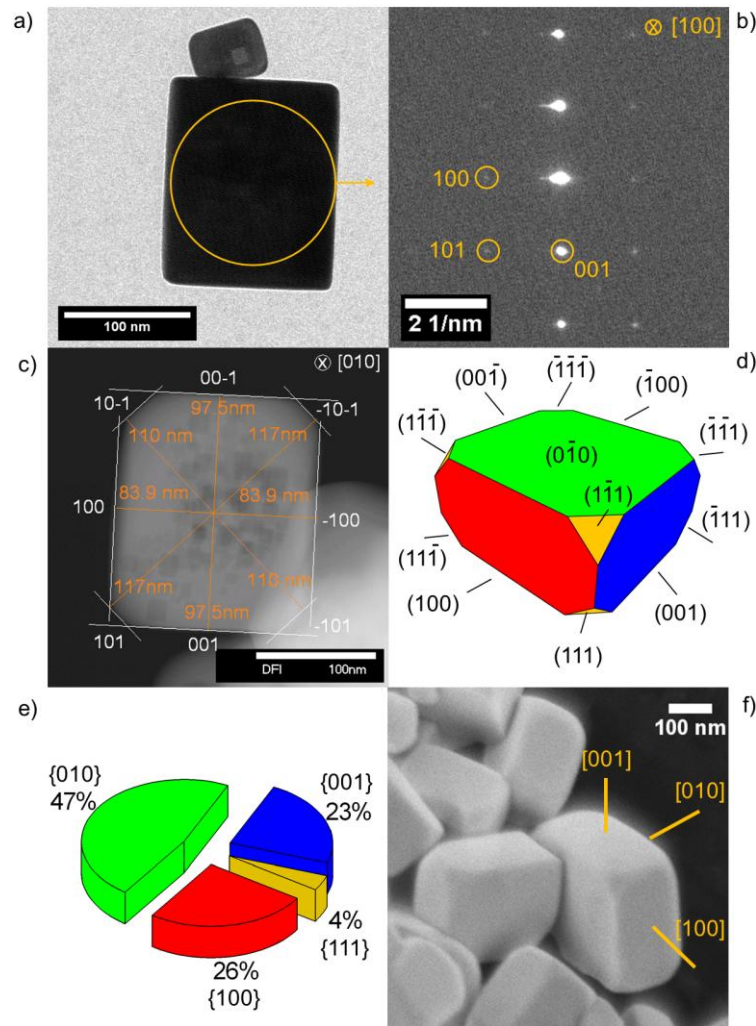
**Figure 15:** Shape analysis for pure NaTaO$_3$ nanoparticles: a) TEM bright-field micrograph, b) electron diffraction pattern of circa 100 nm circular area in a indexed according to [010] zone axis, c) STEM annular dark-field micrograph with normal distances of polyhedron facets to center of crystal, d) reconstructed polyhedron shape, e) relative abundance of crystal facets (same color index applies for as in d). f) Secondary electron micrograph of pure NaTaO$_3$.

Based on the relative surface energies from the theoretical calculations[124] the relevant distance was assumed to be 50 nm for reconstructing the polyhedron in Figure 15 d. The image brightness becomes weaker if the edge of the crystal is approached along the three non-supported {101} directions in the projection of Figure 15 c. This is interpreted as appearance of {111} facets, which is supported by the SEM micrograph in Figure 15 f. This was taken into account for the construction of the polyhedron in Figure 15 d. All of the fourteen bounding facets are labeled except (-100) and (-11-1) which are hidden in the perspective view.

The polyhedron shape in Figure 15 d refers to the following surface normal of the relevant facets: h({100}) = 97 nm; h({010}) = 50 nm; h({001}) = 98 nm; h({111}) = 120 nm. The relative distances should match the relative surface energies for an equilibrium Wulff shape.[124] The surface normal of the {101} facets has to be at least 133 nm to not appear as bounding facets.

It is important to note the relevance of surface energies in an equilibrium Wulff shape. For a polyhedron with a shape according to Figure 15 d, the relative abundances for the individual symmetry-equivalent facets are given in Figure 15 e. Again it is worth noting, that high-resolution SEM micrographs confirm plate-like nanoparticles formation. In Figure 15 f, the principal normal axes are drawn to one nanocrystal. Note the triangular facets on the corners of several crystals in Figure 15 f.

### 4.1.3   Cocatalyst loaded sodium tantalate

The covering of the $NaTaO_3$ surface loaded with different cocatalysts, *i.e.*, noble metals (Pt, Rh, and Au) and metal oxides (NiO, CuO, CoO, $RuO_2$, and AgO) was investigated by means of high-resolution transmission electron microscopy (HRTEM). Selected cocatalysts (Pt, $RuO_2$, and CoO) showing the most significant enhancement of the photocatalytic activity for $H_2$ and $O_2$ evolution as observed within this work will be presented in this chapter. The HRTEM micrographs of the remaining cocatalysts loaded on the La-doped $NaTaO_3$ surface employed in this work are collected in the appendix (section 8.1).

Figure 16 illustrates the HRTEM micrographs of pure (a and b) and La-doped $NaTaO_3$ (0.83 wt%La) (c and d) modified with 0.2 wt% Pt cocatalyst. In both cases several Pt clusters of not more than 5 nm in diameter were found to be adherent to the surface of appropriate catalyst particles.
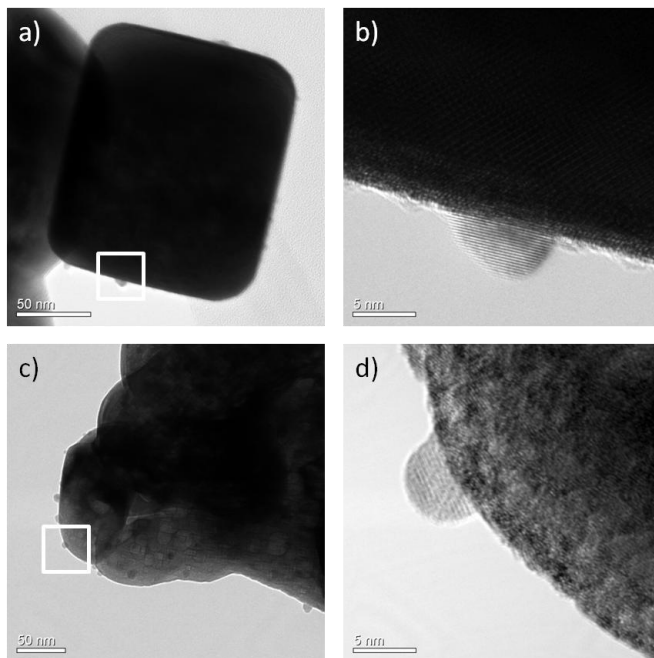
**Figure 16:** High-resolution transmission electron microscopic (HRTEM) analysis of Pt modified pure (a and b) and La-doped $NaTaO_3$ particles (c and d) at different scale bars, i.e., 50 and 5 nm of the corresponding material.

Figure 17 demonstrates the HRTEM micrographs of La-doped $NaTaO_3$ particles loaded with CoO (a and b) and $RuO_2$ (c and d) cocatalysts. It is clearly seen that in both cases less metal oxides cluster of 3-5 nm in diameter were found to be adherent to the surface of La-doped $NaTaO_3$ particles as compared to the Pt-loaded material (see Figure 16). Mostly, the La-doped $NaTaO_3$ particles are covered by a continuous film of CoO or $RuO_2$ of 1-2 nm in thickness.
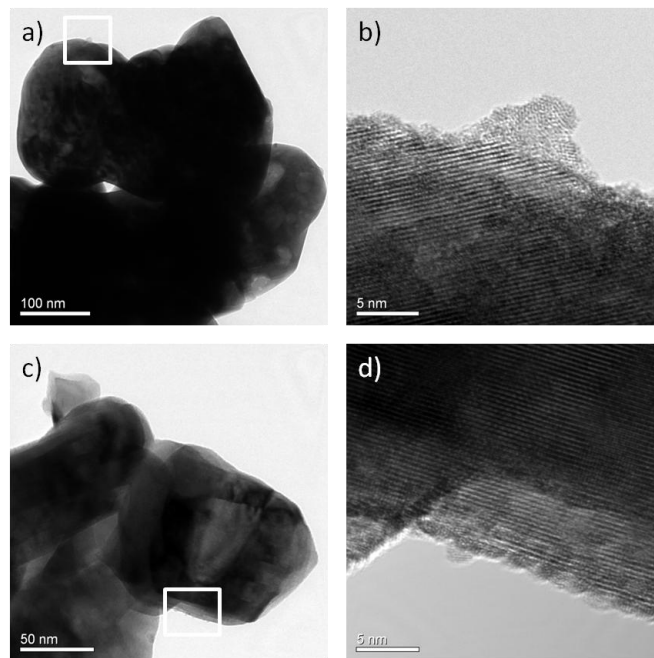
**Figure 17**: High-resolution transmission electron microscopic (HRTEM) analysis of La-doped NaTaO$_3$ particles loaded with CoO (a and b) and RuO$_2$ (b and c) at different scale bars, i.e., 100, 50 and 5 nm of the corresponding material.

## 4.2  Photocatalytic splitting of pure water

### 4.2.1  Sodium tantalate *vs.* titanium dioxide

Pure and lanthanum doped sodium tantalates were examined concerning their activity for the splitting of pure water under UV-vis irradiation. In order to enhance the photocatalytic activity of the studied materials their surface was modified by the deposition of different cocatalysts on it.

Figure 18 illustrates the typical time course of the photocatalytic $H_2$ evolution employing platinized a) bare and b) La-doped $NaTaO_3$ from pure water. In the absence of any cocatalyst, these materials did not exhibit any photocatalytic activity for $H_2$ evolution from pure water.
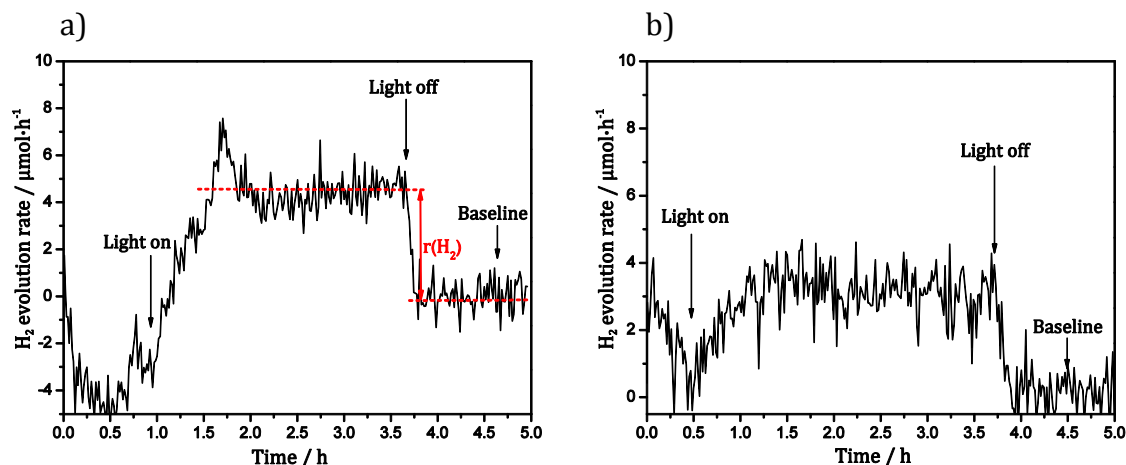


**Figure 18**: Photocatalytic $H_2$ evolution from pure water on a) bare $NaTaO_3$ and b) La-doped $NaTaO_3$ modified with 0.2 wt% Pt. Photocatalyst concentration: $1\ g\cdot L^{-1}$, Reactor volume: 50 ml, Irradiation intensity: $I_{250\text{-}400}=41\ mW\cdot cm^{-2}$.

Before starting with illumination, the time course of the investigated gaseous compounds is monitored (30-60 min) until their signals became stable. After the light is switched on, 30-40 min are required to reach nearly constant $H_2$ evolution rates (Figure 18). The system is then exposed to the light for further 2.5-3 h. Afterwards, the light is switched off whereby a rapid decay of the $H_2$ evolution rate is observed until reaching the baseline again. Usually, the data points measured at the end of each photocatalytic run are slightly higher than those at the very beginning monitored before illumination (see Figure 18 a). Thus, the measuring points at the very end of each experimental run are considered as baseline of the corresponding

gaseous compound. Therefore, the $H_2$ evolution rates were determined from the difference between the baseline (at the end) and the average of the values obtained in the part with so far constant $H_2$ evolution rate (indicated in Figure 18 in red color).

It should be noted here that the chosen way of the data treatment of the obtained gas evolution rates rather leads to an underestimation of the real values. Since, however, this method to determine the gas evolution rates has been consistently applied for all photocatalytic tests performed within this thesis all values given here can be quantitatively compared with one another.

Platinized bare and La-doped $NaTaO_3$ exhibit quite similar photocatalytic activities for $H_2$ evolution from pure water (3.5 and 4.5 $\mu mol \cdot h^{-1}$). Because of the noisy signals being observed for all experiments performed in pure water, the obtained values for $H_2$ evolution rate are rather close to the detection limit of the present system being 2 $\mu mol \cdot h^{-1}$ of $H_2$. Furthermore, no oxygen gas was detected by the mass spectrometer in this system which, however, is readily explained by the fact that the expected maximum amount of $O_2$ evolved under the given experimental conditions is approximately 2 $\mu mol \cdot h^{-1}$ $O_2$ being equal to the detection limit for the $O_2$ determination. Thus, it can be concluded that the investigated tantalates show no detectable activity for photocatalytic water splitting under the current experimental conditions.
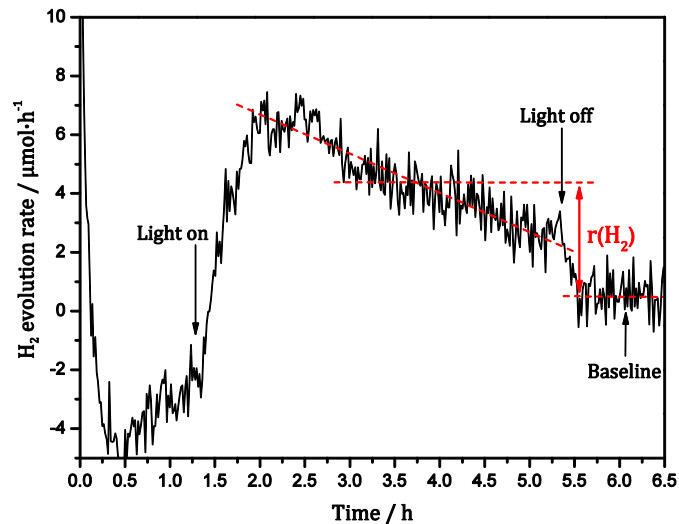
**Figure 19:** Photocatalytic $H_2$ evolution from pure water employing $TiO_2$-P25 modi-
fied with 0.2 wt% Pt. Photocatalyst concentration: 1 g·$L^{-1}$, Reactor volume: 50 ml,
Irradiation intensity: $I_{250-450}$=41 mW·$cm^{-2}$.

Titanium dioxide P25 was employed as a reference material in the present study.
The typical time course of the photocatalytic $H_2$ evolution from pure water is
shown in Figure 19. The obtained $H_2$ evolution rates were found to be unstable
decreasing with the irradiation time. In such cases $H_2$ evolution rates were deter-
mined from the difference between the baseline (at the end) and the average of all
measuring points obtained in the middle part of the curve as indicated in Figure 19
in red color. Similar to the system of sodium tantalates, no other gases besides $H_2$
were detected by means of the mass spectrometer in pure water.

The photocatalytic activity for $H_2$ evolution from pure water was compared
between three platinized photocatalysts, *i.e.*, $NaTaO_3$, La-doped $NaTaO_3$ and $TiO_2$-
P25 considering in particular the determined quantum yields (see Figure 20). The
typical calculation of the quantum yield is exemplarily given below for pure
$NaTaO_3$ modified with Pt exhibiting a $H_2$ evolution rate of 5 μmol·$h^{-1}$ (see
Figure 20):
The quantum yield is defined as

$$\phi \, [\%] = \frac{r}{I_0 \cdot A} \times 100 = \frac{5 \cdot 10^{-6} \, mol \cdot s \cdot cm^2}{3600 \, s \cdot 1.353 \cdot 10^{-8} mol \cdot 7.065 \, cm^2} \times 100 = 1.45\%$$

where *r* is the rate of gas evolution, $I_0$ is the number of absorbed photons and *A* is
the irradiated area. $I_0$ has been calculated as follows:

$$I_0 = \frac{I_a \cdot \lambda}{N_A \cdot h \cdot c} = \frac{5.29 \cdot 10^{-3} \; J \cdot s^{-1} \cdot cm^{-2} \cdot 306 \cdot 10^{-9} \, m}{6.022 \cdot 10^{23} \; mol^{-1} \cdot 6.626 \cdot 10^{-34} \; J \cdot s \cdot 2.998 \cdot 10^{8} \; m \cdot s^{-1}} = 1.353 \cdot 10^{-8} \; mol \cdot s^{-1} \cdot cm^{-2}$$

with    $I_a$  :      the total energy which can be absorbed by the $NaTaO_3$ particles

        $\lambda$  :      the wavelength corresponding to the band gap energy of $NaTaO_3$

       $N_A$  :      Avogadro constant

       $h$  :      Planck constant

       $c$  :      speed of light

$I_a$ has been determined according to the following equation:

$$I_a = I_\lambda \cdot F_s = 40.9 \, mW \cdot cm^{-2} \cdot 0.129 = 5.29 \, mW \cdot cm^{-2} = 5.29 \cdot 10^{-3} \, J \cdot s^{-1}$$

where $I_\lambda$ is the light intensity of the employed lamp being determined by the integration of the irradiance of the lamp in the wavelength range between 250-400 nm (see Figure 8 right axis). $F_s$ is the integrated absorption fraction of the $NaTaO_3$ particles in the wavelength range between 250-400 nm which has been determined using the following equation:

$$F_s = \frac{\int_{\lambda 1}^{\lambda 2} I_\lambda f_\lambda^s d\lambda}{\int_{\lambda 1}^{\lambda 2} I_\lambda d\lambda} = \frac{5.29}{40.9} = 0.129 \quad \text{with} \quad f_\lambda^s = 1 - 10^{-A_\lambda^s}$$

where $A_\lambda^s$ is the absorbance of the suspended $NaTaO_3$ particles in the wavelength range from 250 to 400 nm measured by means of an UV-vis spectrophotometer (see Figure 8 left axis).

The highest quantum yield of 1.5 % was obtained in the case of undoped $NaTaO_3$ under the current experimental conditions. It should be noted here that it is only through the determination of the quantum yields that it is clearly seen that sodium tantalate materials exhibit significantly higher photocatalytic acivity for $H_2$ evolution than $TiO_2$-P25. The simple comparison of the corresponding $H_2$ evolution rates obtained for all three materials does not provide any significant difference in their photocatalytic activity for $H_2$ evolution because of the differences in the absorption capacity between tantalates and titanates under illumination with Xe arc lamp employed in this work (see Figure 8 and Figure 9).
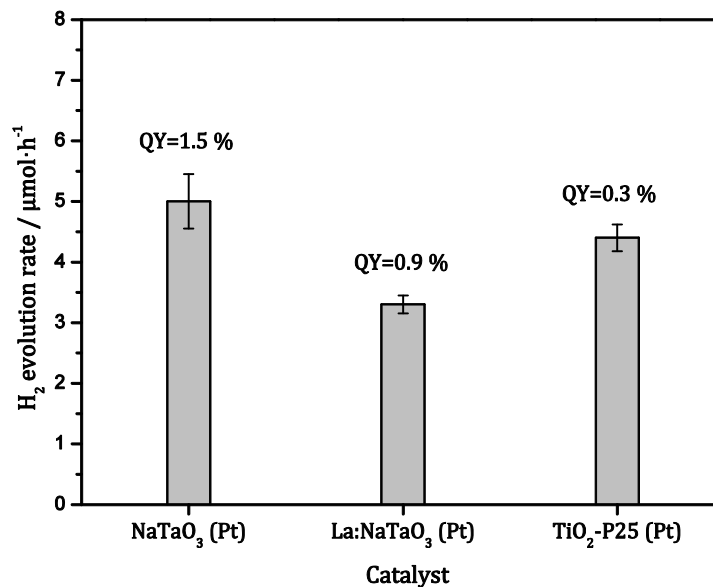
**Figure 20:** Comparison of the photocatalytic activity for $H_2$ evolution between NaTaO₃ (pure and La-doped) and TiO₂- P25 from pure water. Photocatalyst concentration: 1 g·L⁻¹, Pt loading: 0.2 wt%, Reactor volume: 50 ml, Irradiation intensity: $I_{250-450}$=41 mW·cm⁻².

### 4.2.2 Cocatalyst loaded La-doped sodium tantalate

The photocatalytic activity for water splitting can usually be improved by the utilization of different cocatalysts loaded onto the catalyst surface. Owing to the creation of active sites and/or the apparent decrease of the activation energy for gas evolution both noble metals (*e.g.*, Pt, Rh,) and transition metal oxides (*e.g.,* NiO, $RuO_2$) have been widely used as cocatalysts in photocatalytic water splitting systems showing significant enhancement of the photocatalytic activity for $H_2$ and $O_2$ evolution.[40] Since noble metal cocatalysts, in particular Pt, are usually very expensive and may also catalyze the undesired backward reaction, *i.e.*, the water formation, more research is needed to identify low-cost cocatalyts exhibiting a notable enhancement of the photocatalytic activity.[125] Transition metal oxide cocatalysts seem to be suitable candidates because they are less expensive demonstrating high stability and photocatalytic activity for overall water splitting.[40]

Thus, within this work it was of high importance to investigate the effect of different low-cost metal oxide cocatalysts, *i.e.*, NiO, CuO, CoO, $RuO_2$ and AgO on the photocatalytic activity for $H_2$ evolution or even on the photocatalytic splitting of pure water. These transition metal oxides are known to be very stable exhibiting

metallic properties. Although Pt is very expensive, no other cocatalyst being more effective has been found until now. Therefore, it is important to investigate other less expensive noble metal cocatalysts such as Rh and Au on the photocatalytic activity for $H_2$ evolution.

Thus, the surface of La-doped $NaTaO_3$ (0.83 wt% La) was modified noble metals (Pt, Rh and Au) and metal oxides (NiO, CuO, CoO, $RuO_2$ and AgO) in order to enhance the photocatalytic activity for $H_2$ evolution or even to enable the photocatalytic splitting of pure water. Additionally, so-called core/shell cocatalysts were employed in order to investigate the photocatalytic activity for stoichiometric water splitting into molecular $H_2$ and molecular $O_2$.

Figure 21 shows that Pt is the most active cocatalyst for $H_2$ evolution from pure water among the noble metals tested here, however, without really significant differences in the photocatalytic activity among these materials. $RuO_2$, on the other hand, shows the highest catalytic activity for $H_2$ evolution among the metal oxide cocatalysts.
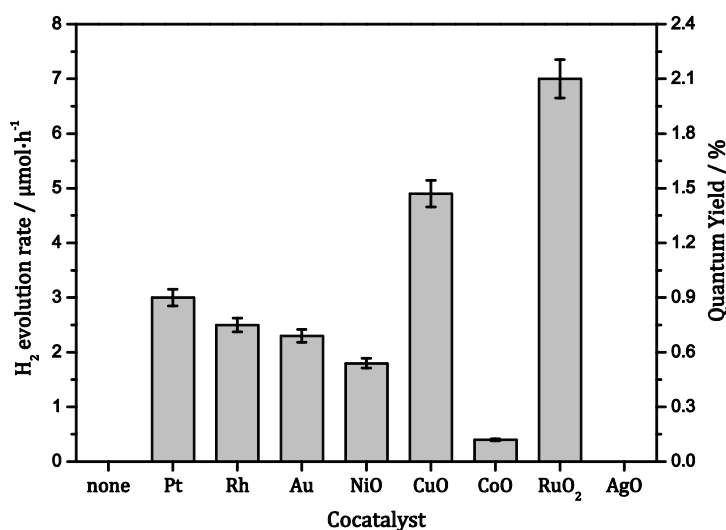


**Figure 21:** Photocatalytic $H_2$ evolution from pure water employing La-doped $NaTaO_3$ (0.83 wt% La) modified with different cocatalysts. Photocatalyst concentration: 1 g/L, Cocatalyst loading: 0.2 wt%, Reactor volume: 50 ml, Irradiation intensity: $I_{250-450}$=41 mW/cm$^2$.

Taken as a whole it is obvious that $RuO_2$ (7 $\mu mol \cdot h^{-1}$, QY=2.1 %) and CuO (5 $\mu mol \cdot h^{-1}$, QY=1.5 %) exhibit the highest activities for the photocatalytic $H_2$ evolution among all investigated cocatalysts. CoO shows a very low activity for $H_2$

evolution while AgO exhibited almost no photocatalytic activity (less than 0.2 µmol/h $H_2$ being the detection limit for the present system). In all systems only $H_2$ and no $O_2$ was detected. This can be explained either by the formation of adsorbed peroxide species or by an enhanced solubility of the produced molecular oxygen in the aqueous photocatalyst suspensions.

The possible formation of $H_2O_2$ during the irradiation was examined in the case of the most efficient cocatalyst, *i.e.*, for La-doped $NaTaO_3$ modified with $RuO_2$ according to the method described in experimental part (chapter 3.4.3). The formation of the fluorescent product was indeed detected, indicating that $H_2O_2$ was photocatalytically formed. Assuming that for the formation of one $H_2O_2$ molecule 2 holes are required, the amounts of $H_2O_2$ and $H_2$ formed are expected to be similar. However, the detected amount of $H_2O_2$ was 60 times lower than that of $H_2$ evolved in the same experiment (see Table 2).

**Table 2:** Quantitative analysis of photocatalytically formed products during water splitting reaction over La-doped $NaTaO_3$ (0.83 wt% La) modified with 0.2 wt% $RuO_2$. Photocatalyst concentration: 1 g·$L^{-1}$, Reactor volume: 50 ml, Irradiation intensity: $I_{250-450}$=41 mW·$cm^{-2}$. Irradiation time: 6 h

| Detected products | Concentration / µmol·$l^{-1}$ |
|---|---|
| Molecular hydrogen ($H_2$) | 840 |
| Hydrogen peroxide($H_2O_2$) | 14 |

In order to enhance the simultaneously formation of both gases, *i.e.*, $H_2$ and $O_2$ a new system consisting of two different cocatalysts was designed. For this purpose a mixture of $RuO_2$- and CoO-loaded La: $NaTaO_3$ was employed in the same photocatalytic run in order to achieve the stoichiometric formation of molecular $H_2$ and molecular $O_2$ from pure water. $RuO_2$ was used as it showed the highest photocatalytic activity for $H_2$ formation for the present system (Figure 21 b). CoO is a well-known cocatalyst for improving the oxidative pathway of water splitting, *i.e.*, enhancing the $O_2$ formation from pure water.[62, 63]
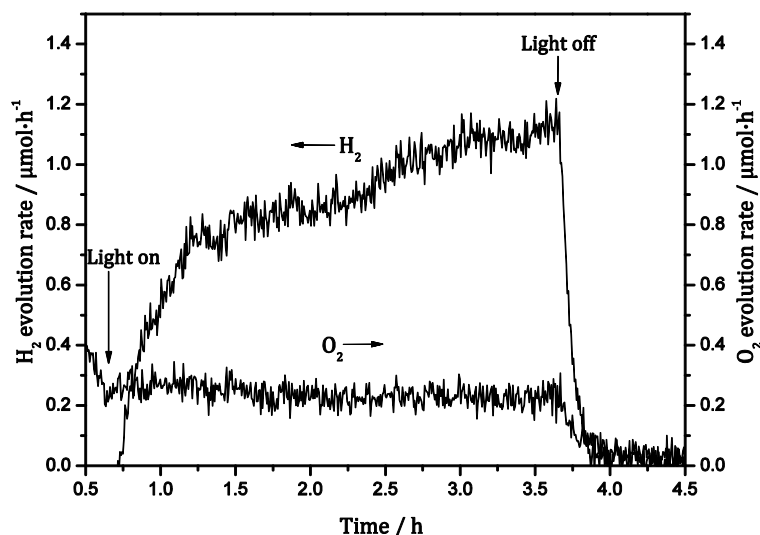
**Figure 22:** Photocatalytic splitting of pure water into $H_2$ and $O_2$ employing a mixture of La-doped $NaTaO_3$ (0.83 wt% La) containing $RuO_2$ and $CoO$ modified particles. Photocatalyst concentration: 1 g·$L^{-1}$, Cocatalyst loading: 0.2 wt%, Reactor volume: 50 ml, Irradiation intensity: $I_{250-450}$=41 mW·$cm^{-2}$.

The results shown in Figure 22 demonstrate the simultaneous formation of both $H_2$ and $O_2$ gases when a combination of $RuO_2$ and $CoO$ cocatalysts was employed at the same time. The obtained rates for $H_2$ and $O_2$ evolution were determined to be 1 and 0.23 μmol·$h^{-1}$, respectively. The $O_2$ evolution rate was found to reach only half of the value expected from the overall water splitting, i.e., 0.5 μmol·$h^{-1}$. Nevertheless, this result gives a strong indication that La-doped $NaTaO_3$ is able to split pure water into $H_2$ and $O_2$.

Another attempt to achieve the overall water splitting on La-doped $NaTaO_3$ is the application of so-called core/shell cocatalysts. Especially, metal-core/$Cr_2O_3$-shell cocatalysts are well-known to exhibit photocatalytic $H_2$ and $O_2$ evolution in stoichiometric ratio from pure water.[73] Therefore, La-doped $NaTaO_3$ was accordingly modified with Pt-core/$Cr_2O_3$-shell cocatalyst and applied in the photocatalytic test reaction. Figure 23 illustrates that both gases *i.e.*, $H_2$ and $O_2$ were detected with significantly higher evolution rates as compared with the results of the previous system (Figure 22). But the obtained ratio of $H_2$:$O_2$ evolution rates was found to be 4:1 which also does not correlate with the stoichiometric ratio of overall water splitting reaction.
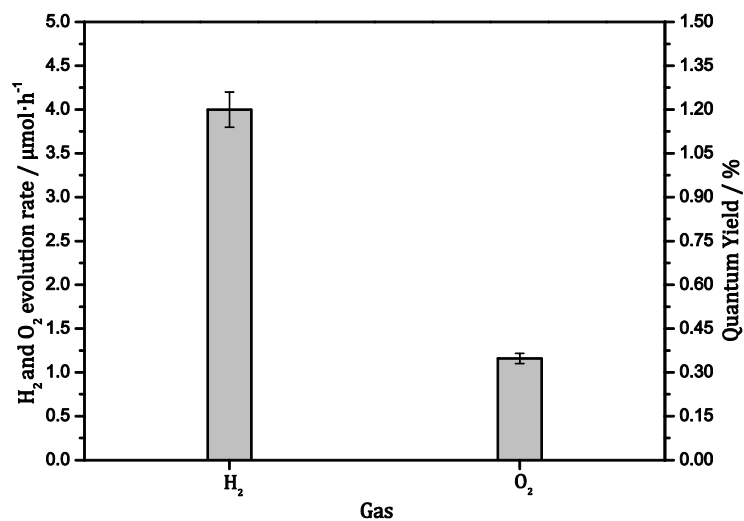
**Figure 23:** Photocatalytic splitting of pure water employing La-doped NaTaO$_3$ (0.83 wt% La) modified with Pt/Cr$_2$O$_3$ core shell cocatalyst. Photocatalyst concentration: 1 g·L$^{-1}$, Cocatalyst loading: 0.2 wt%, Reactor volume: 50 ml, Irradiation intensity: I$_{250-450}$=41 mW·cm$^{-2}$.

## 4.3 Photocatalytic alcohol reforming

### 4.3.1 Optimal conditions

The results presented in chapter 4.2 have clearly shown that sodium tantalate materials exhibit rather poor photocatalytic activity for H$_2$ and O$_2$ evolution from pure water. For a better evaluation of their photocatalytic activity for H$_2$ evolution and to determinate the most efficient photocatalyst for the reductive pathway, a so-called sacrificial system was employed here. In particular, methanol was added to the system since alcohols are known to act as efficient electron donors for the photogenerated holes.[6] Consequently, the reactions of the remaining electrons can be studied in detail in these systems. Thus, the aim of this chapter is to determine the optimal conditions for the reductive photocatalytic H$_2$ evolution in the presence of the sacrificial agent methanol. Different effects as the employed amount of lanthanum doping, the amount of cocatalyst loading and the deposition method will be considered in detail.

The optimal percentage of lanthanum doping among the available La-doped NaTaO$_3$ materials (0.57 wt% La, 0.83 wt% La and 1.11wt% La) was determined by measuring the photocatalytic activity for H$_2$ evolution after photodeposition of the Pt cocatalyst (0.5 wt%) in the presence of methanol. As shown in Figure 24 a 0.83 wt% lanthanum doping of NaTaO$_3$ demonstrated the highest photocatalytic activity for H$_2$ evolution (98 µmol·h$^{-1}$, QY=30 %) among all tested materials. NaTaO$_3$ containing 0.57 wt% La exhibited identical photocatalytic activity for H$_2$ evolution (45 µmol·h$^{-1}$, QY=13.5 %) as that of undoped material, indicating that this amount of lanthanum doping is insufficient to enhance the photocatalytic activity of the undoped catalyst. On the other hand, a 1.11 wt% lanthanum doping obviously exceeds the optimal amount of dopant since the photocatalytic H$_2$ evolution rate (61 µmol·h$^{-1}$, QY=18 %) decreased as compared with that obtained in the case of the 0.83 wt% lanthanum doping.
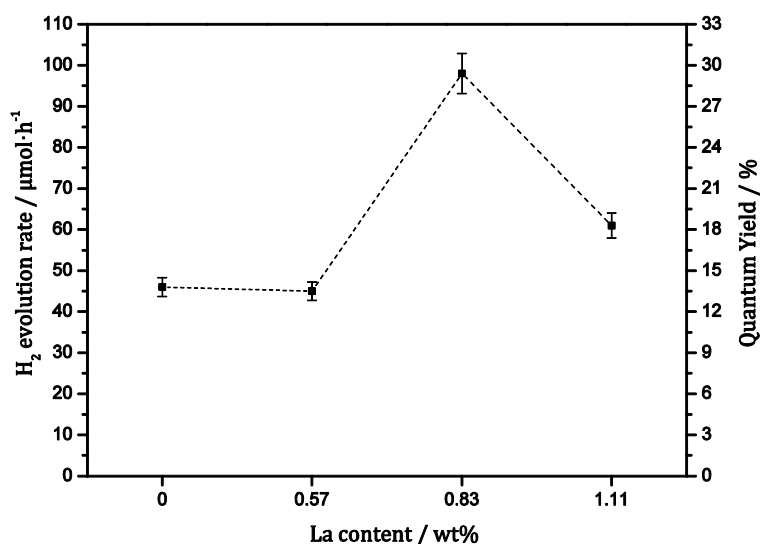


**Figure 24:** Effect of lanthanum doping of NaTaO$_3$ on the photocatalytic activity for H$_2$ evolution in the presence of methanol. Photocatalyst concentration: 1 g·L$^{-1}$, Methanol concentration: 2.5 M, Pt loading: 0.5 wt%, Reactor volume: 50 ml, Irradiation intensity: I$_{250-450}$=41 mW·cm$^{-2}$.

Based upon these results, NaTaO$_3$ with a 0.83 wt% lanthanum doping was chosen as a model photocatalyst to be employed for all further investigations carried out in this work.

The preparation method of the cocatalyst particles has been reported to play an important role for the overall photocatalytic activity of different catalysts.[40] For instance, the deposition of metallic cocatalysts such as Pt, Rh or Au can be accomplished by the conventional photodeposition method either directly within the photocatalytic test for $H_2$ evolution (*in situ*) or employing already metalized photocatalysts at the beginning of the photocatalytic test reaction (*ex situ*). More detailed information about these deposition methods can be found in 3.2.1and 3.2.2.

In this respect, the effect of the employed deposition method on the photocatalytic $H_2$ evolution was exemplarily investigated using La-doped $NaTaO_3$ (0.57 wt% La). This material was chosen because it shows constant $H_2$ evolution rates in the steady state region over 24 h of irradiation time indicating high stability of this photocatalyst.
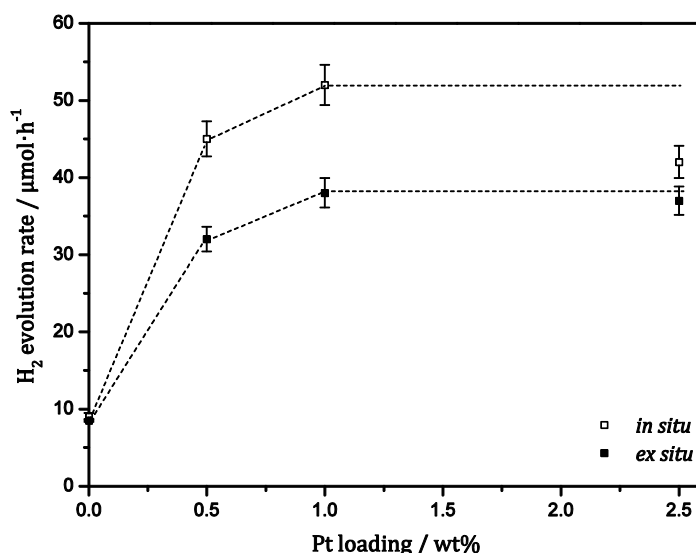


**Figure 25:** Effect of the method employed for Pt deposition on the photocatalytic $H_2$ evolution employing La-NaTaO$_3$ (0.57 wt% La). Photocatalyst concentration: 1 g·L$^{-1}$, Methanol concentration: 2.5 M, Reactor volume: 50 ml, Irradiation intensity: I$_{250-450}$=41 mW·cm$^{-2}$.

Figure 25 shows that for the three different Pt loadings employed here, *i.e.*, 0.5 wt%-, 1.0 wt%- and 2.5 wt%-Pt, the *in situ* photodeposition method leads to higher $H_2$ evolution rates as compared with the *ex situ* method. On account of these results the *in situ* photodeposition method was also applied for the deposition of

other noble metal cocatalysts, *i.e.*, Rh and Au employed in this work expecting similar results as obtained in the case of Pt photodeposition.

In order to determine the optimal amount of Pt loading for the photocatalytic $H_2$ evolution, Pt loadings from 0 to 2.6 wt% were varied as shown in Figure 26. Evidently that even in the absence of any cocatalyst a $H_2$ evolution rate of 9 μmol·h$^{-1}$ was observed. After addition of a small amount of Pt (0.1 wt%) into the system the $H_2$ evolution rate was increased almost four times, *i.e.*, from 9 to 37 μmol·h$^{-1}$. The increase of Pt loading up to 0.2 wt% resulted in further enhancing of $H_2$ evolution rate (48 μmol·h$^{-1}$). It should be noted that the further increase of Pt loading from 0.2 up to 2.6 wt% did not affect the photocatalytic activity for $H_2$ evolution with nearly constant $H_2$ evolution rates of about 45 μmol·h$^{-1}$.
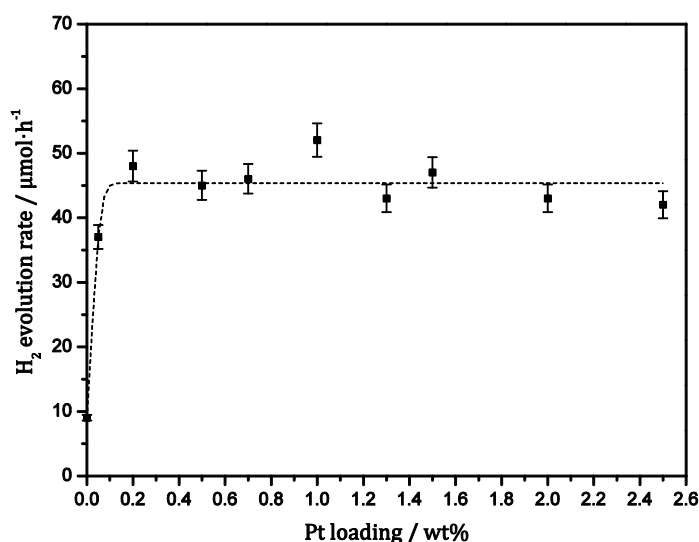


**Figure 26:** Effect of Pt concentration on the photocatalytic $H_2$ evolution employing La-doped NaTaO$_3$ (0.57wt% La). Photocatalyst concentration: 1 g·L$^{-1}$, Methanol concentration: 2.5 M, Reactor volume: 50 ml, Irradiation intensity: $I_{250-450}$=41 mW·cm$^{-2}$.

The obtained results demonstrated that Pt loading of only 0.2 wt% already suffices to reach, *e.g.*, similar photocatalytic $H_2$ evolution rates as in the case of 1 wt% Pt loading. Therefore, the majority of the performed photocatalytic tests in this work have been carried out using the optimal Pt loading of 0.2 wt%.

### 4.3.2 Sodium tantalate *vs.* titanium dioxide

The photocatalytic activity for $H_2$ evolution of La-doped $NaTaO_3$ was compared with that of the commercial $TiO_2$-P25 acting as a reference material. The effect of the presence and absence of the Pt cocatalyst on the surface of the bare $NaTaO_3$, La-doped $NaTaO_3$ and commercial $TiO_2$-P25 was examined in detail.

Figure 27 illustrates the typical time courses of the photocatalytic $H_2$ and $CO_2$ evolution rates from aqueous methanol solution exemplarily shown for a) La-doped $NaTaO_3$ (0.83 wt% La) and b) $TiO_2$-P25. The time course of $H_2$ and $CO_2$ is similar to that of the previously described system of pure water (see 4.2.1). After the light is switched on, the evolved gases, i.e., $H_2$ and $CO_2$, reach the region with constant evolution rates significantly faster in the presence of methanol (less than 30 min) than just in pure water. The only exception here presents the photocatalytic evolution of $CO_2$ in the case of $TiO_2$-P25 where the so-called initiation phase takes more than 30 min (see Figure 27 b). After reaching the region with nearly constant $H_2$ and $CO_2$ evolution rates, the suspension is irradiated for further 6 h. When the lamp is switched off, the $H_2$ and $CO_2$ evolution rates decrease within 10-15 min reaching the baseline. Again, only in the case of $TiO_2$-P25 the decrease of the $CO_2$ signal takes at least 30 min (Figure 27 b). Interestingly, the obtained $H_2$ evolution rates in the case of $TiO_2$-P25 are less stable than those monitored for La-doped $NaTaO_3$ both in the presence and absence of methanol (Figure 19 and Figure 27 b). By analogy with pure water system, the $H_2$ and $CO_2$ evolution rates were determined from the difference between the baseline (at the end) and the average of all measuring points obtained in the middle part of the curve, *i.e.*, the so-called steady state region (indicated in red color in Figure 27 a and b).
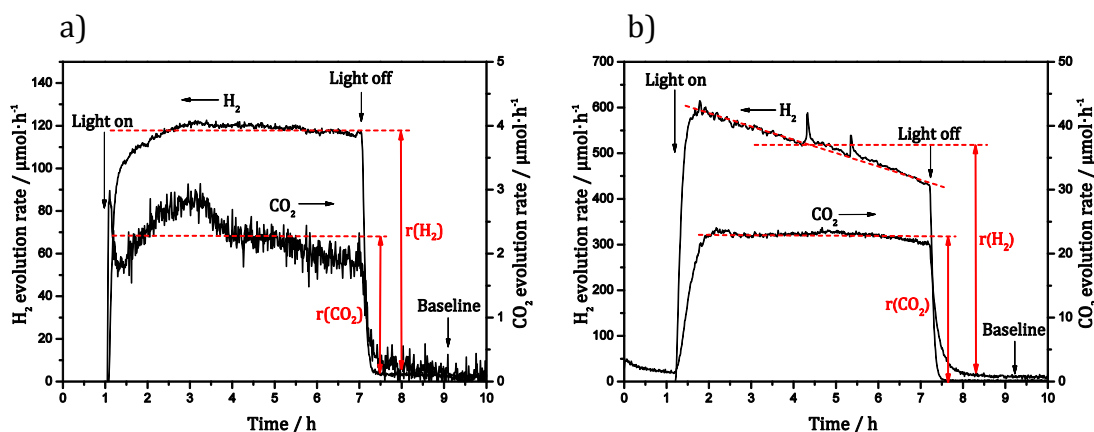
**Figure 27:** Time course of the photocatalytic evolution of $H_2$ and $CO_2$ from aqueous methanol solution employing a) La-doped $NaTaO_3$ (0.83 wt% La) and b) $TiO_2$-P25. Photocatalyst concentration: 1 g·$L^{-1}$, Methanol concentration: 2.5 M, Pt loading: 0.2 wt%, Reactor volume: 50 ml, Irradiation intensity: $I_{250-450}$=41 mW·$cm^{-2}$.

Figure 28 illustrates the effect of Pt deposition on the photocatalytic $H_2$ evolution employing (a) $NaTaO_3$ (pure and La-doped) and (b) $TiO_2$-P25. In the presence of methanol acting as electron donor all three tested catalysts showed photocatalytic activity for $H_2$ evolution even in the absence of any cocatalyst. In particular, pure $NaTaO_3$ exhibited the highest quantum yield of 14 % for photocatalytic $H_2$ production (47 µmol·$h^{-1}$). This is more than ten times as high as that of P25 with QY=1.2 % (20 µmol·$h^{-1}$) while La-doped $NaTaO_3$ exhibited the lowest quantum yield of 0.9 % in this system (3 µmol·$h^{-1}$). Interestingly, Pt loading had no influence on the photocatalytic $H_2$ evolution in the presence of methanol in the case of pure $NaTaO_3$. On the other hand, due to the Pt deposition the photocatalytic activity for $H_2$ evolution could be remarkably enhanced in the case of La-doped $NaTaO_3$ and of P25 reaching quantum yields of 33 % (109 µmol·$h^{-1}$) and 32 % (530 µmol·$h^{-1}$), respectively. Thus, it is clearly seen that both materials exhibit quite identical photocatalytic activity for $H_2$ evolution from aqueous methanol solution under the present conditions.
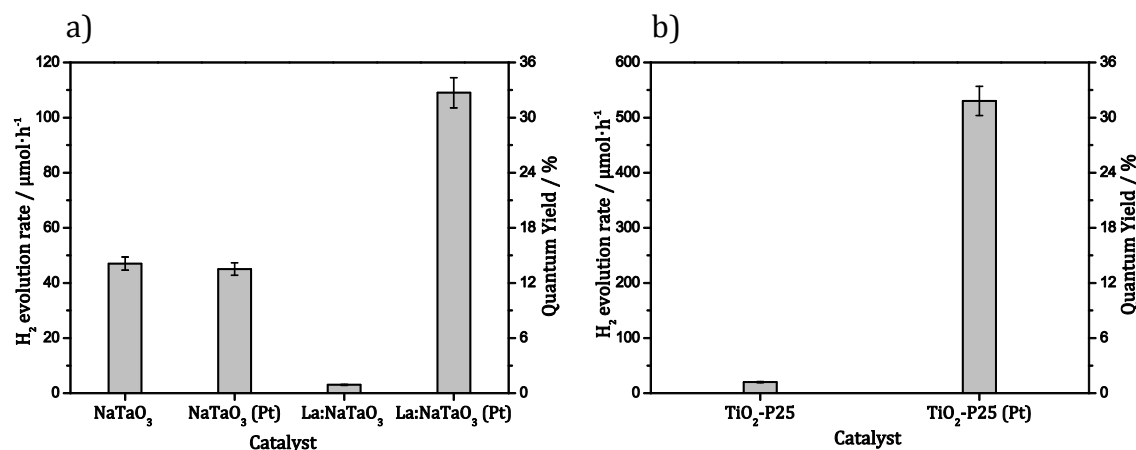
**Figure 28:** Photocatalytic $H_2$ evolution from aqueous methanol solution employing a) $NaTaO_3$ (pure and La-doped) and b) $TiO_2$-P25. Photocatalyst concentration: $1\ g \cdot L^{-1}$, Methanol concentration: 2.5 M, Pt loading: 0.2 wt%, Reactor volume: 50 ml, Irradiation intensity: $I_{250\text{-}450}$=41 mW·cm$^{-2}$.

### 4.3.3 Cocatalyst loaded La-doped sodium tantalate

Different alcohols acting as electron donors or so-called sacrificial agents have shown different activities for the photocatalytic $H_2$ evolution employing various photocatalysts including $TiO_2$. However, a systematic study of the effect of different alcohols on the photocatalytic activity for $H_2$ evolution employing La-doped $NaTaO_3$ has not been performed yet.

Therefore, the effect of the nature and concentration of the alcohol employed on the photocatalytic $H_2$ evolution employing La-doped $NaTaO_3$ (0.83 wt% La) photocatalyst was investigated. Furthermore, the effect of different cocatalysts on the photocatalytic $H_2$ evolution determining the most efficient system for the reductive pathway in the presence of sacrificial agents was examined in detail.

Figure 29 illustrates the obtained $H_2$ evolution rates in the presence of different alcohols employing 0.2 wt% Pt-loaded 0.83 wt% La-doped $NaTaO_3$ photocatalysts. Aqueous solutions of methanol (MeOH), ethanol (EtOH), 2-propanol (2-PrOH), butanol (BuOH), and 2-methyl-2-propanol (tert-BuOH) were employed instead of pure water. It is clearly seen that all employed alcohols enhanced the photocatalytic $H_2$ evolution rates to a great extend as compared with that measured in pure water (Figure 29). It should be noted that the investigated La-doped

55

$NaTaO_3$ exhibited a rather poor photocatalytic activity for $H_2$ evolution even from pure water (3 µmol/h, QY=0.9 %).
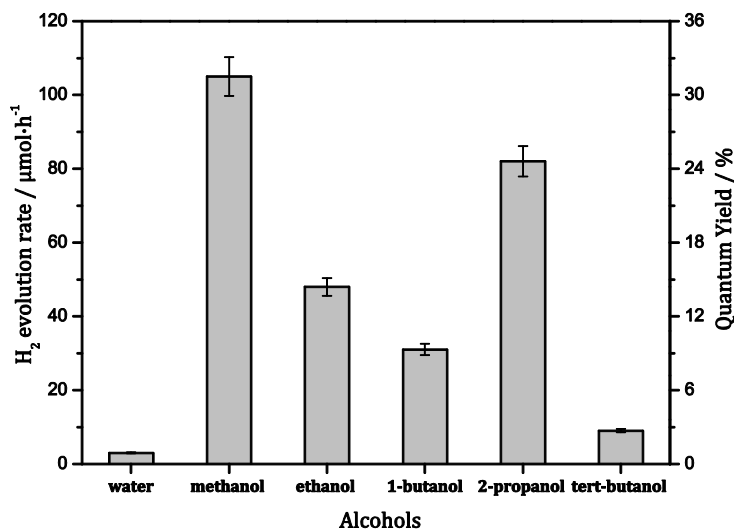


**Figure 29:** Photocatalytic $H_2$ evolution from different aqueous alcoholic solutions employing La-doped $NaTaO_3$ (0.83 wt% La). Photocatalyst concentration: 1 g·L$^{-1}$, Alcohol concentration: 2.5 M, Pt loading: 0.2 wt%, Reactor volume: 50 ml, Irradiation intensity: $I_{250-450}$=41 mW·cm$^{-2}$.

Obviously, employing methanol and 2-propanol as sacrificial agents, the highest photocatalytic activities for $H_2$ evolution were achieved under the experimental conditions used here. The $H_2$ evolution rates were reduced almost by a factor of two when ethanol or 1-butanol were employed. The lowest $H_2$ evolution rates were observed when 2-methyl-2-propanol (*i.e.*, tert-butanol) was used as sacrificial agent. According to these results, methanol was chosen as the most efficient sacrificial agent among the alcohols tested here for all further investigations regarding the photocatalytic $H_2$ evolution on La-doped $NaTaO_3$.

Since methanol was fond to be the most efficient sacrificial agent for the present system, the effect of its initial concentration on the photocatalytic $H_2$ evolution was investigated (Figure 30). The initial methanol concentrations were varied between 0 and 25 mol l$^{-1}$. Up to a methanol concentration of 4 mol l$^{-1}$ the shape of the $H_2$ evolution rate vs. $C_{methanol}$ curve resembles that of a hyperbolic curve. In the saturation region of this curve the $H_2$ evolution rate reaches a value of 100 µmol h$^{-1}$. When the initial methanol concentration exceeds 4 mol l$^{-1}$ the $H_2$ evolution rate

decreases to 75 μmol h$^{-1}$ and remained constant without significant changes thereafter.
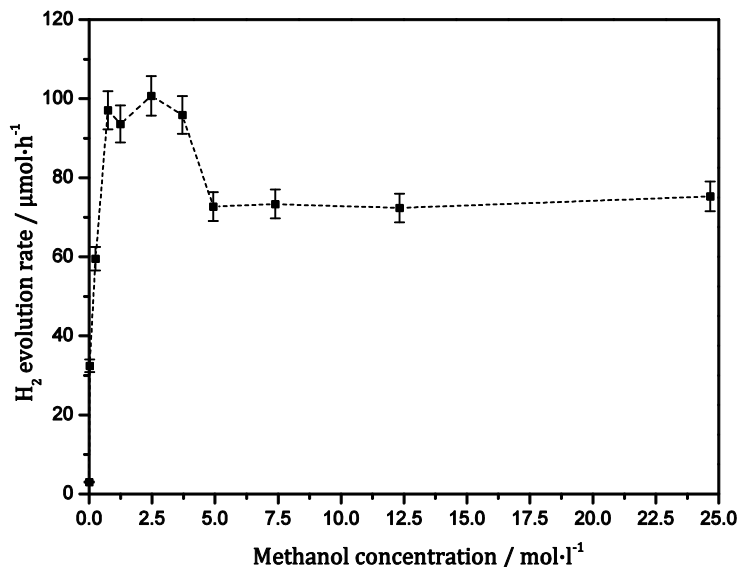


**Figure 30:** Effect of methanol concentration on the photocatalytic H$_2$ evolution employing La-doped NaTaO$_3$ (0.83 wt% La). Photocatalyst concentration: 1 g·L$^{-1}$, Pt loading: 0.2 wt%, Reactor volume: 50 ml, Irradiation intensity: I$_{250-450}$=41 mW·cm$^{-2}$.

The most interesting result shown in Figure 30 is that the addition of a very small quantity of methanol (0.05 M) into the system already suffices to increase the H$_2$ evolution rates by at least one order of magnitude. Obviously that methanol acts as a hole acceptor reducing the electron-hole recombination rate to a great extent. According to these results the optimal methanol concentration for the photocatalytic H$_2$ evolution under current conditions was found to be 2.5 M.

Figure 31 shows the H$_2$ evolution rates from aqueous methanol solutions on modified La-doped NaTaO$_3$ employing different cocatalysts. It is clearly seen that noble metal cocatalysts exhibit higher photocatalytic activities for H$_2$ evolution than metal oxides. Among the different noble metal cocatalysts Pt (105 μmol h$^{-1}$, QY=31.5 %) and Rh (99 μmol h$^{-1}$, QY=30 %) showed quite similar catalytic activity for H$_2$ evolution followed by Au (76 μmol h$^{-1}$, QY=23 %) exhibiting slightly lower catalytic activity. Among the metal oxides tested here NiO shows the highest catalytic activity for H$_2$ evolution (53 μmol h$^{-1}$, QY=16 %) while RuO$_2$ and AgO exhibit the lowest ones (9 μmol h$^{-1}$, QY=3 %).
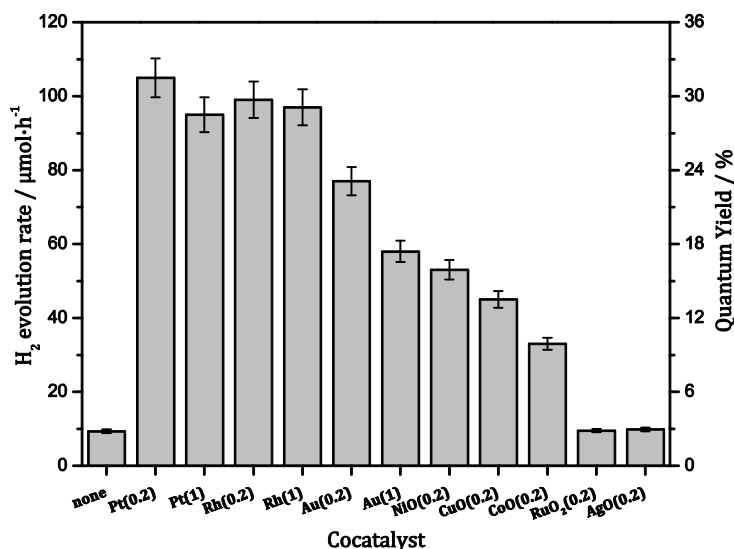
**Figure 31:** Photocatalytic $H_2$ evolution from aqueous methanol solution employing La-doped $NaTaO_3$ (0.83 wt% La) modified with different cocatalysts. Photocatalyst concentration: 1 g·$L^{-1}$, Methanol concentration: 2.5 M, Cocatalyst loading: 0.2 or 1 wt%, Reactor volume: 50 ml, Irradiation intensity: $I_{250-450}$=41 mW·$cm^{-2}$.

Additionally, in the case of noble metal cocatalysts the effect of the loading amount was investigated. The results revealed that higher $H_2$ production rates are obtained by lower cocatalyst loading of 0.2wt% in the case of all noble metals used here. This result can be explained by the fact that the excess cocatalyst loading might reduce the photocatalytic activity by hindering the light absorption by the host photocatalyst as reported elsewhere.[40]

### 4.3.4  Long-term investigation of La-doped sodium tantalate

Methanol is frequently used as an electron donor in the so-called sacrificial systems and has been reported to yield a remarkable improvement of the photocatalytic $H_2$ production. However, only few mechanistic studies of this system employing mainly $TiO_2$ have been published until now. Since the role of methanol during the photoctalytic reactions has not been clarified yet fundamental investigations aiming for the understanding of such sacrificial systems are still required. Moreover, it is important to investigate the role of methanol during the photocatalytic reactions employing other photocatalysts besides $TiO_2$.

The complete methanol oxidation process was investigated in order to clarify the role of methanol as sacrificial agent on the photocatalytic hydrogen production employing La-doped $NaTaO_3$ (0.83 wt% La). For this purpose a long-term experiment was carried out employing platinized La-doped $NaTaO_3$ (0.83 wt% La) in the presence of a very low methanol concentration in water (30 mM).
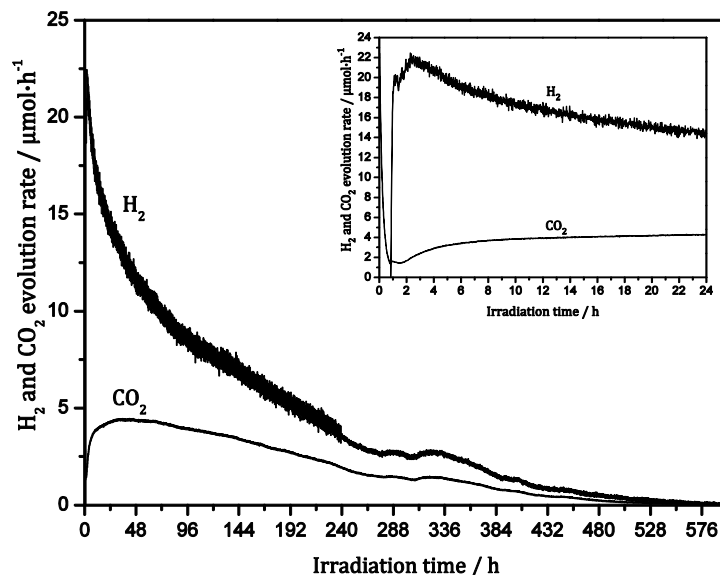


**Figure 32:** Time course of the photocatalytic $H_2$ and $CO_2$ evolution on platinized La-doped $NaTaO_3$ (0.83 wt% La) from 30 mM aqueous methanol solution. Photocatalyst concentration: 1 g·L$^{-1}$, Pt loading: 0.2 wt%, Reactor volume: 50 ml, Irradiation intensity: $I_{250-450}$=41 mW·cm$^{-2}$.

During this photocatalytic reaction only molecular $H_2$ and molecular $CO_2$ were formed and no traces of other gases, *i.e.*, CO, $O_2$, or $CH_4$ were detected (Figure 32). The inset of Figure 32 shows that the evolution of $H_2$ and $CO_2$ occurred almost directly after the light was switched on reaching their maximal evolution rates after 2.5 and 30 h, respectively. The formation of $CO_2$ confirms the complete methanol mineralization apparently through the oxidation of formaldehyde and formic acid intermediates. By reason of the reactor design, being equipped with only two outputs, *i.e.*, a connection to a gas supply (mass flow controller) and to a gas analyzer (mass spectrometer), the simultaneous monitoring of the time profiles of these intermediates (formaldehyde and formic acid) has not been performed. Within the further course of the irradiation time the $H_2$ and $CO_2$ evolution rates

were slowly decreasing, presumably due to the consumption of methanol in the system.

The overall amounts of evolved $H_2$ and $CO_2$ were determined by integration of the signals shown in Figure 32. The results revealed that about 2500 µmol of molecular $H_2$ and 1000 µmol of molecular $CO_2$ were evolved during this photocatalytic reaction (Figure 33).
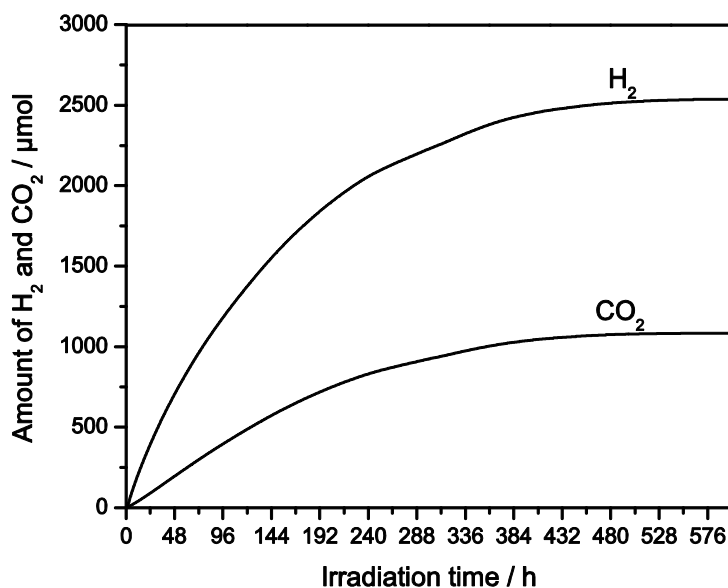


**Figure 33:** Amounts of the photocatalytically evolved $H_2$ and $CO_2$ on platinized La-doped $NaTaO_3$ (0.83 wt% La) from 30 mM aqueous methanol solution. photocatalyst concentration: 1 g·L$^{-1}$, Pt loading: 0.2 wt%, Reactor volume: 50 ml, Irradiation intensity: $I_{250-450}$=41 mW·cm$^{-2}$.

If methanol oxidation process occurs according to the mechanism proposed by Kawai and Sakata [79] (see chapter 2.3.1), the amounts of evolved $H_2$ and $CO_2$ are expected to be 4500 and 1500 µmol, respectively. Because of the long duration time of this experiment, *i.e.*, approximately 600 h (25 days), lower amounts of evolved gases could be explained by the partly evaporation of methanol. For instance, in the case of $TiO_2$-P25 the complete photooxidation of methanol occurred readily after 150 h under identical experimental conditions where the amounts of evolved $H_2$ and $CO_2$ were in a good agreement with the expected

ratio.[90] A more detailed analysis and interpretation of the obtained results will be given later (chapter 5.6).

Thus, the present work demonstrates for the first time a long-term stability study carried out over a period of 25 days employing La-doped $NaTaO_3$ (see Figure 32). The realization of such an extended test reaction time was achieved due to the continuous photocatalytic flow through system connected to a mass spectrometer allowing the simultaneous detection of several gaseous compounds.

### 4.3.5 Isotopic studies of the photocatalytic hydrogen evolution

Only few studies are known dealing with isotopic labeling experiments aiming for the further elucidation of the mechanisms of the photocatalytic hydrogen production and the concomitant methanol oxidation.[90, 126] Moreover, all these valuable studies were carried out on the intensively studied photocatalysts $TiO_2$. The isotopic study presented here was performed for the first time employing La-doped $NaTaO_3$ in order to identify the origin of the evolved $H_2$ in the presence of low amounts of methanol.

The photocatalytic tests concerning the hydrogen evolution over platinized La-doped $NaTaO_3$ were performed employing the following (deuterated) water and (deuterated) methanol mixtures: a) $CH_3OH$-$H_2O$, b) $CD_3OD$-$D_2O$, c) $CD_3OD$-$H_2O$, and d) $CH_3OH$-$D_2O$. The initial concentration of $CH_3OH$ or $CD_3OD$ in each system was 30 mM. The evolution of $H_2$, HD, and $D_2$ was detected by means of a mass spectrometer. Figure 34 illustrates the time course of the evolved gaseous compounds during the photocatalytic tests performed in the four different systems (cases a - d).
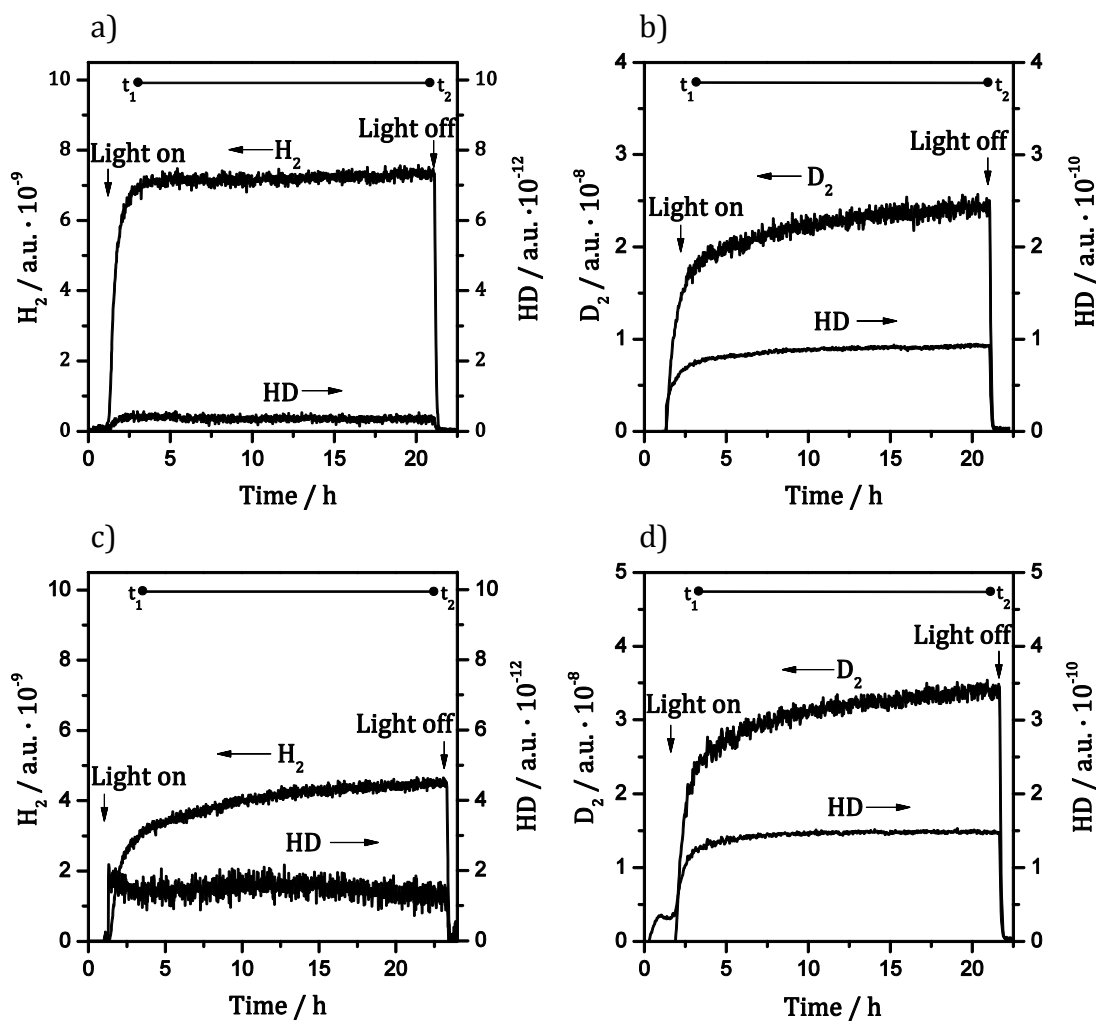
**Figure 34:** Time courses of the photocatalytic $H_2$, HD, and $D_2$ evolution on platinized La-doped $NaTaO_3$ (0.83 wt% La) from a) $CH_3OH$-$H_2O$, b) $CD_3OD$-$D_2O$, c) $CD_3OD$-$H_2O$, d) $CH_3OH$-$D_2O$ solutions. Methanol or deuterated methanol concentration: 30 mM. Photocatalyst concentration: 1 g·L$^{-1}$, Pt loading: 0.2 wt%, Reactor volume: 50 ml, Irradiation intensity: $I_{250-450}$=41 mW·cm$^{-2}$.

It is clearly seen that the signals of the appropriate gaseous compounds increase directly after the lamp is switched on. Since the methanol concentrations employed here were quite low (30 mM), the values of evolved gases at the time $t_1$ were reached only after approximately 2 h of irradiation time. Consequently, all four systems were irradiated for further the light was switched off, the gas evolution rates rapidly decreased reaching the baseline of the corresponding compounds in the system.

In "pure" systems containing either H atoms (case a) or D atoms (case b) accordingly $H_2$ or $D_2$ were found to be formed as major products. In "mixed" systems (cases c and d) containing both H and D atoms, either $H_2$ or $D_2$ were detected as major products depending on the nature of the solvent employed (Figure 34 ). Additionally, traces of signals at $m/z$=3 (HD) were detected in all four systems due to the possible overlap of the $H_2$ or $D_2$ signal with that of HD. Moreover, the natural abundance of deuterium should be taken into account which is approximately 0.015% of the hydrogen present in water.[127]

## 4.4 Photocatalytic oxygen evolution from aqueous silver nitrate solution

The results presented in chapter 4.2 have shown that the investigated La-doped $NaTaO_3$ materials exhibit rather poor photocatalytic activity for the $O_2$ evolution from pure water. Taking into account the usually very rapid recombination of the photogenerated charge carriers (electrons and holes), the achievement of the overall water splitting reaction is still a challenging target. It has been shown that the employment of so-called sacrificial agents acting as electron acceptors can enhance the photocatalytic $O_2$ formation.[128-130] In particular, oxidizing reagents (electron acceptors) such as $Ag^+$ and $Fe^{3+}$ are frequently employed to enhance the photocatalytic $O_2$ evolution due to the scavenging of the photogenerated electrons thus improving the charge carrier separation to a great extent. Moreover, this half reaction of water splitting is often used as a test reaction to evaluate whether a certain photocatalyst satisfies the thermodynamic and kinetic requirements for $O_2$ evolution.

The photocatalytic activity for $O_2$ evolution was evaluated employing La-doped $NaTaO_3$ modified with different cocatalysts, *i.e.*, noble metals (Pt, Rh and Au) and metal oxides (NiO, CuO, CoO, $RuO_2$ and AgO) in the presence of silver ions as oxidizing reagents in the system. Figure 35 illustrates the typical time course of the $O_2$ evolution exemplarily shown for La-doped $NaTaO_3$ modified with 0.2wt% CoO cocatalyst in an aqueous silver nitrate solution. Similar to the system of pure water 30-40 min are required to reach the maximum $O_2$ evolution rate at time $t_1$ after the light is switched on (Figure 35). Consequently, the suspensions were irradiated for further 6 h. A typical feature being characteristic also for all other systems was a

continuous decrease of the $O_2$ evolution rate within the course of the irradiation time between $t_1$ and $t_2$ (Figure 35). Such a behavior can be explained either by an enhanced solubility of $O_2$ in water or by the deactivation of the photocatalyst by the deposition of metallic silver ($Ag^0$) on its surface.

When the light is switched off (at time $t_2$), a rapid decay of the $O_2$ evolution rate is observed until the baseline was reached. Similar to the system with pure water, the measuring points at the end of each photocatalytic run are also slightly higher as compared with those at the very beginning monitored before illumination. Also in this system, the measuring points at the very end of each experimental run are considered as a baseline. Accordingly, the $O_2$ evolution rates were determined from the difference between the baseline (at the end) and the average of all measuring points obtained in the time range between $t_1$ and $t_2$ as indicated in Figure 35.



**Figure 35:** Time course of the photocatalytic $O_2$ evolution from 0.01 M aqueous silver nitrate solution employing La-doped $NaTaO_3$ (0.83 wt% La) modified with 0.2 wt% CoO. Catalyst concentration: 1 g·L$^{-1}$, Reactor volume: 50 ml, Irradiation intensity: $I_{250-450}$=41 mW·cm$^{-2}$.

This method for the determination of the $O_2$ evolution rates has been analogously applied for the La-doped $NaTaO_3$ modified with the remaining cocatalysts investigated in this work. The overall amount of the photocatalytically evolved $O_2$ can be

determined by the integration of the curve shown in Figure 35. The obtained amount of $O_2$ in the case of La-doped $NaTaO_3$ modified with CoO is calculated to be approximately 74 µmol (Figure 36) corresponding to an $O_2$ evolution rate of approximately 12 µmol/h considering an irradiation time of 6 h. This is in a good agreement with the $O_2$ evolution rate determined according to the method described above. Identical curves were obtained also for La-doped $NaTaO_3$ loaded with other cocatalysts and are therefore not shown here.
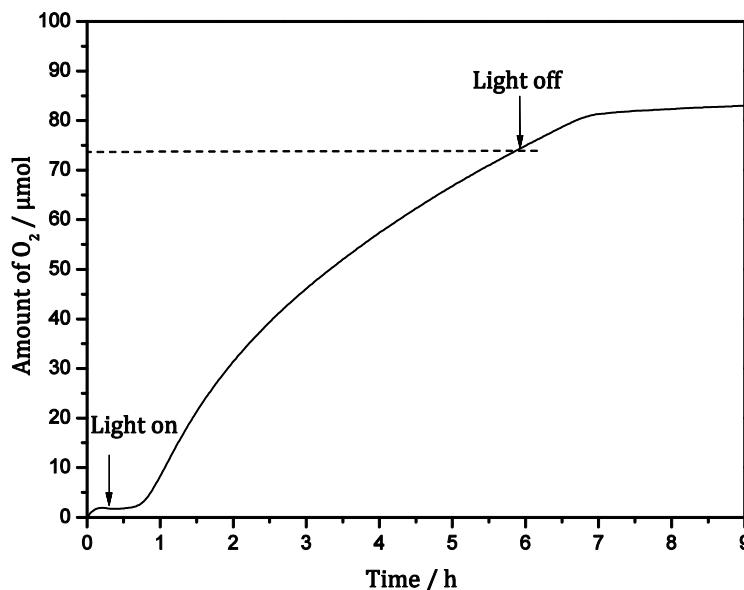


**Figure 36**: Amount of the photocatalytically evolved $O_2$ on La-doped $NaTaO_3$ modified with 0.2 wt% CoO cocatalyst from 0.01 M silver nitrate solution. Catalyst concentration: 1 g·L$^{-1}$, Reactor volume: 50 ml, Irradiation intensity: $I_{250-450}$=41 mW·cm$^{-2}$.

Figure 37 summarizes the results obtained for the photocatalytic $O_2$ evolution rates and the corresponding quantum yields employing La-doped $NaTaO_3$ modified with different cocatalysts. It is clearly seen that the highest $O_2$ evolution rate was obtained when CoO cocatalyst was employed (12 µmol·h$^{-1}$, QY=3.6 %). All other modified materials exhibit almost the same photocatalytic activity for $O_2$ evolution without really significant changes. The $O_2$ evolution rates are varying between 4 and 6 µmol·h$^{-1}$ (QY=1.2-1.8 %). CuO cocatalyst exhibits the lowest catalytic activity for $O_2$ evolution (2 µmol·h$^{-1}$. QY=0.6 %) which is comparable with that of unmodified La-doped $NaTaO_3$ (indicated as none). It should be noted that the

unmodified La-doped $NaTaO_3$ indicated as "none" could possibly be loaded by small amounts of metallic silver particles during the photocatalytic reaction resulting for an enhanced $O_2$ evolution. However, no photocatalytic activity for $O_2$ evolution was observed when the dry La-doped $NaTaO_3$ apparently loaded with metallic Ag was re-used again.
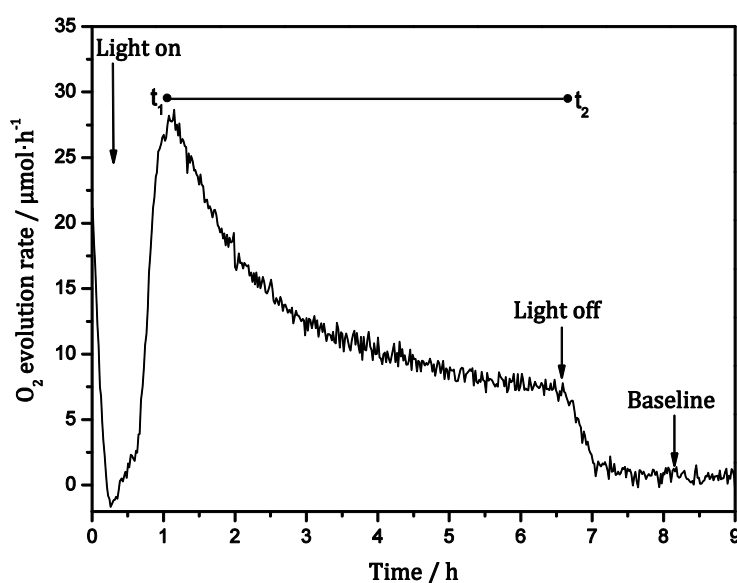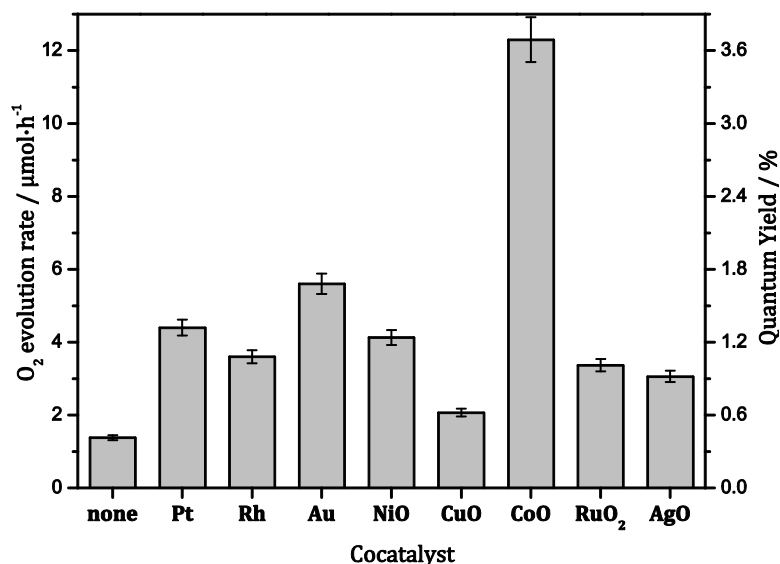


**Figure 37:** Photocatalytic $O_2$ evolution from 0.01 M aqueous silver nitrate solution employing La-doped $NaTaO_3$ (0.83 wt% La) modified with different cocatalysts. Catalyst concentration: 1 g·L$^{-1}$, Cocatalyst loading: 0.2 wt%, Reactor volume: 50 ml, Irradiation intensity: $I_{250-450}$=41 mW·cm$^{-2}$.

## 4.5   Laser flash photolysis studies

Lanthanum doping and surface modification of sodium tantalate materials affect their overall photocatalytic activity for $H_2$ and $O_2$ evolution to a great extent. Hereby, the life time of the photogenerated charge carriers (electrons and holes) plays an important role. Laser flash photolysis spectrometry is a powerful tool to study light induced electron transfer processes thus providing important mechanistic information for a better understanding of the photocatalytic activity of the investigated photocatalysts. The majority of the laser flash photolysis studies have so far been performed employing $TiO_2$ as the photocatalyst.[131] In this work this technique has been applied for the first time on $NaTaO_3$ in order to detect the trapped charge carriers and to determine their lifetime. Moreover, the effect of different cocatalysts deposited on the photocatalyst surface on the lifetime of the photogenerated charge carriers has been investigated in detail.

The inset of Figure 38 illustrates the decay of the transient absorption signal at 310 nm of pure $NaTaO_3$ after band-gap excitation with a laser irradiation wavelength of 248 nm.
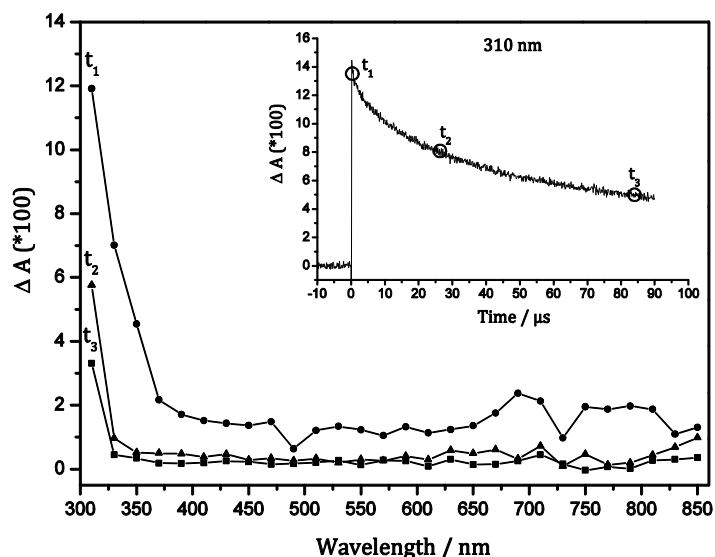


**Figure 38:** Transient absorption spectra of pure $NaTaO_3$ taken at three different times ($t_1$=0.34 µs, $t_2$= 25 µs and $t_3$=85 µs) after band-gap excitation at laser $\lambda_{ex}$=248 nm. The inset shows the transient absorption measured at the absorption maximum at 310 nm indicating $t_1$, $t_2$ and $t_3$. The powder was purged for ½ h with $N_2$ prior to the measurement.

It is worth mentioning that the signal at 310 nm does not reach zero within measured period of time, indicating to a stable and long-living species. Figure 38 shows the transient absorption spectra of pure $NaTaO_3$ taken at three different times ($t_1$=0.34 µs, $t_2$= 25 µs and $t_3$=85 µs). These transient absorption spectra have been measured in the wavelength range between 300 and 850 nm. Laser flash photolysis measurements at wavelengths lower than 300 nm were not possible due to the own absorption of the investigated materials in this region. It is clearly seen that the highest absorption value of pure $NaTaO_3$ is observed at 310 nm within the analyzed wavelength range 300-850 nm. Additionally, an absorption band at around 700 nm was observed exhibiting significantly lower transient absorption values as compared with that of the absorption at 310 nm (Figure 38).

By analogy to the well-investigated $TiO_2$ the highest absorption value at 310 nm could be attributed to the trapped holes of pure $NaTaO_3$. In order to verify this assumption, methanol acting as a holes scavenger was added to the system. Figure 39 shows the decays of the signals at 310 nm after addition of different amounts of methanol.
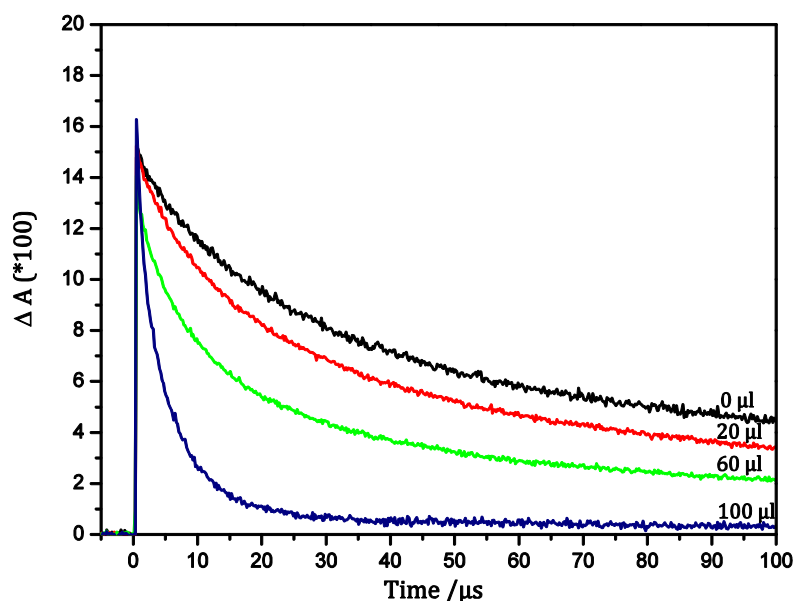


**Figure 39**: Transient absorption of the photogenerated holes at λ=310 nm of pure $NaTaO_3$ in the absence and presence of different amounts of methanol (20, 60 and 100 µl) after laser irradiation at 248 nm. All powders were purged for ½ h with $N_2$ prior to the measurement.

Obviously that with the increased methanol amount in the system, the signals decay faster. After addition of 100 µl of methanol, the signal at 310 nm has even disappeared after 40µs. These results confirm the fact that the detected signal at 310 nm can really be attributed to the trapped holes of pure $NaTaO_3$. Moreover, it is obvious that in the case of $NaTaO_3$ the photogenerated holes are first trapped and do not immediately react with adsorbed methanol molecules since the initial intensity of the signal stays constant in the case of different amounts of methanol added to the system (see Figure 39).

Figure 40 shows the transient absorption spectra of La-doped doped $NaTaO_3$ (0.83 wt% La) at three different times ($t_1$=0.34 µs, $t_2$= 25 µs and $t_3$=85 µs) after band-gap excitation with a laser irradiation wavelength of 248 nm. The inset of Figure 40 demonstrates the transient absorption signal at 310 nm indicating $t_1$, $t_2$ and $t_3$.
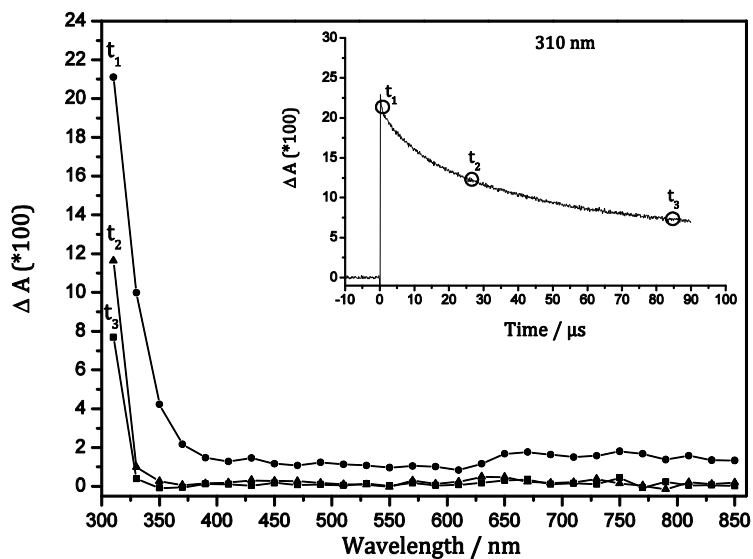


**Figure 40:** Transient absorption spectra of La-doped $NaTaO_3$ (0.83 wt% La) taken at three different times ($t_1$=0.34 µs, $t_2$= 25 µs and $t_3$=85 µs) after band-gap excitation at laser $\lambda_{ex}$=248 nm. The inset shows transient absorption measured at the absorption maximum at 310 nm indicating $t_1$, $t_2$ and $t_3$. The powder was purged for ½ h with $N_2$ prior to the measurement.

Both the transient absorption spectra and the decay of the signal at 310 nm are very similar to those measured in the case of pure $NaTaO_3$. By analogy to the pure

NaTaO$_3$ the highest absorption value at 310 nm can also be attributed to the photo-generated holes. The initial intensity of the transient absorption signals shown in Figure 40 is higher as that detected in the case of pure NaTaO$_3$ under identical conditions. Apparently, the higher intensity of the signals correlates with a higher density of the photogenerated charge carriers (holes) in the system.

In order to generalize this finding, the life-time of the photogenerated charge carries (holes) of sodium tantalate doped with different amounts of lanthanum were investigated as well. Figure 41 illustrates the decays of the photogenerated holes measured at 310 nm. It is clearly seen that the intensity of the signals depends on the lanthanum loading in the system. The lowest intensity of the signal was found by a La loading of 0.57 wt%. A 0.83 wt% La loading seems to be the optimal loading for the present system since the measured signal showed the highest intensity. The further increase of the La loading has a negative effect on the intensity of the signal.
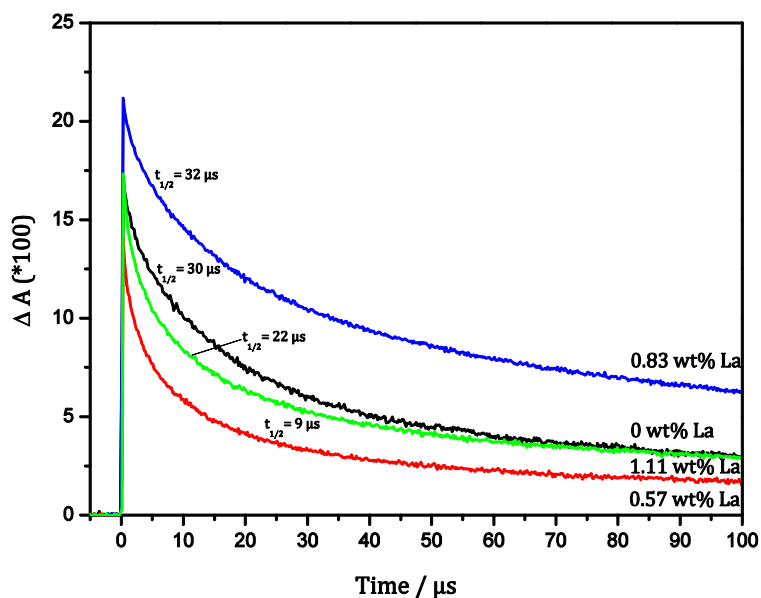


**Figure 41**: Transient absorption of photogenerated holes at λ=310 nm of pure and La-doped NaTaO$_3$ (0.57, 0.83 and 1.11wt% La) after band-gap excitation with laser excitation wavelength of 248 nm. All powders were purged for ½ h with N$_2$ prior to the measurement.

Table 3 clearly demonstrates that for the investigated pure and La-doped NaTaO$_3$ both the values obtained for the half lifetime and those measured for the initial intensity of the transient absorption signal at 310 nm show, a similar trend:

$\Delta$ $I_0$ and $t_{1/2}$ of 0.83 wt% La $NaTaO_3$ > 0 wt% La $NaTaO_3$ > 1.11 wt% La $NaTaO_3$ > 0.57 wt% La $NaTaO_3$.

**Table 3**: Summary of the values obtained for the initial intensities ($\Delta$ $I_0$) and the half lifetimes ($t_{1/2}$) of the transient absorption signals at 310 nm for pure and for La-doped $NaTaO_3$ adapted from Figure 41.

| $NaTaO_3$ | $\Delta$ $I_0$ (*100) | $t_{1/2}$ ($\mu s$) |
|---|---|---|
| 0 wt% La | 17 | 30 |
| 0.57 wt% La | 13 | 9 |
| 0.83 wt% La | 21 | 32 |
| 1.11 wt% La | 17 | 22 |

Figure 42 illustrates an enlarged view of the transient absorption spectra of pure and La-doped $NaTaO_3$ (0.83 wt% La) in the wavelength range between 400 and 850 nm. The inset of Figure 42 shows the corresponding transient absorption signals at 710 nm of both materials. In the wavelength range of 600 to 800 nm a broad absorption band is clearly seen which is more pronounced in the case of pure $NaTaO_3$ than in the case of La-doped $NaTaO_3$. The transient absorption signal at 710 nm (inset) of La-doped $NaTaO_3$ also decays faster than that of pure material.
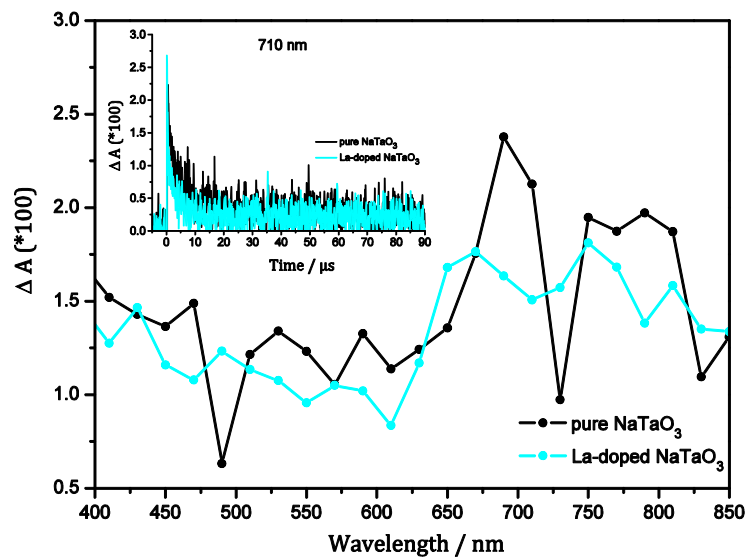


**Figure 42**: Transient absorption spectra of pure and La-doped $NaTaO_3$ (0.83 wt% La) after band-gap excitation with laser excitation wavelength of 248 nm. The inset shows the corresponding transient absorption signals at $\lambda$=710 nm. All powders were purged for ½ h with $N_2$ prior to the measurement.

It should be noted that the signals in this wavelength range are quite noisy, so that the determination of the half lifetimes was not possible in this case.

The influence of the surface modification by the loading of pure and La-doped NaTaO$_3$ with different cocatalyst nanoparticles on the life-time of the photogenerated holes was investigated. Figure 43 a) and b) shows the transient absorption kinetics of the photogenerated holes at 310 nm of pure NaTaO$_3$ modified with noble metals and metal oxides, respectively. The intensity of the signals at 310 nm is normalized for a better comparison of the decays of the photogenerated holes of surface modified NaTaO$_3$. The corresponding half lifetimes and the intensities of the signals are summarized in Figure 44 a) and b), respectively.
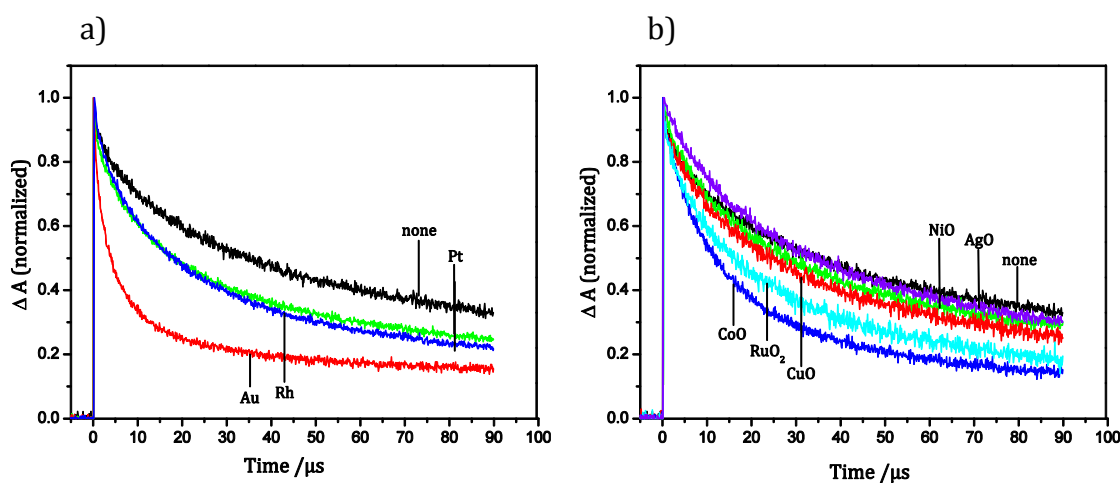


**Figure 43:** Transient absorption of photogenerated holes at λ=310 nm of pure NaTaO$_3$ modified with a) noble metal cocatalysts and b) metal oxide cocatalysts after band-gap excitation with laser excitation wavelength of 248 nm. All powders were purged for ½ h with N$_2$ prior to the measurement.

Figure 44 a) clearly shows higher intensities of the signals in the case of the noble metal loaded sodium tantalates as compared with those of the pure and of the metal oxide loaded material. Loading with NiO, CuO and AgO had no effect on the half lifetime of the photogenerated holes (~30 µs) as compared with that of pure NaTaO$_3$. All other cocatalyst loadings seem even to reduce the half lifetime of the photogenerated charge carriers. In particular, the shortest half lifetime of 5 µs was found in the case of Rh-loaded NaTaO$_3$.
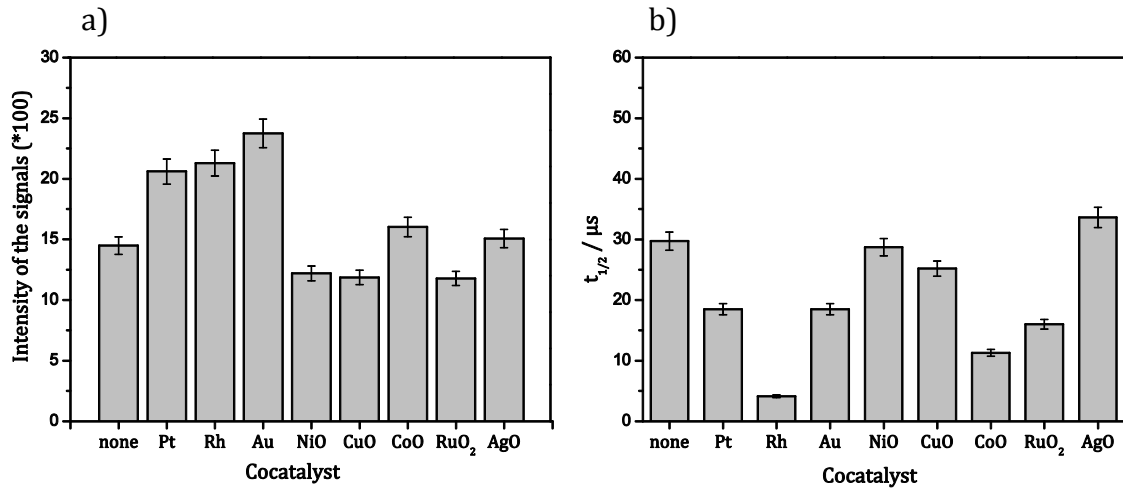
**Figure 44:** a) Intensities and b) half lifetimes of the cocatalyst modified pure NaTaO₃ deduced from the corresponding absorptions measured at 310 nm shown in Figure 44 a) and b).

The same series of measurements was carried out for the La-doped sodium tantalate materials. Figure 45 a) and b) illustrates the transient absorption kinetics of the photogenerated holes of the modified La-doped NaTaO₃ measured at 310 nm.
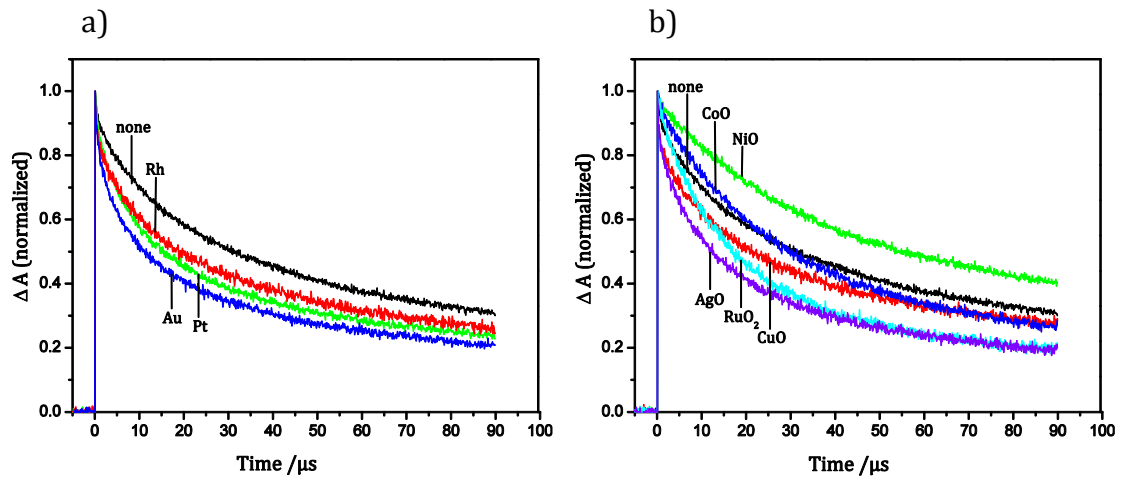


**Figure 45:** Transient absorption of photogenerated holes at λ=310 nm of 0.83wt% La-doped NaTaO₃ modified with a) noble metal cocatalysts and b) metal oxide cocatalysts after band-gap excitation with laser excitation wavelength of 248 nm. All powders were purged for ½ h with N₂ prior to the measurement.

It can be clearly seen that in the case of noble metal loaded materials the order of the determined half lifetimes of the holes for the La-doped NaTaO₃, *i.e.*, none > Rh > Pt > Au is found to be identical with that of pure NaTaO₃.

Generally, the modification of La-doped NaTaO$_3$ with noble metal cocatalyts seems to lower the life-time of the photogenerated holes as compared with that of unmodified system. On the other hand, the life-time of the photogenerated holes was significantly prolonged when NiO was loaded on the surface of La-doped NaTaO$_3$ as shown in Figure 45 b).

The corresponding intensities of the signals and calculated half lifetimes shown in Figure 45 are summarized in Figure 46 a) and b). It is interesting to note that the intensity of all signals measured at 310 nm was found to be constant independent of the cocatalyst employed. The half lifetimes of most of the modified systems is lower than that of the unmodified La-doped NaTaO$_3$. Only NiO modification significantly increased the half lifetime of La-doped NaTaO$_3$ from 32 to 56 μs.
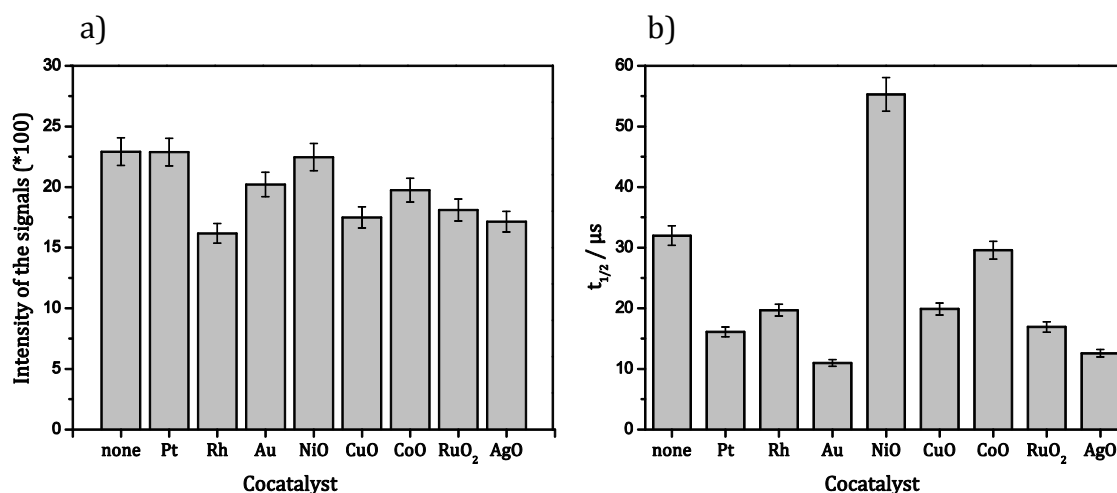


**Figure 46:** a) Intensities and b) half lifetimes of the cocatalyst modified 0.83wt% La-doped NaTaO$_3$ deduced from the corresponding absorptions measured at 310 nm shown in Figure 45 a) and b).

# 5. Discussion

In this chapter the results of the experimental work will be discussed and interpreted in detail.

The first chapter deals with the optical and morphological aspects of sodium tantalate materials. In the following chapter the particular features of the newly within this thesis developed reactor design will be considered. In the next three chapters the effect of lanthanum doping, nature of alcohol and different cocatalysts on the photocatalytic $H_2$ and $O_2$ evolution will be discussed. Based on the long-term investigations, isotopic studies, and laser flash photolysis measurements the respective mechanisms of the photocatalytic $H_2$ and $O_2$ evolution employing three different systems, *i.e.*, pure water, aqueous silver nitrate solution and aqueous methanol solution will be proposed.

## 5.1 Optical and morphological properties

### 5.1.1 Direct and indirect electronic transitions

Using the method described in 4.1.1 it is not possible to distinguish between two different kinds of electronic transitions (direct and indirect) of a semiconductor. Assuming that the scattering coefficient is constant throughout the entire wavelength range of the measurement, the so-called Kubelka-Munk function ($F(R)E)^{1/n}$ is usually employed instead of $\alpha$ ( see Equation 3) and plotted vs. the energy of the exciting light (Figure 47 and Figure 48).

As shown in Figure 47 two straight lines can be drawn, whereby their abscissa intercepts, 3.95 and 4.15 eV correspond to the band gaps for the assumed indirect and direct transition, respectively. Assuming the forbidden direct electronic transition with n=3/2, a band gap of 4.02 eV is obtained as shown in Figure 48. It is often unclear which transition mode should be preferred for a given semiconductor. One possibility is to compare the range of the linear part of both plots, giving preference to the transition mode the plot of which exhibits the longest linear part. According to this method, for the materials prepared here the indirect transition has to be preferred because of its slightly longer range of the linear part (0.20 eV)

as compared with the allowed (0.17 eV) and the forbidden direct transitions as shown in Figure 47 and Figure 48.
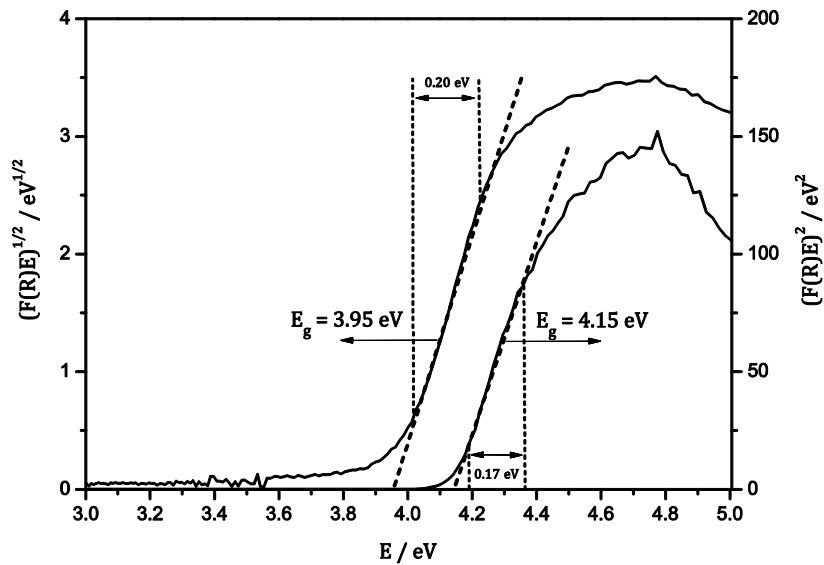


**Figure 47:** Diffuse reflectance spectra of pure $NaTaO_3$ powder. The Tauc plots of the modified Kubelka-Munk function $(F(R)E)^{1/n}$ versus the energy of light absorbed for the direct (right) and indirect (left) allowed transitions.
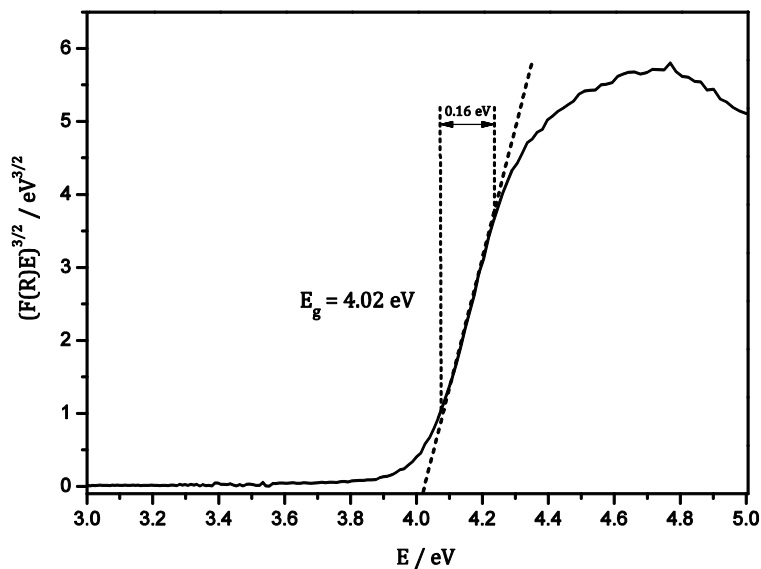


**Figure 48**: Diffuse reflectance spectrum of pure $NaTaO_3$ powder. The Tauc plots of the modified Kubelka-Munk function $(F(R)E)^{1/n}$ versus the energy of light absorbed for the forbidden direct transitions.

It is worth to note that the estimated band gap values are quite close to one another making a differentiation between these three kinds of electronic transitions almost impossible (Figure 47 and Figure 48). Similar difficulties and the drawback of using the Kubelka-Munk function for the determination of the kind of the electronic transition have been already discussed in the literature.[132]

The reported band gap type and optical properties of sodium tantalate differs depending on its modification, space group, and synthesis route.[120, 133] According to the literature data the sol-gel synthesis (SG) of $NaTaO_3$ provides mostly a cubic structure with band gap energy of approximately 4.1 eV while the solid state route provides an orthorhombic structure with a slightly narrower band gap of 4.0 eV.[120, 133-135] Recently, Kanhere *et al*. also reported for the pristine $NaTaO_3$ synthesized by the solid state method a band gap of 4.01 eV.[136] Kudo *et al*. reported band gap energy values of 4.0 and 4.07 eV for pure and La doped $NaTaO_3$, respectively.[18, 58, 60] Similar to the results of this thesis, no significant shift in the absorption of $NaTaO_3$ by the La doping has been observed either. However, these publications do not consider the nature of the allowed or forbidden transition modes of $NaTaO_3$. Hu and Teng reported band gap energies of 3.9 and 4.1 eV for the direct and the indirect transition, respectively, for the $NaTaO_3$ using the SG method. These results are consistent with the present data, *i.e.*, yielding larger band gap energy values for the direct (allowed and forbidden) transition as compared with those of the indirect one.[121]

The detailed analysis of the optical band gap determination has shown that it is obviously not unambiguous to merely employ tauc plots derived from the Kubelka-Munk function to distinguish between direct and indirect allowed transitions for the present semiconductor. The estimated band gap energy values for sodium tantalate are very close to one another independent whether the direct (allowed and forbidden) or the indirect electronic transition is assumed. They are ranging between 3.95 and 4.15 eV. In very good agreement with these experimental data, theoretical calculations regarding the electronic transitions of $NaTaO_3$ particles have demonstrated that both direct and indirect transitions are quasi degenerate showing also very similar band gap energy values for the direct (4.34eV) and for the indirect (4.43eV) electronic transitions .[124]

### 5.1.2 Effect of La-doping

Scanning electron microscopic (SEM) investigations of pure and La-doped $NaTaO_3$ showed that La-doping led to a marked decrease of the particle size with simultaneous increasing of inhomogeneity and irregularity in the system (Figure 14). In fact, the measurements of the specific surface area (BET) have shown, that La-doped $NaTaO_3$ particles exhibit almost twice the specific surface area (5.4 m$^2$/g) as compared with that of pure $NaTaO_3$ ( 2.4 m$^2$/g).

Similar observations were reported in the literature where the particle size of $NaTaO_3$ was found to decrease from 2-3 µm to 0.1-0.7 µm upon La-doping.[58, 137] It should be noted that the La-doped $NaTaO_3$ particles reported in the literature are at least 10 times larger than those investigated in the present work ranging from 80 to 250 nm. It was reported that due to La-doping a characteristically ordered nanostep surface structure of $NaTaO_3$ particles (0.1-0.7 µm) was observed while the non-doped particles showed flat structure.[58, 137] In the present work the La-doping did not lead to the formation of such an ordered nanostep structure. Similar results were obtained by Zang *et al.* who demonstrated well-crystallized La-doped $NaTaO_3$ particles of 100-200 nm in diameter exhibiting also flat surface structure.[138] Apparently, the observed nanostep structure is only obtained for large particles of 0.1-0.7 µm in diameter. It is generally agreed that since La-doping occurs at the A site (Na of the perovskite-type oxide $ABO_3$) within the lattice, the crystal growth is suppressed due to the difference in the ionic radii (see Figure 49).[18, 136]

Additionally, the results of this work revealed that the morphology of $NaTaO_3$ particles strongly depends on the amount of La-doping employed. It was found that up to 0.83 wt% La-doping the inhomogeneity and irregularity of the particles was significantly increased. Higher La-doping of 1.11 wt% La led to a reduced both inhomogeneity and irregularity of the particles whereby a characteristic for undoped particles rectangular shape was observed again.
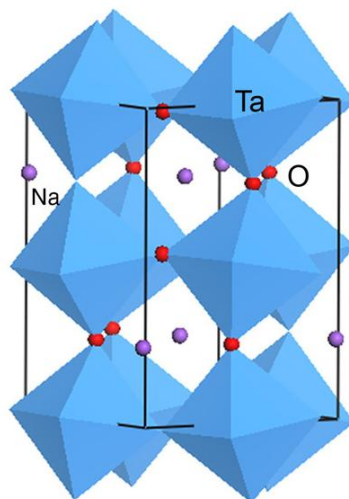
**Figure 49**: Crystal structure in the polyhedron model for orthorhombic $NaTaO_3$.[133]

The results obtained within this thesis clearly indicate that La doping notably affects not only the morphology of $NaTaO_3$ but also its photocatalytic activity for $H_2$ evolution. It is widely agreed that apart from the doping of a photocatalyst especially its specific surface structure and the coordination of the exposed surface atoms greatly influences the photoreactivity.[114] Thus, design and morphological control of specific crystal facets became a commonly employed strategy to enhance the photocatalytic activity of semiconductor materials.[139]

Therefore, it was also important within this work to predict the three dimensional shape of sodium tantalate particles and to determine their predominant crystallographic surfaces. This kind of analysis has been performed for the first time for $NaTaO_3$ by means of a combinatorial method of the geometric estimations by TEM and the Wulff-type construction according to the method suggested by Feldhoff *et al.* (see chapter 4.1.2).[114] Accordingly, the predicted shape of the $NaTaO_3$ crystals is a polyhedron as has also been confirmed by the SEM micrographs (Figure 15 f). As clearly shown in Figure 15 d and e this polyhedron is enclosed by a majority of {010} (47 %) and minority of {111} (4 %) facets. It was found that the relative abundance of the two further crystallographic facets, *i.e.*, {100} and {001}, is very similar being 26 and 23 %, respectively. According to the theoretical calculations the {010} surface was found to be the energetically preferred surface of $NaTaO_3$ whereby the $TaO_2$ termination is more stable than the

NaO termination. The {001} - and {100} -surfaces were found to be energetically quite similar to each other in good agreement with the experimental data of this work.[124]

For instance, the facets of the type (100) and (001) are widely assumed to constitute the majority of exposed facets on anatase nanoparticles surfaces as shown in Figure 50.[139, 140]
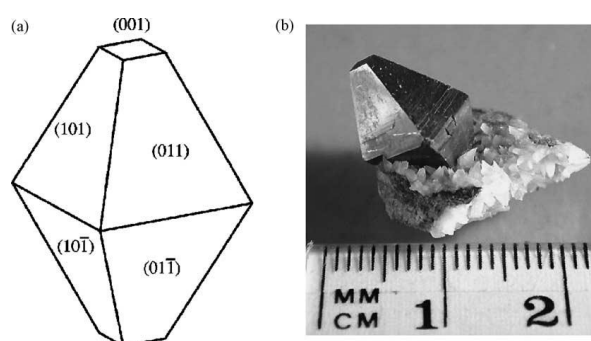


**Figure 50**: a) The equilibrium shape of TiO$_2$ crystal in the anatase phase according to the Wulff construction and surface energy calculated by Lazzeri et al. [141] b) Picture of an anatase mineral crystal.[140]

However, Feldhoff *et al*. investigated a series of commercial TiO$_2$ anatase nanoparticles demonstrating that the facets of the type (100) and (001) are indeed presenting the minority. On the contrary, surfaces of powder nanoparticles studied herein are rather dominated by (100) or (111) facets depending on the particle shape as shown in Figure 51.[114]
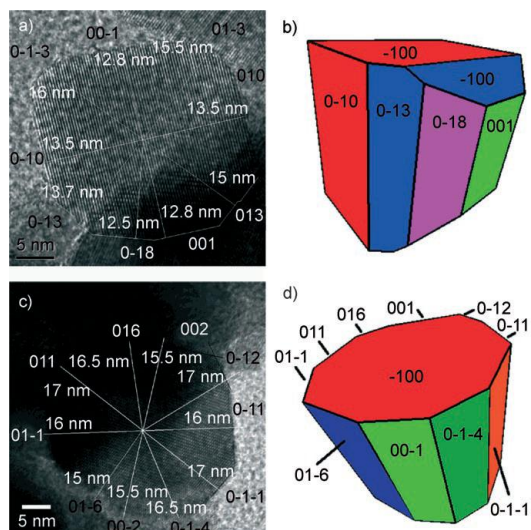
**Figure 51**: HRTEM micrographs and reconstructed shapes of anatase nanoparticles from PC50 powder: a), b) truncated cube; c), b) prism. [114]

These investigations clearly show that the shape of naturally occurring macroscopic anatase is not the key to a better understanding of nanocrystalline materials.[114] Moreover, it should be noted that the shape of the crystallites rather varies with the employed preparation technique, so that the findings concerning one material do not allow a general extrapolation to other materials.

## 5.2 Novel photocatalytic setup for $H_2$ and $O_2$ evolution

Within this thesis a novel photocatalytic setup has been successfully developed and constructed for the evaluation of the photocatalytic activity for water splitting allowing both quantitative and qualitative determination of the reaction products. Such a photocatalytic setup enables an in line monitoring of the entire course of the reaction detecting several gaseous compounds, *e.g.*, $H_2$, $O_2$ or $CO_2$ simultaneously formed during the photocatalytic reaction.

In a typical photocatalytic run an appropriate quantity of gas (mol) to any point of time was typically monitored first in the dark before starting with illumination, then upon illumination reaching the so-called steady state region and subsequently again in the dark when the light is switched off and the gas evolution decays reaching the baseline of the system (see Figure 18). Such a detailed measuring

procedure of the photocatalytically formed products provides much more essential information regarding the photocatalytic water splitting as compared to the rather poor data set obtained by a convential batch system. The detection limit of the present system is in the range of 0.2 to 2 $\mu$mol·h$^{-1}$ of the evolved gases (H$_2$ or O$_2$).

The simultaneously detection of several gaseous compounds during the same photocatalytic test reaction is achieved due to the utilization of a quadrupole mass spectrometer in this work. Additionally, the employment of the mass spectrometer enabled the detection of isotopes allowing mechanistic investigations performed in the present work. Due to the continuously operated reactor design as shown in Figure 52, the undesired overpressure generated inside of the reactor is success-fully avoided allowing the performance of the photocatalytic test reactions over a long period of time (up to one month). This is one of the very important advantages of the newly developed photocatalytic setup as compared with a classical batch type reactor being utilized in the majority of scientific studies in this field.



**Figure 52:** Quartz glass double jacket photoreactor with stainless steel flanges

## 5.3 Effect of La-doping on H$_2$ evolution

Kudo and Kato reported a significant enhancement of the photocatalytic activity for H$_2$ evolution due to the La-doping and a cocatalyst loading of pure NaTaO$_3$. [18, 57, 142] In principle, this is in a good agreement with the results obtained in this work

(see chapter 4.3.3). The photocatalytic activity for water splitting employing $NaTaO_3$ reported in the literature is usually just given as a rate of gas evolution in $\mu mol \cdot h^{-1}$, making the direct comparison across the published results from different photocatalytic systems very difficult.

Therefore, within this thesis the overall quantum yields have been determined for the first time for this Tantalate system to achieve a quantitative evaluation of the photocatalytic activity for $H_2$ or $O_2$ evolution. The highest quantum yield of 33 % (at 340 $\mu mol \cdot h^{-1}$ photon flux) for the photocatalytic $H_2$ evolution has been obtained in this work employing 0.2 wt% Pt modified La-doped $NaTaO_3$ (0.83 wt% La). Kato *et al.* reported a significantly higher apparent quantum yield of 56 % (at 300 $\mu mol \cdot h^{-1}$ photon flux) for the La-doped $NaTaO_3$ modified with NiO cocatalysts while, however, this group did not determine any overall quantum yields.[18]

The main differences in the properties between the $NaTaO_3$ particles investigated in this work and those synthesized by Kato *et al.* are the particle size and the surface structure. The La-doped $NaTaO_3$ particles investigated in this work have significantly smaller particle sizes (100-200 nm) as compared to those synthesized by Kato et al. (100-700 nm). It is usually assumed that larger particles can absorb more photons creating more charge carriers and hence increasing the recombination rate and thus consequently lowering the photocatalytic activity. However, the surface of the La-doped $NaTaO_3$ particles investigated in this work is flat while that of the La-doped $NaTaO_3$ particles synthesized by Kato *et al.* exhibits ordered surface nanostep structure. The authors claim that owing to such a characteristic nanostep structure created at the surface of the La-doped $NaTaO_3$ crystal, the reaction sites can be effectively separated with the edges acting as reduction sites ($H_2$ evolution) and the grooves as oxidation sites ($O_2$ evolution).[18]

Figure 28 a clearly showed that in the case of pure $NaTaO_3$ Pt photodeposition did not play any positive role for $H_2$ evolution. In contrast, in the case of smaller photocatalyst particles, *i.e.*, La-doped $NaTaO_3$ and $TiO_2$ P25, the surface modification significantly enhanced the photocatalytic activity (Figure 28 a and b). For a better understanding of these results it is important to consider the effect of both parameters, *i.e.*, the surface area and the particle size, on the photocatalytic $H_2$

evolution separately. The surface area mainly affects the number of active sites on the catalyst surface while the particle size influences the distance and the time that the charge carriers (electrons and holes) have to migrate from the bulk of the catalyst particle to reach the active sites at its surface.[58] Since methanol is employed and the photogenerated holes are scavenged, the charge carrier recombination rate is supposing reduced thus playing only a secondary role for the photocatalytic activity. Hence, one would expect that in the case of larger particles, *i.e.*, smaller surface area (*e.g.*, pure $NaTaO_3$), the effect of the surface modification on the photocatalytic activity should be less significant than in the case of smaller particles, *i.e.*, higher surface area (e.g., La-doped $NaTaO_3$). The results obtained in this work confirm this hypothesis.

Charge carrier recombination plays, in the case of photocatalytic reactions performed in pure water a more important role as compared to a system where sacrificial reagents, *e.g.*, methanol are used. Consequently, in pure water the photocatalytic $H_2$ evolution was observed only when Pt was deposited on the surface of $NaTaO_3$ and $TiO_2$ P25. Comparing the three materials shown in Figure 20, it is clearly seen that in the case of larger particles (pure $NaTaO_3$) the enhancement of the photocatalytic activity for $H_2$ evolution by Pt deposition was more notable (QY=1.5 %) than in the case of smaller particles, *i.e.*, La-doped $NaTaO_3$ (QY=0.9 %) and $TiO_2$ P25 (QY=0.27 %). In this case the charge carrier recombination plays an important role changing the mechanism of the photocatalytic reaction. Accordingly, the obtained results indicate that in the case of larger particles (pure $NaTaO_3$) the charge carrier recombination rate is slower than in the case of smaller particles (La-doped $NaTaO_3$, $TiO_2$ P25). On the one hand, these results are in agreement with the well-known fact that in the case of smaller particles the distance between the charge carriers (electrons and holes) is shorter with the consequence of a higher possibility of their recombination than in the case of

larger particles.[103, 143] On the other hand, larger particles can absorb more photons creating consequently more charge carriers which again could result in a higher recombination rate. Obviously, the higher photocatalytic activity for $H_2$ evolution of Pt/$NaTaO_3$ as compared to that of Pt/La-doped $NaTaO_3$ and

Pt/P25-TiO$_2$ cannot be interpreted only in relation to the respective particle size. Such parameters as crystallinity, morphology, and dopant concentration might also significantly affect the photocatalytic activity of a photocatalyst.

Since the photocatalytic activity of Pt/NaTaO$_3$ for H$_2$ evolution from pure water is found to be lowered due to the La-doping (Figure 20), it is assumed that the lanthanum could act as a recombination center thus increasing the recombination rate of the photogenerated charge carriers. In order to prove whether the employed La concentration (0.83 wt% La) corresponds to the optimal dopant concentration of NaTaO$_3$ or not, a newly developed theoretical model suggested by Bloh *et al*. describing the correlation between photocatalytic activity, doping ratio, and particle size has been applied in this work.[144] This model is based on the optimal doping data collected for different particle sizes of doped titanium dioxide and zinc oxide (see Figure 53)
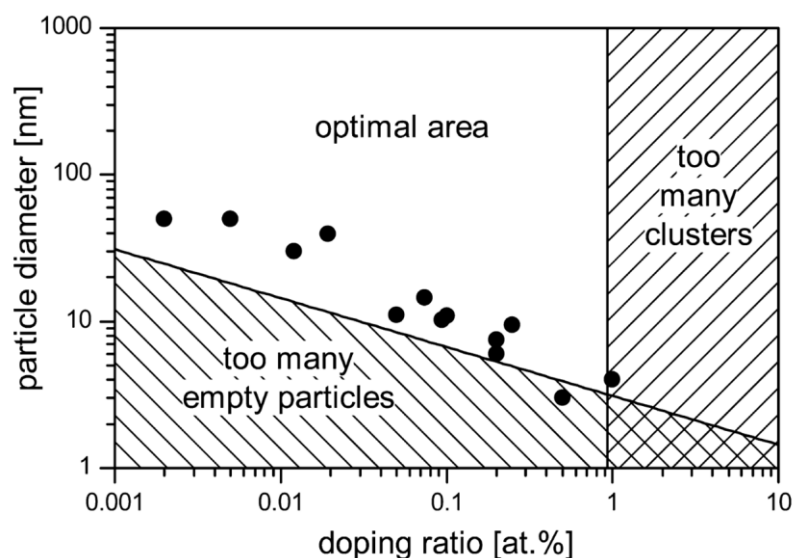


**Figure 53**: Optimal combinations of particle size and doping ratio, where neither too many recombination centers nor too many empty particles are present.[144]

It is important to emphasize, that this model is not material specific and therefore it schould be applicable for any semiconductor photocatalyst considering its molar mass, its density, and its particle size. When assuming that the optimal number of dopants per particle is 2.40 nm$^{-1}$ of particle size, as determined by Bloh *et al*., the

optimal dopant concentration for $NaTaO_3$ can be calculated employing the following formula:[144]

$$r_{d,opt} \approx \frac{6M}{N_A \cdot \rho \cdot \pi \cdot d^2} \times (2.40 \, nm^{-1})$$

29

with
$M$ : Molar mass of $NaTaO_3$ =251.8 g mol$^{-1}$
$N_A$ : Avogadro constant =6.022·10$^{23}$ mol$^{-1}$
$\rho$ : Density of $NaTaO_3$ =7.141 g·cm$^{-3}$
$\pi$ : Mathematical constant =3.14
$d$ : Diameter of $NaTaO_3$ particles =250 nm

Accordingly, the calculated optimal dopant concentration for $NaTaO_3$ is 0.0004 at %. The lanthanum concentration employed in this work is 0.3 at% La (0.83 wt% La), *i.e.*, a value which is three orders of magnitude higher as compared with the theoretically calculated dopant concentration according to the applied model.

Since the photocatalytic activity of $NaTaO_3$ at such low dopant concentration has been not investigated yet, the existence of two optimal dopant concentrations cannot be excluded. On the one hand, this model was developed based on experimental data for $TiO_2$ and ZnO where significantly smaller particle sizes and different crystallographic structures were considered. Therefore, this model might not be applicable for $NaTaO_3$. On the other hand, the doping itself might play different role for $NaTaO_3$ materials on the one side and for $TiO_2$ or ZnO on the other side. Consequently, completely different mechanisms might affect the photocatalytic activity of $NaTaO_3$ photocatalyst.

However, based on the results obtained from the XRD measurements indicating the majority of La atoms are rather localized near the surface than in the bulk of $NaTaO_3$ (see Figure 13), the real dopant concentration might be in this case significantly lower than 0.3 at% La (0.83 wt% La). Accordingly, it cannot be excluded that the real dopant concentration of La used in this work might indeed be very close to the theoretical value of 0.0004 at %.

## 5.4 Effect of the nature of alcohol on H₂ evolution

The results of the present thesis clearly show significantly lower photocatalytic activity for $H_2$ evolution from pure water as compared with that from aqueous alcoholic solutions. As proposed by Tamaki *et al.* this can be explained by the much lower water oxidation efficiency by the photogenerated holes as compared with the alcohol oxidation efficiency.[145] This is evinced by the fact that the endergonic water dehydrogenation (Equation 30) is associated with a free energy change being on average 10 times higher than that of the alcohol dehydrogenation as exemplary shown for the case of methanol (Equation 31).[146]

$$H_2O + 2\,hv \rightarrow \frac{1}{2}O_2(\uparrow) + H_2(\uparrow) \qquad\qquad \Delta G^0_{298} = 237\,kJ\cdot mol^{-1} \qquad\qquad 30$$

$$CH_3OH(l) + H_2O(l) \xrightarrow{\ hv, catalyst\ } CO_2(g) + 3H_2(g) \quad \Delta G^0_{298} = 16.1\,kJ\cdot mol^{-1} \qquad\qquad 31$$
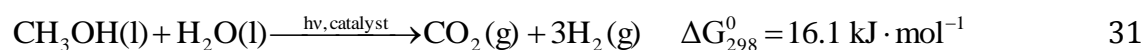
Figure 29 illustrated that the photocatalytic activity for $H_2$ evolution depends on the nature of alcohol employed in such photocatalytic reactions. Apparently, for La-doped $NaTaO_3$ (0.83 wt% La) methanol is the most efficient electron donor among the investigated alcohols being consistent with many other studies mostly performed on $TiO_2$.[15, 147-149]

Generally, it is assumed, that due to the small dimensions of the methanol molecule its surface coverage is higher as compared with that of larger alcohol molecules thus enabling a more efficient interference of the electron/hole recombination and yielding higher amounts of $H_2$ .[147] Assuming higher affinity of methanol with holes as compared with that of the larger alcohol molecules the first might prevent the back reaction of the photocatalytically formed $H_2$ and $O_2$, *i.e.*, water formation more efficiently.

For instance, an adsorption study of different alcohols on an anatase surface of $TiO_2$ in the gas phase also showed that the total amount of adsorbed alcohol is decreasing with the higher dimensions of alcohol molecules as follows: MeOH = EtOH > 1-PrOH > 2 PrOH > 1-BuOH.[150] Thus, the obtained order of the photocatalytic $H_2$ evolution activity seems to be related with the adsorption properties of the alcohols. An identical order of reactivity can be predicted comparing the one electron reduction potentials for alcohols vs. NHE at pH 7:

$E^0$ (MeOH) = 0.96 V=$E^0$ (EtOH) = 0.96 V < $E^0$ (2-PrOH) = 1.14 V.[151] Figure 54 summarizes the reduction potentials of one-electron couples in aqueous solution for alcohols and water.
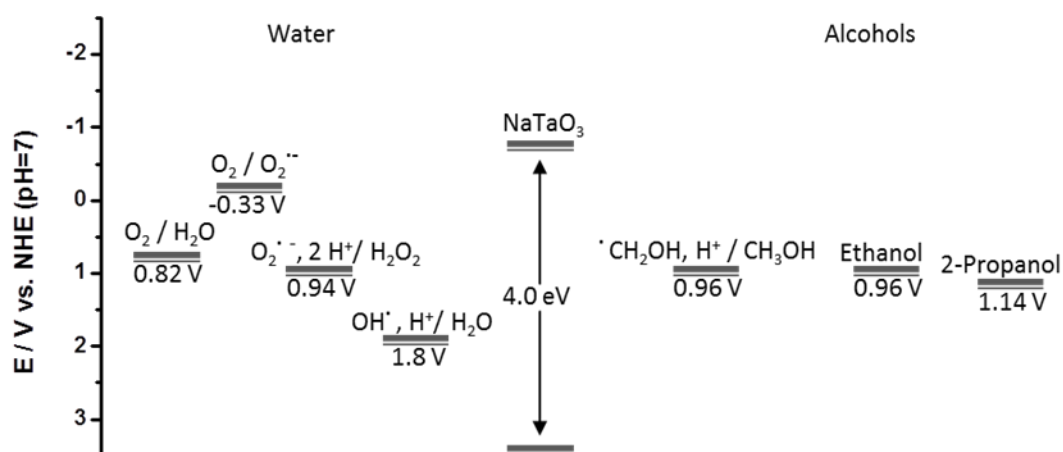


**Figure 54**: Reduction potentials of one-electron couples in aqueous solution for Water and for Alcohols. [151, 152]

Moreover, using transient absorption spectroscopy Tamaki *et al.* found for the oxidation efficiency of alcohols by trapped holes the following order: MeOH > EtOH > 2-PrOH, which is also in agreement with the other data mentioned above.[145]

Comparing the order of different alcohols for the photocatalytic activity for $H_2$ evolution obtained in this work with those obtained from adsorption and kinetic studies, it is clearly seen, that the order of ethanol and 2-propanol are exchanged. Normally, the inductive effects of the two methyl groups linked to the α-carbon in the case of 2-propanol should make the abstraction of the hydroxylic hydrogen atom more difficult.[15] However, it was found that the photocatalytic activity for $H_2$ evolution of 2-propanol (QY=25 %) is higher than that of ethanol (QY=15 %) for the present photocatalyst. In agreement with the results of this thesis, most studies published on this topic showed the same sequence of the photocatalytic activity for $H_2$ evolution, *i.e.*, methanol, butanol followed by 2-methyl-2-propanol. The order of

ethanol and 2-propanol in the above mentioned sequence was found to differ from publication to publication.[15, 147, 153-156]

The effect of the methanol concentration on the photocatalytic $H_2$ evolution was investigated in detail as shown in Figure 30. Interestingly, the $H_2$ evolution rate was found to be decreased from 100 to 75 µmol h$^{-1}$ when the initial methanol concentration exceeded 4 mol·l$^{-1}$. Employing P25-TiO$_2$ as photocatalyst no decrease in the $H_2$ evolution rate has been observed [91] However, it should be taken into account that with an increase of the methanol concentrations in the system, an enhanced competition between alcohol and water molecules for the adsorption sites might take place. Furthermore, the difference in dispersion characteristics of the photocatalyst in water and in water/alcohol mixtures might also result in a slightly lower photocatalytic activity for $H_2$ evolution. On the other hand, the photocatalytic $H_2$ evolution at higher methanol/water ratios could also be affected by the significantly higher $H_2$ solubility in methanol (3.9 mmol·L$^{-1}$) than in water (0.78 mmol·L$^{-1}$). However, slightly lower amounts of $H_2$ are expected to be dissolved because the equilibrium is usually not reached in the argon flow through system. Nevertheless, the effect of the $H_2$ solubility in methanol should not be totally neglected at this point.

## 5.5  Selectivity of the cocatalysts for $H_2$ and $O_2$ evolution

Considering the results from the photocatalytic tests for $H_2$ and $O_2$ evolution from three different systems, *i.e.*, pure water, aqueous methanol solution and aqueous silver nitrate solution, it was observed that certain cocatalysts show selective behavior either towards the enhanced $H_2$ or $O_2$ evolution (Figure 21, Figure 31 and Figure 37). It is worth noting, that such a selectivity can be clearly observed in systems containing pure water and aqueous silver nitrate solution while, however, it is found to be very different from the selectivity obtained for the system containing methanol (cf. Figure 55 and Figure 56).

Figure 55 summaries schematically the obtained selectivity and photocatalytic activity (indicated as best, middle and worst) of the investigated cocatalysts for $H_2$ and $O_2$ evolution over La-doped NaTaO$_3$ from pure water and aqueous silver

solution, respectively. The obtained results demonstrate that the cocatalysts, *i.e*, RuO$_2$ or CuO with the highest photocatalytic activity for H$_2$ evolution exhibit, however, the lowest photocatalytic activity for O$_2$ evolution. Similar results were observed in the case of CoO, *i.e.*, being the cocatalyst with the highest photocatalytic activity for O$_2$ evolution while exhibiting the lowest activity for H$_2$ evolution (Figure 21). Furthermore, it was observed that AgO showed the lowest activity for both H$_2$ and O$_2$ evolution. Noble metal cocatalysts, *i.e.*, Pt, Rh and Au showed neither the highest not the worst photocatalytic activities for both H$_2$ and O$_2$ evolution classifying them as cocatalysts with medium activity.
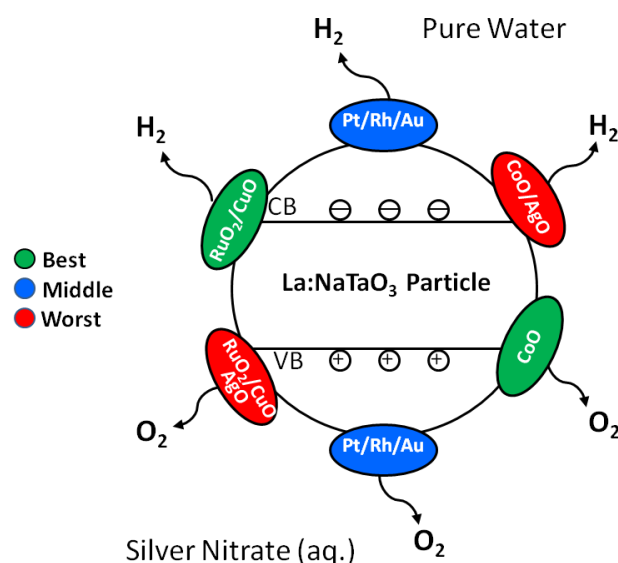


**Figure 55:** Selectivity and photocatalytic activity of the employed cocatalysts for hydrogen and oxygen evolution over La-doped NaTaO$_3$ (0.83 wt% La) in the presence of pure water and aqueous silver nitrate solution.

Cocatalyst nanoparticles deposited on the surface of a photocatalyst play mainly two roles for photocatalytic water splitting reactions: the extraction of the photogenerated charge carriers (electrons or holes) from the photocatalyst and the creation of active sites decreasing the activation energy for gas evolution.

In pure water system the highest photocatalytic activity for H$_2$ evolution is expected in the case where noble metal cocatalysts are employed because of their strong ability of extracting the electrons from the photocatalyst. It is well-known that in the presence of noble metal deposits on the surface of a semiconductor

90

photocatalyst an efficient charge carrier separation can be achieved by suppressing the electron-hole recombination.[36]

In particular these noble metal islands act as very effective electron traps due to the formation of a Schottky barrier at the respective metal-semiconductor contact (see Figure 5).[37, 43] A serious disadvantage of the employment of noble metals is, however, that they do not only catalyze the water splitting but also the undesirable back reaction, *i.e.*, the water formation from $H_2$ and $O_2$.[54] On the other hand, metal oxide nanoparticles exhibiting metallic behavior (such as $RuO_2$ or $NiO$) do not exhibit activity for water formation from $H_2$ and $O_2$.[40] Therefore, these metal oxides have been utilized in the past as efficient cocatalysts for similar systems using another photocatalysts, *e.g.*, $TiO_2$.[5, 12, 55, 56]

The obtained results clearly show that noble metals exhibit lower catalytic activity for $H_2$ evolution from pure water as compared with the metal oxides employed here. This can be explained by the fact that apparently the undesired back reaction seems indeed to take place on the surface of noble metal particles, *i.e*, the reaction of $H_2$ with $O_2$ resulting in water formation. Interestingly, in pure water system a selective behavior for either $H_2$ or $O_2$ formation can be clearly seen among the deposited metal oxide cocatalysts. At the same time looking to the results for $O_2$ evolution from aqueous silver nitrate solution (lower part of Figure 55) it is clearly seen, that the cocatalyst with the lowest catalytic activity for $H_2$ evolution, *i.e.*, CoO (upper part of Figure 55) exhibits the highest catalytic activity for $O_2$ evolution.

Considering the system of pure water the sequence of the catalytic activity of metal oxide cocatalaysts was found to be as follows: $RuO_2$ > CuO > NiO > CoO. It can be assumed that in the absence of any sacrificial agent in the system the recombination rate of the photogenerated charge carriers is high. In order to explain the obtained sequence, the chemical properties of these materials have to be considered in more details. The employed metal oxides have properties of Bronsted acids with characteristic bond interaction M-O···H, whereby the strength of an acid refers to its ability or tendency to loose a proton. It is well-known that the tendency to loose a proton depends on the oxidation state, size, and electronegativity of the corresponding metal. $RuO_2$ has both the highest oxidation state (IV) and the

highest electronegativity (3.5) among the investigated metal oxides. Accordingly, $RuO_2$ is considered to be the strongest Bronsted acid thus exhibiting the highest catalytic activity for $H_2$ evolution in pure water. While, CuO, NiO, and CoO exhibit the same oxidation state (II) and similar electronegativity ($\sim$2), the respective cations have different sizes with their ionic radii decreasing in the following sequence: Co > Ni > Cu. Thus, the smaller the ionic radius of the transition metal ion, the stronger is the band interaction between the metal and the oxygen atom (M-O$\cdots$H), making the bond between the oxygen and the proton weaker and the proton release easier. Accordingly, the catalytic activity for $H_2$ evolution is expected to be higher in the case of the metal ions with smaller ionic radius being in a good agreement with the obtained sequence of the catalytic activity for $H_2$ evolution, *i.e.*, CuO > NiO > CoO (see Figure 21).

According to the results presented in Figure 56, it is obviously that Pt, Rh, and Au are the most efficient electron transfer catalysts in the presence of methanol in the system. All other metal oxides exhibit lower catalytic activity for $H_2$ evolution without significant differences in their activities. Therefore, this group of cocatalysts have been assigned as "others" being middle active cocatalysts. $RuO_2$ exhibits the lowest values for $H_2$ evolution and can be therefore classified as the worst cocatalyst together with AgO showing catalytic activity closed to the detection limit of the instrument.
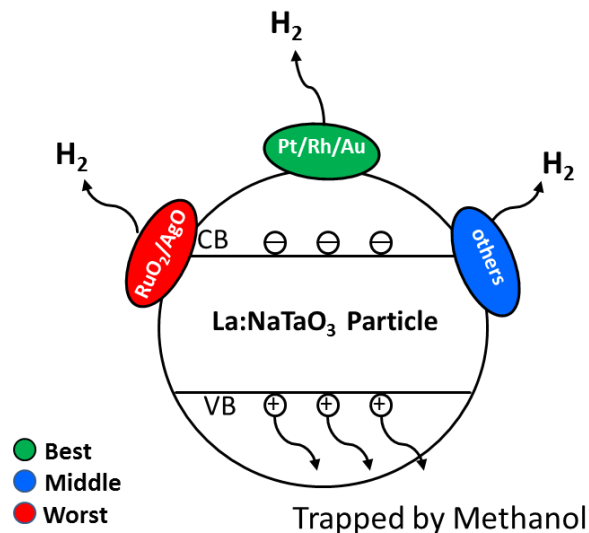
**Figure 56:** Selectivity and photocatalytic activity of the employed cocatalysts for hydrogen evolution over La-doped NaTaO$_3$ (0.83 wt% La) in the presence of aqueous methanol solution.

It is well-known that noble metals exhibit higher values for work function as compared with that of metal oxides and subsequently higher Schottky barrier which can serve as an efficient barrier preventing the undesired electron migration back to the semiconductor (see Figure 5).[39] While the electrons are trapped at the cocatalyst (noble metal partcles) surface, the holes remain at the host photocatalyst and migrate to its free surface ensuring an efficient charge separation. Anpo and Takeuchi have demonstrated the electron transfer from TiO$_2$ to Pt particles by means of Electron Spin Resonance measurements.[157]

The first step of the H$_2$ formation at the Pt catalyst surface is supposed to involve the transfer of excess electrons from Pt to adsorbed $H_{ads}^+$ and $H_2O_{ads}$ generating $H_{ads}^\bullet$ atoms via the Volmer reaction:[158]

$$H_{ads}^+ + e^- \left( Pt^0 \right) \rightarrow H_{ads}^\bullet \left( Pt^0 \right) \qquad 32$$

$$H_2O_{ads} + e^- \left( Pt^0 \right) \rightarrow H_{ads}^\bullet \left( Pt^0 \right) + OH^- \qquad 33$$
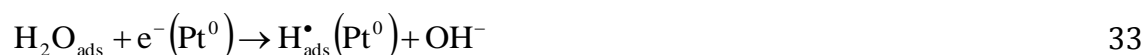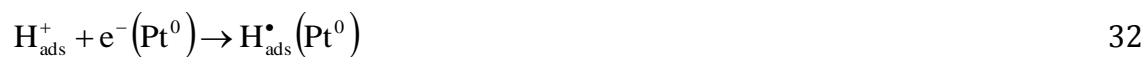
The formation of the molecular hydrogen can occur via two reaction mechanisms, namely, the Heyrovsky reaction involving an electrochemical-desorption step or the Tafel reaction involving a recombination step, as shown in Equation 34 and Equation 35, respectively:[159]

$$H^{\bullet}_{ads}\left(Pt^0\right)+e^-\left(Pt^0\right)+H^+_{ads}\left(Pt^0\right)\rightarrow H_2\left(g\right) \qquad\qquad 34$$

$$H^{\bullet}_{ads}\left(Pt^0\right)+H^{\bullet}_{ads}\left(Pt^0\right)\rightarrow H_2\left(g\right) \qquad\qquad\qquad 35$$
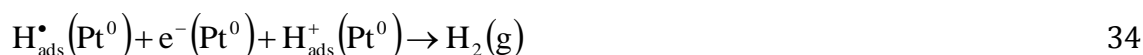
Interestingly, $RuO_2$ demonstrates the highest catalytic activity for $H_2$ evolution from pure water while in the presence of methanol it exhibits rather poor catalytic activity for $H_2$ evolution (Figure 55 and Figure 56). This can be explained by the proposed mechanism schematically shown in Figure 57. Assumingly, the proton coupled electron transfer (PCET) from the $^{\bullet}CH_2OH$ radical does not take place on the $RuO_2$ surface thus lowering the catalytic activity of $RuO_2$ to a great extent. Moreover, the extraction of the CB electrons by $RuO_2$ in the presence of methanol seems to be not very efficient either.
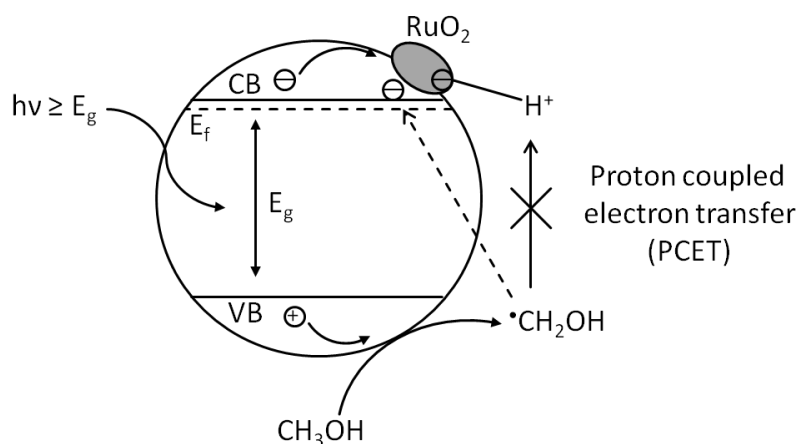


**Figure 57**: Proposed mechanism to explain the high catalytic activity of $RuO_2$ for $H_2$ evolution from water and the low catalytic activity for $H_2$ evolution from aqueous methanol solution.

Due to the complexity of the mechanisms being involved in all three systems, *i.e.*, pure water, aqueous silver nitrate solution, and aqueous methanol solution, they will be separately discussed in the next chapter 5.6 in more detail.

## 5.6 Mechanisms of $H_2$ and $O_2$ evolution

### 5.6.1 In pure water

The photocatalytic tests performed in pure water evince that only the photocatalytic $H_2$ evolution is observed employing La-doped $NaTaO_3$ loaded with different cocatalysts (Figure 21). In none of the investigated systems was any $O_2$ gas detected. However, instead of $O_2$ evolution, the formation of $H_2O_2$ was confirmed in all investigated systems.

Figure 58 illustrates the proposed mechanism of the photocatalytic $H_2$ evolution employing cocatalyst loaded La-doped $NaTaO_3$ powder in pure water. It is assumed that in the absence of any sacrificial agent, the $e^-/h^+$ recombination rate is very high. The low fraction of charge carriers able to escape this recombination migrate to the surface of the La-doped $NaTaO_3$ photocatalyst. Thus, the $H_2$ evolution occurs by the reduction of adsorbed protons ($H^+_{ads}$) on the surface of the cocatalysts whereby the overpotential for the gas formation could be reduced. Supposedly, the photogenerated holes oxidize the $OH^-$ ions forming two $OH^\bullet$ radicals which subsequently dimerize yielding mainly $H_2O_2$ species adsorbed on the La-doped $NaTaO_3$ surface. This is the reason for the considerably lower concentration of detected $H_2O_2$ as compared with the expected value assuming that the formed surface bound peroxo species are not sensitive for the horseradish peroxidase test employed here.

One reason for the absence of any $O_2$ detection during the photocatalytic tests carried out in pure water (Figure 21) could be associated with the solubility of $O_2$ in water. For instance, taking an $H_2$ evolution rate of 5 $\mu mol \cdot h^{-1}$ as measured in the case of CuO being the cocatalyst 0.6 $mmol \cdot l^{-1}$ of $H_2$ will be evolved within 6 h of reaction time. Accordingly, the expected amount of evolved $O_2$ is 0.3 $mmol \cdot l^{-1}$. In fact, taking the solubility values of 1.28 $mmol \cdot l^{-1}$ for $O_2$ and 0.78 $mmol \cdot l^{-1}$ for $H_2$ [160] in water a considerably lower fraction of the photogenerated $O_2$ can be expected to enter the gas phase which is analyzed by mass spectrometry in the experimental setup used here. This effect has to be considered even though lower values for the solubility of $H_2$ and $O_2$ should be assumed for the present system as no

thermodynamic equilibrium between the evolved gases and aqueous suspension is achieved under the current experimental conditions. Hence, only a rather small portion of the photogenerated holes need to be accounted for by this hydrogen peroxide formation while the majority of the photoformed holes might still lead to the (dissolved) $O_2$ formation.
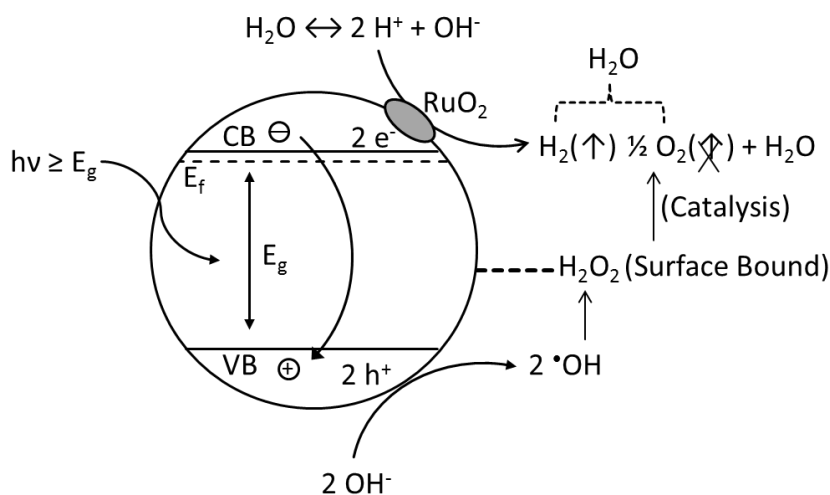


**Figure 58**: Proposed mechanism of photocatalytic $H_2$ evolution employing cocatalyst loaded La-doped $NaTaO_3$ in pure water.

It is interesting to note that noble metal cocatalysts exhibit unexpectedly lower photocatalytic activity for $H_2$ evolution than metal oxide cocatalysts. This might be explained by the fact that if $O_2$ is indeed formed, noble metal cocatalysts may readily catalyze the back reaction, *i.e.*, water formation thus lowering the overall photocatalytic activity for $H_2$ evolution.

In summary, it can be said that in none of the employed systems discussed above the photocatalytic stoichiometric splitting of pure water into $H_2$ and $O_2$ could be achieved. Therefore, new concepts are required to enhance the photocatalytic $H_2$ evolution ensuring the simultaneously evolution of $O_2$ gas.

The photocatalytic tests shown in Figure 19 and Figure 20 reveal that the simultaneous application of two cocatalysts on the photocatalyst surface can enable the overall photocatalytic water splitting reaction. When, for example, $RuO_2$ and $CoO$

were used in the same photocatalytic test reaction, the simultaneous formation of both $H_2$ and $O_2$ was indeed observed.

It seems that for both pathways of the photocatalytic water splitting process, *i.e.*, the reductive ($H_2$ formation) and oxidative ($O_2$ formation) reactions, one cocatalyst for each is the essential prerequisite. Similar results were obtained when $Pt/Cr_2O_3$ core shell structures were employed yielding the simultaneous formation of both $H_2$ and $O_2$ gases. The ratio of the evolved gases was found to be quite close to the stoichiometric one with, however, slightly lower amounts of $O_2$ gas being detected in each of these cases. As previously mentioned, the lower $O_2$ amounts detected in these photocatalytic tests could be associated with the better solubility of $O_2$ in water as compared with that of $H_2$.
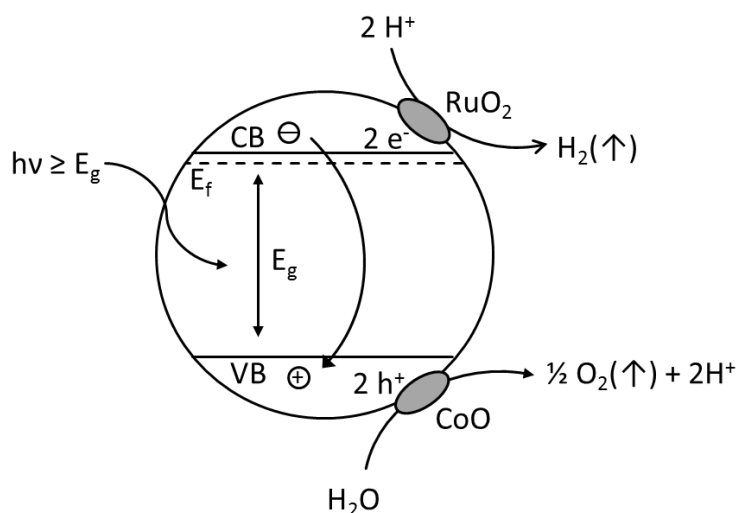


**Figure 59**: Concept of efficient water splitting into molecular $H_2$ and molecular $O_2$ employing La-doped $NaTaO_3$ loaded with two cocatalysts.

### 5.6.2   In aqueous silver nitrate solutions

The choice of the reported electron acceptors for the so-called sacrificial photocatalytic water splitting is rather limited. By far, $Ag^+$ cations are most frequently used as electron acceptors usually resulting in an enhanced photocatalytic activity for the photocatalytic $O_2$ evolution.

In fact, the results presented in chapter 4.4 also confirmed that in the presence of $Ag^+$ ions the photocatalytic $O_2$ evolution can be significantly increased as compared with that obtained in pure water (Figure 23).

It is generally assumed that the photocatalytic formation of molecular oxygen is accompanied by the deposition of metallic silver nanocontacts ($Ag_n^0$) on the semi-conductor's surface as shown in Equations 15-17. While it is commonly taken into account that the presence of $Ag^+$ does not change the anodic reaction pathway, it has recently been proposed that another possible pathway of $O_2$ formation, *i.e.*, through the oxidation reaction of $Ag^+$ ions by the photogenerated holes might be operative (see Equations 18-20).[96] Owing to the rather high one-electron oxidation potential of the holes photogenerated in most oxide semiconductors (3 V *vs*. NHE at pH 0)[26], this oxidative pathway should be also taken into account for the tanta-late materials studied here.

Assuming that the photooxidation of water occurs according to Equations 15-17, the expected amount of $O_2$ formed from the complete reduction of $Ag^+$ ions employed in this study, *i.e.*, 500 µmol can be calculated to be 125 µmol. This value is in a good agreement with experimentally detected amount being 72±4 µmol (CoO loaded La-doped $NaTaO_3$) considering the rather high $O_2$ solubility in water (Figure 37).

It should be noted that while employing different cocatalysts, the detected amounts of $O_2$ did under no circumstances exceed the amount expected from the complete consumption of the available $Ag^+$ ions. Moreover, based on the dark grey coloration of the suspension observed at the end of the photoreaction when silver nitrate solutions are employed, it is very likely that the pathway according to Equations 15-17 takes place in the present system.

Figure 60 schematically illustrates the proposed mechanism of $O_2$ evolution in the presence of $Ag^+$ ions. It is assumed that due to the efficient trapping of electrons by the Ag+ ions and the therefore reduced $e^-/h^+$ recombination rate, a significant enhancement of the photocatalytic $O_2$ evolution can be achieved.
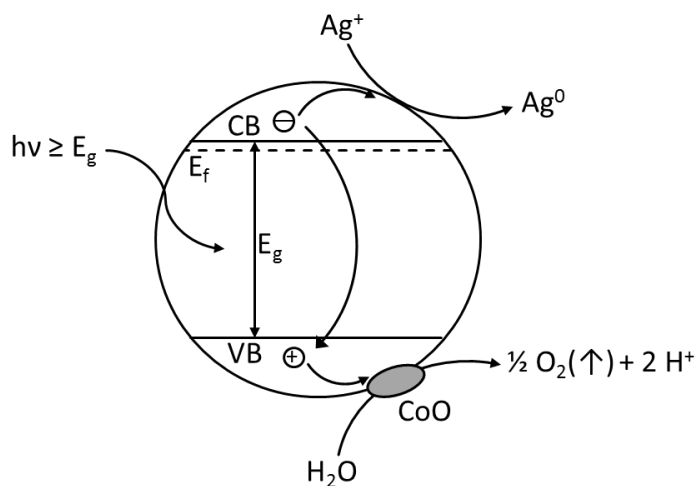


**Figure 60**: Proposed mechanism of the photocatalytic $O_2$ evolution employing cocatalyst loaded La-doped $NaTaO_3$ in aqueous silver nitrate solution.

The usage of nanoparticulate cocatalysts (noble metals and metal oxides) generally improves the photocatalytic activity for $O_2$ evolution to a great extent. In particular, CoO was found to be the most efficient cocatalyst for enhanced $O_2$ evolution under the present conditions (QY=3.6 %). In fact, the utilization of cocatalysts is essential but they alone are not sufficient for a significant enhancement of the $O_2$ gas evolution since in the absence of $Ag^+$ in related systems no $O_2$ was detected (Figure 21).

### 5.6.3   In aqueous methanol solutions

The attained results of the long-term study evince that methanol acts as sacrificial agent up to its complete oxidation yielding $H_2$ and $CO_2$ (Figure 32). It is, however, important to emphasize that the evolved amount of $H_2$ did not exceed the amount expected from the complete consumption of methanol, evidencing that no $H_2$ was produced by the direct photooxidation of water (Equation 36).
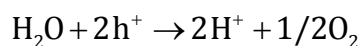
$$H_2O + 2h^+ \rightarrow 2H^+ + 1/2O_2 \hfill 36$$

Therefore, it can be assumed that no competition for scavenging of the photogenerated holes between methanol and water molecules occurs when NaTaO3 is used as photocatalyst. This observation is in a good agreement with the recently published work on Pt/TiO$_2$-P25 and other TiO$_2$ photocatalysts performed under identical experimental conditions.[90] Since no molecular oxygen was detected, the probability of the water splitting reaction to occur in the presence of even very low methanol concentrations is very unlikely in the present system.

According to the proposed mechanism shown in Figure 61, it is assumed that the e$^-$/h$^+$ recombination rate is notably suppressed due to the reaction of methanol with the photogenerated valence band holes. In the first oxidation step the formation of an α-hydroxyalkyl radical occurs by the abstraction of a proton from the methyl group of methanol. This radical is very reactive, thus, apparently injecting an electron either into the conduction band or even directly into the Pt cocatalyst deposited on the surface of the semiconductor (Current-Doubling).
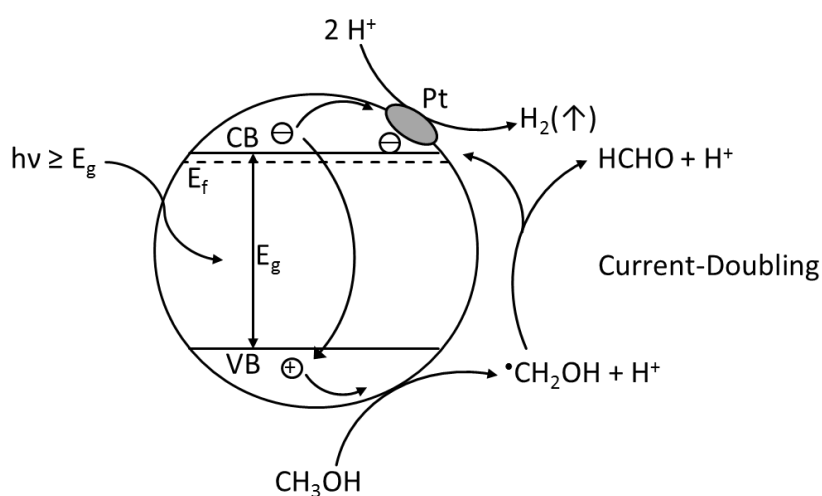


**Figure 61**: Proposed mechanism of the photocatalytic H$_2$ evolution employing cocatalyst loaded La-doped NaTaO$_3$ in aqueous methanol solution.[87]

Based on the results from the isotopic study carried out here, it can be assumed that this electron injection play an important role for the photocatalytic H$_2$ evolution. It is, in fact, not possible to distinguish between the (dark) electrons injected by an α-hydroxyalkyl radical and the (photo) electrons originating from the

semiconductor. However, in the presence of methanol the drastic increase of the quantum yields for $H_2$ evolution from 1 to 30 % cannot only be attributed to the suppression of the $e^-/h^+$ recombination. Otherwise, the enhancement for the $H_2$ evolution would be expected to be more similar to that observed in the case when silver nitrate solution was employed, *i.e.*, only 10 times higher quantum yields for $O_2$ evolution in the case of the best cocatalysts (CoO).

## 5.7 Long-term investigations of the photocatalytic methanol reforming

Long-term investigations were carried out on platinized La-doped $NaTaO_3$ employing methanol as a model compound. Hereby, the amount of molecular $H_2$ and $CO_2$ evolved from a known amount of oxidized methanol were both measured and calculated.

Figure 32 shows that the complete methanol oxidation occurred within 600 hours (25 days) of irradiation time under typical experimental conditions. Assuming that the photocatalytic methanol oxidation occurs according to the mechanism proposed in the literature (Equations 11-14), the expected amounts of $H_2$ and $CO_2$ formed from the complete reforming of methanol employed in this work (i.e., 1.5 mmol) can be calculated to be 4500 and 1500 µmol, respectively. The obtained amounts of the evolved molecular $H_2$ and molecular $CO_2$ were found to be lower than the calculated ones, *i.e.*, about 2500 and 1000 µmol, respectively (Figure 33). Accordingly, the ratio of evolved $H_2$ to $CO_2$ was found to be 2.5 to 1 instead of the theoretical ratio 3 to 1 as shown in Equation 14. Supposedly, lower amounts of evolved $H_2$ and $CO_2$ can be explained by the fact, that after 600 h of reaction some amount of methanol has been evaporated from the reaction mixture due to the continuous flow of Ar gas through the experimental setup employed in this work.

The ratio of $CO_2$ to $H_2$ evolution rates within the photocatalytic methanol oxidation obtained from the long-term experiment on platinized La-doped $NaTaO_3$ (0.83 wt% La) is shown in Figure 32.
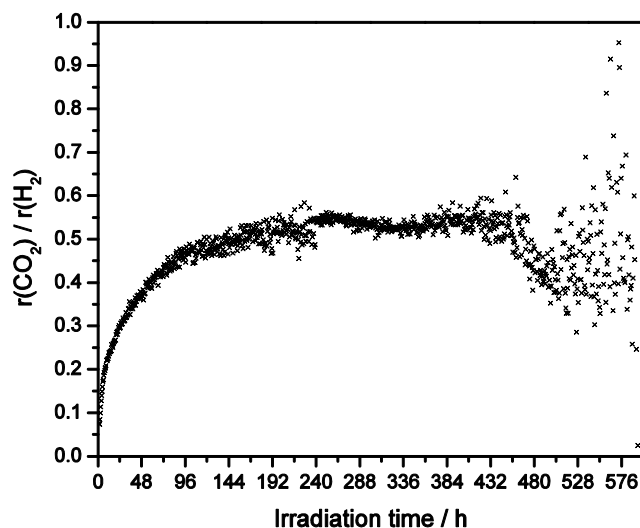
**Figure 62**: Ratio of the evolution rates of $CO_2$ and $H_2$ evolved on platinized La-doped $NaTaO_3$ (0.83 wt% La) from 30 mM aqueous methanol solution. Photocatalyst concentration: $1\,g \cdot L^{-1}$, 0.2 wt% Pt cocatalyst loading. Reactor volume: 50 ml, Irradiation intensity: $I_{250\text{-}400}$=41 mW$\cdot$cm$^{-2}$.

Figure 62 clearly shows that within the first 24 h of the experiment more $H_2$ than $CO_2$ gas is evolved approaching the ratio of 0.3 expected according to the proposed mechanism (Equation 5). At the initial steps of the methanol oxidation the higher quantity of evolved $H_2$ as compared with $CO_2$ can be easily explained by the fact that even when already two $H_2$ molecules have been formed no $CO_2$ molecule has to be generated (Eqn. 11-13). In the range between 24 to 144 h of irradiation the ratio of the evolved gases ($CO_2$:$H_2$) is further increasing up to approximately 0.5 staying nearly constant up to 480 h. This means that the observed ratio of $H_2$ to $CO_2$ evolution rates remains at 2:1 during almost the entire photocatalytic oxidation of methanol. It should be noted that within initial 150 h of irradiation time already 40 % of the initially present methanol have been converted to $CO_2$ (585 µmol) and $H_2$ (1591 µmol) with the overall amount of the evolved $H_2$ being lower than the expected one of 1755 µmol. Supposedly, the photocatalytic oxidation of methanol to formaldehyde is a fast reaction and almost all methanol remaining in the system should have been oxidized to formaldehyde within first 144 h of illumination. The observed ratio 2:1 of $H_2$ to $CO_2$ evolution rates after 144 h corresponds apparently to the last two methanol oxidation steps, *i.e.*, the

oxidation of formaldehyde to formic acid and then to $CO_2$ yielding two $H_2$ molecules (Equation 12 and 13). This assumption readily explains the observed ratio of the $H_2$ to $CO_2$ evolution rates being 2:1 instead of 3:1.

## 5.8   Origin of the evolved $H_2$ gas

When methanol is used as the sacrificial agent for the enhanced photocatalytic hydrogen formation, the question whether the evolved hydrogen gas originates from water or from methanol is still controversial. Answering this question is not only very exciting from the scientific point of view but is also very important from the technical point of view.

In order to identify the origin of the evolved hydrogen gas an isotopic study was carried out on platinized La-doped $NaTaO_3$ employing aqueous methanol solution (0.03 M). Long-term photocatalytic hydrogen evolution tests were performed using several mixtures of (deuterated) water and (deuterated) methanol whereby $H_2$, $D_2$ and HD were detected (Figure 34). It was found that depending on the solvent used, *i.e.*, $H_2O$ or $D_2O$, $H_2$ or $D_2$ were formed accordingly as major products (Figure 34 c and d).

Under the used experimental conditions a rapid $H^+/D^+$ exchange has to be taken into account as follows:[161].

$$CH_3OH + D_2O \leftrightarrow CH_3OD + HOD \qquad\qquad 37$$

$$CD_3OD + H_2O \leftrightarrow CD_3OH + HOD \qquad\qquad 38$$

Moreover, it can be assumed that this $H^+/D^+$ exchange takes place already before starting the illumination. The equilibrium of these reactions is supposed to be mainly on the product side taking into account the equilibrium constant $K$ being 1.761[161] for Equation 37.

Considering the case where deuterated water was used as the solvent (Equation 37), the notable amount of HD would be expected to be formed through the abstraction of $H^+$ from the methyl group and $D^+$ from the OD-group of the partially deuterated methanol molecule ($CH_3OD$). However, the main product detected in this system was $D_2$ and not HD (Figure 34 d). Therefore, it is more likely that in the

first step of the methanol oxidation the abstracted $H^+$ rapidly exchanges with $D^+$ originating from $D_2O$ as schematically shown in

Figure **63**. The predominant evolution of $D_2$ (Figure 34 d) from the $CH_3OH$-$D_2O$ system can moreover be explained by statistical considerations. For instance, the ratio of D atoms to H atoms is cal-culated to be 1000 to 1 under the current experimental conditions. Therefore, due to the rapid $H^+/D^+$ exchange in the present system, it is rather difficult to distinguish between protons originating from methanol and those originating from water. However, it can still be assumed that methanol plays a crucial role for the $H_2$ ($D_2$) formation with the initially formed α-hydroxyalkyl radical injecting either an electron or even an H-atom (D-atom) directly into the Pt catalyst whereby two of H-atoms (D-atoms) can be reduced on the Pt surface yielding $H_2$ ($D_2$) gas.
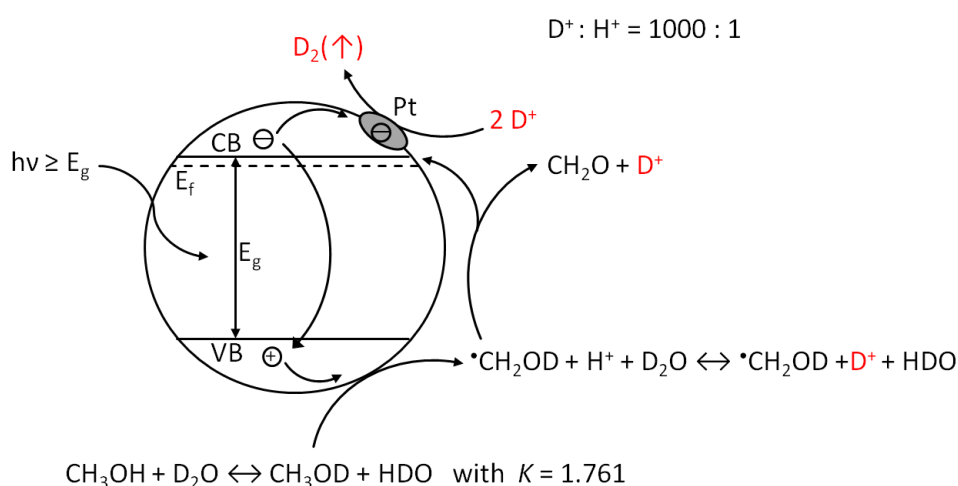


**Figure 63**: Proposed mechanism of the photocatalytic $H_2$ or $D_2$ formation from the mixtures of (deuterated) water and (deuterated) methanol.

## 5.9 Interpretation of the laser flash photolysis studies

Transient laser flash photolysis measurements were performed on pure and on La-doped sodium tantalate powders. Additionally, the effect of the surface modification by the deposition of different cocatalysts on the lifetime of the photogenerated charge carriers was investigated.

### 5.9.1 Photogenerated holes and electrons

The transient absorption maximum at 310 nm and a broad transient absorption band in the range of 650 to 800 nm with low intensity were observed in the case of both pure and La-doped $NaTaO_3$ (0.83 wt% La) (Figure 38 and Figure 40). Since no laser flash photolysis measurements have been carried out on sodium tantalates to date, the results of this study are compared here to those obtained for $TiO_2$.

The absorption maximum at 310 nm is attributed to trapped holes since this transient absorption signal has been found to decrease in the presence of different amounts of hole scavengers, *i.e.*, of methanol, until it completely disappeared after the addition of 100 µl methanol (Figure 39). In $TiO_2$ nanoparticles the respective transient absorption maximum for the trapped holes was found to be at 430 nm supporting the assignment of the transient absorption signal of the trapped holes at 310 nm in the case of the sodium tantalates.[99] Although the half lifetimes of the trapped holes in pure and in La-doped $NaTaO_3$ are similar (~30 µs), the intensity of the signals were found to be quite different. Due to the La doping, the initial intensity of the transient absorption signals 310 nm (trapped holes) increases from 0.17 to 0.22 (see Figure 38). Apparently, the higher intensity of the signals correlates with a higher density of the photogenerated charge carriers (holes) in the system.

Similar to $TiO_2$ the trapped holes in $NaTaO_3$ can chemically be equivalent either to the surface-bound hydroxyl radicals [108, 109] or to the subsurface oxygen anion radicals.[110] Bahnemann *et al*. reported for $TiO_2$ two kinds of the trapped holes being trapped in energetically shallow and deep traps, respectively.[104] The holes trapped in shallow traps apparently posseses an electrochemical potential close to that of free holes because they are readily detrapped. They can be excited thermally into the valence band achieving an equillibrium with free holes. Holes

trapped in deep traps can be characterized by their transient absorption around 430 nm. In analogy, the observed trapped holes with the transient absorption maximum at 310 nm are attributed to the holes trapped in deep traps.

By analogy to colloidal $TiO_2$ particles where the transient absorption maximum of the trapped electrons was found to be at 750 nm, the observed band in the range of 650 to 800 nm could accordingly be attributed to trapped electrons in $NaTaO_3$.[99] The respective transient absorption band is expected to increase after addition of methanol since the holes can be effectively scavenged. However, because of the noisy transient absorption signals in the range of 650 to 800 nm, no effect of the methanol addition could be observed.

It is interestingly to note that, for $TiO_2$, the absorption coefficient of the trapped electrons is reported to be much lower than that of the trapped holes. For instance, for nanosized $TiO_2$ the reported absorption coefficients for the trapped holes and electrons were found to be $9200 \, M^{-1} \cdot cm^{-1}$ (at 475 nm) and $800 \, M^{-1} \cdot cm^{-1}$ (at 700 nm), respectively.[98, 99] For the tantalates investigated here, the transient absorption signals around 750 nm were also found to be much weaker that those detected at 310 nm. Moreover, the intensity of the band in the range of 650 to 800 nm was found to be further reduced with La doping with the decay of the transient absorption signal at 710 nm in the case of La-doped $NaTaO_3$ being faster than that in the pure material (Figure 42).

Supposedly, $La^{3+}$ ions incorporated in the bulk of $NaTaO_3$ are able to trap the photogenerated electrons thus lowering their transient absorption and also the lifetime of the trapped electrons. In analogy of the laser flash photolysis measurements performed on $TiO_2$, it can be assumed that the conduction band electrons could be trapped at two different $Ta^{4+}$ sites (Equation 39 and 40).[103, 111, 162] It is worth mentioning, that no direct evidence of the existence of $Ta^{4+}$ species has been reported yet!

$$e_{CB}^- + Ta^{5+} - OH \leftrightarrow Ta^{4+} - OH \qquad\qquad 39$$

$$e_{CB}^- + Ta^{5+}(bulk) \rightarrow Ta^{5+}(bulk) \qquad\qquad 40$$

Hoffmann *et al.* postulated that for $TiO_2$ the trapping of an electron trapped at the surface (Equation 39) is a reversible process while the trapping of an electron in a

deep trap is irreversible (Equation 40).[162] Henderson *et al.* showed that the photoexcited electrons are preferentially trapped at surface traps, *i.e.*, at surface OH groups of $TiO_2$.[163]

The results of the laser flash measurements clearly show that the lifetime of the trapped electrons is significantly shorter as compared with that of the trapped holes. This trapped electrons move then to the deeper trap states and become less reactive. In contrast, the trapped holes lives longer and react with methanol within a μs time scale (Equation 49). Based on the transient absorption at 310 nm of the trapped holes, their oxidation power should be rather high. Therefore, it might be that in the case of $NaTaO_3$ there are two different electrons being trapped at different deep traps. One of these electrons could be trapped at $Ta^V$ (Equation 44) or it could competitively react with a proton yielding molecular hydrogen (Equation 45). The reaction of the trapped holes with $Ta^{IV}$ leads subsequently to a recombination (Equation 46). The other electron could be trapped at $La^{III}$ as shown in Equation 47. The subsequent reaction of $La^{II}$ with the protons leads to a molecular hydrogen formation (Equation 48).

$$NaTaO_3 \xrightarrow{h\upsilon} e^- + h^+ \tag{41}$$

$$e^- \rightarrow e^-_{tr} \ (\lambda_{max} : 600 - 800 \ nm) \tag{42}$$

$$h^+ \rightarrow h^+_{tr} \ (\lambda_{max} : 310nm) \tag{43}$$

$$e^-_{tr} + Ta^V \rightarrow Ta^{IV} \ (no \, transient \, absorption) \tag{44}$$

$$e^-_{tr} + H^+ \rightarrow \frac{1}{2} H_2 \tag{45}$$

$$h^+_{tr} + Ta^{IV} \rightarrow recombination \tag{46}$$

$$e^-_{tr} + La^{III} \rightarrow La^{II} \tag{47}$$

$$La^{II} + H^+ \rightarrow \frac{1}{2} H_2 + La^{III} \tag{48}$$

$$h^+_{tr} + CH_3OH \rightarrow {}^\bullet CH_2OH + H^+ \tag{49}$$
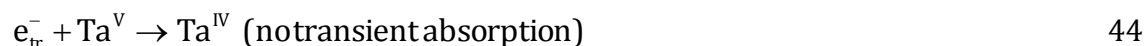
### 5.9.2 Effect of La doping

Figure 41 clearly shows that the La doping of 0.57 and 1.11 wt% La significantly decreases the half lifetime of the trapped holes as compared with those of pure $NaTaO_3$. Interestingly, the La doping of 0.83 wt% slightly increases the half lifetime of the trapped holes while the transient absorption intensity was notable increased. Based on this observation it seems to be important to consider not only the half lifetimes of the trapped holes but also the intensities of their transient absorption signals. Thus, the intensity of the transient absorption signals and the half lifetimes of the trapped holes were plotted versus the La content (Figure 64). It is clearly seen that both the intensity and the half lifetime values of La-doped $NaTaO_3$ materials correlate with their photocatalytic activity for $H_2$ evolution at the respective La content exhibiting the maximum at a 0.83 wt% La doping. It is obvious that for pure $NaTaO_3$ the incorporation of 0.57 wt% La into the structure has a negative effect on both the intensity of the transient absorption and the half lifetime.
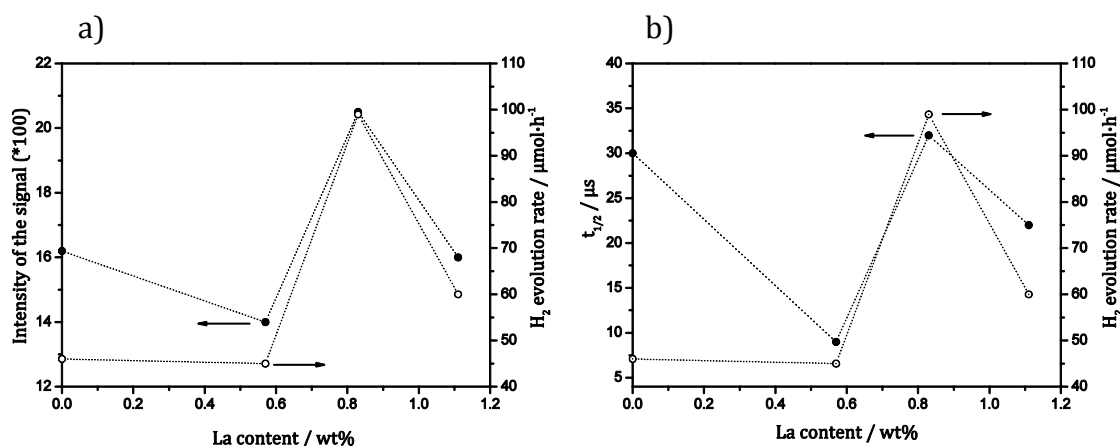


**Figure 64**: a) Correlation between the intensity of the transient absorption at 310 nm and photocatalytic activity for $H_2$ evolution with the La content of $NaTaO_3$. b) Correlation between the half lifetime of the trapped holes and photocatalytic activity for $H_2$ evolution with the La content of $NaTaO_3$. Experimental conditions of the photocatalytic tests: catalyst concentration: 1 g·L$^{-1}$, methanol concentration: 2.5 M, Pt loading: 0.5 wt%, reactor volume: 50 ml, irradiation intensity: $I_{250-450}$=41 mW·cm$^{-2}$.

Comparing SEM micrographs of pure and La-doped $NaTaO_3$ particles (Figure 14) it is clearly seen that the strongest agglomeration degree of the particles was observed in the cases of 0.83 and 1.11 wt% La doping. Apparently, the enhanced

agglomeration facilitates an efficient charge carries separation thus increasing the photocatalytic activity for $H_2$ formation. Such a positive effect of the agglomeration of the particles on the photocatalytic activity can be explained by means of the so-called antenna mechanism.[164] The antenna effect involves the transfer of energy of a photon through a self-assembled aggregate in which the particles have the same crystallographic orientation. [165] Consequently, an electron generated by light absorption within one of the nanoparticles forming the network will subsequently be available to promote redox processes anywhere within the structure.[166]

According to this mechanism, it is supposed that in the case of a 0.83 wt% La doping the well pronounced agglomeration of the particles could contribute to the prolonged lifetime of the excited charge carriers resulting in an enhanced photocatalytic activity. It can be assumed that at a higher La doping of 1.11wt%, lanthanum acts as a recombination center since the decrease of both the half life-time of the trapped holes and the photocatalytic activity has been observed.

### 5.9.3  Effect of cocatalysts

The effect of the surface modification by the deposition of noble metal and metal oxide cocatalyst nanoparticles on the lifetime of the photogenerated charge carriers has also been investigated. Hereby, the laser flash photolysis measu-rements were performed on pure $NaTaO_3$ as the reference (Figure 44) and, 0.83 wt% La-doped $NaTaO_3$ (Figure 46) since the latter material was employed for the majority of the photocatalytic tests performed in this work.

The surface modification of pure $NaTaO_3$ with different cocatalysts did not affect the half lifetime of the transient absorption signals assigned to the trapped holes to a great extent. The half lifetime was found either to be comparable with that of the bare material (NiO, CuO and AgO) or to be even reduced (Pt, Rh, Au, CoO, and, $RuO_2$) (Figure 44 b). On the other hand, the intensity of the transient absorption signal was significantly enhanced when noble metals (Pt, Rh and Au) were depo-sited onto the pure $NaTaO_3$ (Figure 44 a). Supposedly, the noble metal deposits on the surface of pure $NaTaO_3$ can effectively trap the photogenerated electrons increasing the intensity of the transient absorption of the trapped holes.

The evaluation of the transient absorption at around 700 nm being observed in the case of cocatalysts modified pure and La-doped $NaTaO_3$ was not possible because of the strong noise of the measured signals. The deposition of the remaining cocatalysts did not show any effect on the intensity of the transient absorption signals as compared with that of the pure material. In summary, it can be stated that these results are consistent with those obtained from the photocatalytic activity measurements as no enhancement for the $H_2$ evolution was observed in the present of Pt (Figure 28 a).

In contrast, in the case of La-doped $NaTaO_3$ no effect of the cocatalyst deposits on the intensity of the transient absorption signals was noted. Apparently, as discussed above, due to the La doping the highest intensities of the signals have been already achieved so that no further effect of the addition of the cocatalyst nanoparticles can be observed. Interestingly, for most cocatalyst deposits the half lifetime of the trapped holes was reduced as compared with that of the unmodified La-doped $NaTaO_3$. Only the NiO cocatalyst loading significantly enhanced the half lifetime of the trapped holes. These results do not show a direct correlation with those obtained from the measurements of the photocatalytic activity for $H_2$ evolution (Figure 31). Therefore, it can be concluded that the cocatalyst deposits are mainly responsible for surface effects such as, *e.g.*, lowering of the activation energy and of the overpotential for the gas formation ($H_2$ or $O_2$) and that they almost do not affect the bulk properties of the host photocatalyst.

## 6. Summary and conclusions

Due to the successful development and construction of a novel photocatalytic set-up within this thesis, water splitting reactions have been thoroughly investigated utilizing sodium tantalate materials. The new photocatalytic setup enables an in line monitoring of the entire course of the reaction detecting several gaseous compounds, *e.g.*, $H_2$, $O_2$, or $CO_2$ formed during the photocatalytic reaction simultaneously. Thus, this new system allows both the quantitative and the qualitative determination of these reaction products, providing essential information regarding the mechanism of the photocatalytic water splitting process.

The photocatalytic water splitting activity of different materials reported in the literature is usually given in evolution rates ($mol \cdot h^{-1}$), making the true comparison of their activities among each other practically impossible. Therefore, within this thesis the absolute quantum yields ($\phi$) in particulate suspensions has been determined. Based upon these absolute quantum yields of the reaction products a better evaluation of the photocatalytic activity for $H_2$ and $O_2$ evolution obtained in his work has successfully been ensured.

This work demonstrates that the photocatalytic activity for $H_2$ and $O_2$ evolution employing $NaTaO_3$ materials is much more affected by the presence or absence of sacrificial agents in the system than by the doping or by the surface modification of the bare material. For instance, $H_2$ evolution from pure water is observed only after surface modification of $La:NaTaO_3$ with cocatalysts, *e.g.*, Pt (QY=0.9 %), whereby no molecular oxygen was detected. In contrast, employing methanol as a so-called sacrificial agent the photocatalytic activity for $H_2$ evolution of $La:NaTaO_3$ is increased by a factor of three even in the absence of any cocatayst (QY=3 %) and by a factor of ten in the case of a Pt loading (QY=32 %).

The lanthanum doping of platinized $NaTaO_3$ shows no significant effect on the photocatalytic activity for $H_2$ evolution from pure water. Moreover, rather a negative effect is noted lowering the quantum yield of $H_2$ evolution from 1.5 to 0.9 %. Due to the low $H_2$ evolution rates, no $O_2$ evolution from pure water was detected, since the theoretically expected amount of evolved $O_2$ is rather close to the

detection limit of the present system. Instead, hydrogen peroxide was detected during the photocatalytic test reactions in pure water.

On the contrary, when methanol is employed as a sacrificial electron donor platinized La doped $NaTaO_3$ exhibits significantly higher photocatalytic activity for $H_2$ evolution (QY=32 %) as compared with that of undoped $NaTaO_3$ (QY=15 %). Furthermore, it was shown that a positive effect of Pt deposition on the photocatalytic $H_2$ evolution is in the case of small particles (La-doped $NaTaO_3$) more pronounced than in the case of bigger particles (bare $NaTaO_3$). This observation is readily explained by the difference in the specific surface area of both materials playing a crucial role by their surface modification.

Among three different La dopings, *i.e.*, 0.57, 0.83, and 1.11 wt% La employed in this work, a La doping of 0.83 wt% La reveals the highest photocatalytic activity for $H_2$ evolution. The relationship between the photocatalytic activity and the lifetime of the photogenerated charge carriers has been investigated by means of laser flash photolysis studies for the first time.

In agreement with the results from the photocatalytic study it was demonstrated that 0.83 wt% La-doped $NaTaO_3$ exhibits both the highest initial intensity of the transient absorption signal at 310 nm and the highest half lifetimes of the trapped holes. Accordingly, it was assumed that at the optimal dopant concentration (0.83 wt% La) the band bending inside the particles is increased inducing the so-called depletion layer or space charge region whereby the photocatalytic activity can be enhanced due to a more efficient charge carrier separation within the depletion layer.

According to the newly developed model for the optimal dopant concentration suggested by Bloh *et al.*, significant lower optimal dopant concentrations of 0.0004 at % for La doping have been predicted as compared to those employed in this work, *i.e.*, 0.3 at%. Since the photocatalytic activity of $NaTaO_3$ at such low dopant concentration has not been investigated yet, the existence of two optimal dopant concentrations cannot be excluded. On the other hand, this model might be not applicable for $NaTaO_3$ since it has been developed for $TiO_2$ and ZnO considering smaller particle size and different crystallographic structure. Moreover, the doping of $NaTaO_3$ could serve different a purpose as in the case of $TiO_2$ or ZnO, so

that completely different mechanisms might be responsible to explain the enhanced photocatalytic activity of $NaTaO_3$.

During the work performed in this thesis the effect of different cocatalysts including noble metals (Pt, Au, and Rh) and metal oxides (NiO, CuO, CoO, $RuO_2$, and AgO) on the photocatalytic activity of La-doped $NaTaO_3$ for the generation of $H_2$ and/or $O_2$ has been systematically investigated for the first time. The investigated cocatalysts demonstrate a selective behavior either towards enhanced photocatalytic $H_2$ or $O_2$ evolution employing three different systems, *i.e.*, pure water, aqueous methanol solutions and aqueous silver nitrate solutions. The selectivity towards the enhanced $H_2$ formation from pure water is being compared with that for the enhanced $O_2$ formation from aqueous silver nitrate solutions, since no $O_2$ evolution has been detected employing just pure water. During this comparison, it was found that $RuO_2$ or CuO used as cocatalysts exhibit the highest photocatalytic activity for $H_2$ evolution while, however, they show the lowest photocatalytic activity for $O_2$ evolution. Similar results were observed in the case of CoO, *i.e.*, while being the cocatalyst with the highest photocatalytic activity for $O_2$ evolution CoO exhibits the lowest activity for $H_2$ evolution. Noble metal cocatalysts, *i.e.*, Pt, Rh, and Au demonstrate neither the highest nor the worst photocatalytic activity for both $H_2$ and $O_2$ evolution from pure water and from aqueous silver nitrate solutions, respectively. AgO used as cocatalyst exhibits the lowest photocatalytic activity for both $H_2$ and $O_2$ formation.

When methanol is employed as sacrificial reducing agent, noble metal cocatalysts show the highest photocatalytic activity for $H_2$ evolution. Interestingly, $RuO_2$ being the cocatalyst with the highest activity for $H_2$ evolution from pure water, exhibits, on the other hand the lowest activity for $H_2$ evolution in the presence of methanol. This result indicates that different mechanisms for the $H_2$ and/or $O_2$ formation in the presence or absence of methanol as sacrificial agents are operative. Thus, a new mechanism was suggested assuming that in pure water $RuO_2$ acts as an efficient electron transfer catalyst significantly enhancing the photocatalytic activity for $H_2$ formation. In the presence of methanol it is assumed that the proton coupled electron transfer (PCET) from the α-hydroxyalkyl radical ($^•CH_2OH$) to $RuO_2$ is not efficient or even does not occur at all. Here, the injection of

the electrons into the semiconductor rather than directly into $RuO_2$ is the suggested mechanism.

The laser flash photolysis technique was utilized for the first time in this work to investigate the relationship between the photocatalytic activity of different cocatalysts and the lifetime of the photogenerated charge carriers in detail. It was found that the photocatalytic activity of different cocatalysts cannot be easily compared with the lifetime of the photogenerated charge carriers. However, this work demonstrates the importance of considering not only the kinetic data but also the intensities of the transient absorption signals of the photogenerated charge carriers to achieve a better understanding of the reaction mechanisms.

Long-term experiments demonstrated high stability of La-doped $NaTaO_3$ in the aqueous methanol solution within a period of 600 hours. Owing to the detection of the oxidation products of methanol, *i.e.*, $H_2$ and $CO_2$ and the subsequent determination of their amounts evolved during these long-term experiments, the mechanism of the methanol oxidation using La-doped $NaTaO_3$ as photocatalyst was proposed. By means of the isotopic investigations the mechanism of the photocatalytic $H_2$ or $D_2$ formation from the (deuterated) water and (deuterated) methanol mixtures has been elucidated.

Within this thesis it has been demonstrated that no overall water splitting into molecular $H_2$ and molecular $O_2$ was achieved utilizing La-doped $NaTaO_3$ loaded with only one cocatalyst such as Pt or $RuO_2$. However, it was found that due to the usage of two different cocatalysts, *e.g.*, $RuO_2$ for the enhanced $H_2$ evolution and CoO for the enhanced $O_2$ evolution, the simultaneously formation of both gases from pure water was enabled. Based on this result of the present thesis, it can be concluded that the photocatalytic systems containing two different cocatalysts will play significant role by the design of the efficient systems for the future solar energy applications.

# 7. References

(1)    Dorian, J. P.; Franssen, H. T.; Simbeck, D. R., Global challenges in energy. *Energy Policy* **2006,** *34* (15), 1984-1991.

(2)    Zheng, X. J.; Wei, L. F.; Zhang, Z. H.; Jiang, Q. J.; Wei, Y. J.; Xie, B.; Wei, M. B., Research on photocatalytic $H_2$ production from acetic acid solution by $Pt/TiO_2$ nanoparticles under UV irradiation. *Int. J. Hydrogen Energ.* **2009,** *34* (22), 9033-9041.

(3)    Matsuoka, M.; Kitano, M.; Takeuchi, M.; Tsujimaru, K.; Anpo, M.; Thomas, J. M., Photocatalysis for new energy production: recent advances in photocatalytic water splitting reactions for hydrogen production. *Catal. Today* **2007,** *122* (1-2), 51-61.

(4)    Bao, N. Z.; Shen, L. M.; Takata, T.; Domen, K., Self-templated synthesis of nanoporous CdS nanostructures for highly efficient photocatalytic hydrogen production under visible. *Chem. Mater.* **2008,** *20* (1), 110-117.

(5)    Kitano, M.; Takeuchi, M.; Matsuoka, M.; Thomas, J. M.; Anpo, M., Photocatalytic water splitting using Pt-loaded visible light-responsive $TiO_2$ thin film photocatalysts. *Catal. Today* **2007,** *120* (2), 133-138.

(6)    Chen, X. B.; Shen, S. H.; Guo, L. J.; Mao, S. S., Semiconductor-based photocatalytic hydrogen generation. *Chem. Rev.* **2010,** *110* (11), 6503-6570.

(7)    Fujishima, A.; Honda, K., Electrochemical photolysis of water at a semiconductor electrode. *Nature* **1972,** *238* (5358), 37-38.

(8)    Maeda, K.; Domen, K., New non-oxide photocatalysts designed for overall water splitting under visible light. *J. Phys. Chem. C* **2007,** *111* (22), 7851-7861.

(9)    Bard, A. J., Photoelectrochemistry and heterogeneous photocatalysis at semiconductors. *J. Photochem.* **1979,** *10* (1), 59-75.

(10)   Bard, A. J., Photoelectrochemistry. *Science* **1980,** *207* (4427), 139-144.

(11)   Bard, A. J., Design of semiconductor photo-electrochemical systems for solar-energy conversion. *J. Phys. Chem.* **1982,** *86* (2), 172-177.

(12)   Mills, A.; Porter, G., Photosensitized dissociation of water using dispersed suspensions of n-type semiconductors. *J. Chem. Soc., Faraday Trans.* **1982,** *78*, 3659-3669.

(13)   Bard, A. J.; Fox, M. A., Artificial photosynthesis - solar splitting of water to hydrogen and oxygen. *Acc. Chem. Res.* **1995,** *28* (3), 141-145.

(14)   Lehn, J. M.; Sauvage, J. P.; Ziessel, R., Photochemical water splitting continuous generation of hydrogen and oxygen by irradiation of aqueous suspensions of metal loaded strontium-titanate. *New J. Chem.* **1980,** *4* (11), 623-627.

(15)   Pichat, P.; Herrmann, J. M.; Disdier, J.; Courbon, H.; Mozzanega, M. N., Photocatalytic hydrogen production from aliphatic-alcohols over a bifunctional platinum on titanium-dioxide catalyst. *New J. Chem.* **1981,** *5* (12), 627-636.

(16)    Kawai, T.; Sakata, T., Conversion of carbohydrate into hydrogen fuel by a photocatalytic process. *Nature* **1980,** *286* (5772), 474-476.

(17)    Duonghong, D.; Borgarello, E.; Gratzel, M., Dynamics of light-induced water cleavage in colloidal systems. *J. Am. Chem. Soc.* **1981,** *103* (16), 4685-4690.

(18)    Kato, H.; Asakura, K.; Kudo, A., Highly efficient water splitting into $H_2$ and $O_2$ over lanthanum-doped $NaTaO_3$ photocatalysts with high crystallinity and surface nanostructure. *J. Am. Chem. Soc.* **2003,** *125* (10), 3082-3089.

(19)    Kisch, H., Semiconductor photocatalysis - mechanistic and synthetic aspects. *Angew. Chem. Int. Ed.* **2013,** *52* (3), 812-847.

(20)    Memming, R., *Semiconductor Electrochemistry*. Wiley-VCH Verlag GmbH: Weinheim, 2001.

(21)    Binnewies, M., *Allgemeine und Anorganische Chemie*. Elsevier GmbH: München, 2004.

(22)    Weber, M. F.; Dignam, M. J., Splitting water with semiconducting photoelectrodes efficiency considerations. *Int. J. Hydrogen Energ.* **1986,** *11* (4), 225-232.

(23)    Bolton, J. R.; Strickler, S. J.; Connolly, J. S., Limiting and realizable efficiencies of solar photolysis of water. *Nature* **1985,** *316* (6028), 495-500.

(24)    Murphy, A. B.; Barnes, P. R. F.; Randeniya, L. K.; Plumb, I. C.; Grey, I. E.; Horne, M. D.; Glasscock, J. A., Efficiency of solar water splitting using semiconductor electrodes. *Int. J. Hydrogen Energ.* **2006,** *31* (14), 1999-2017.

(25)    Takanabe, K.; Domen, K., Toward Visible Light Response: Overall Water Splitting Using Heterogeneous Photocatalysts. In *Green*, 2011; Vol. 1, p 313.

(26)    Kudo, A.; Miseki, Y., Heterogeneous photocatalyst materials for water splitting. *Chem. Soc. Rev.* **2009,** *38* (1), 253-278.

(27)    Meissner, D.; Memming, R.; Kastening, B.; Bahnemann, D., Fundamental problems of water splitting at cadmium sulfide. *Chem. Phys. Lett.* **1986,** *127* (5), 419-423.

(28)    Ellis, A. B.; Kaiser, S. W.; Bolts, J. M.; Wrighton, M. S., Study of n-type semiconducting cadmium chalcogenide-based photoelectrochemical cells employing polychalcogenide electrolytes. *J. Am. Chem. Soc.* **1977,** *99* (9), 2839-2848.

(29)    Maeda, K.; Takata, T.; Hara, M.; Saito, N.; Inoue, Y.; Kobayashi, H.; Domen, K., GaN : ZnO solid solution as a photocatalyst for visible-light-driven overall water splitting. *J. Am. Chem. Soc.* **2005,** *127* (23), 8286-8287.

(30)    Maeda, K.; Teramura, K.; Takata, T.; Hara, M.; Saito, N.; Toda, K.; Inoue, Y.; Kobayashi, H.; Domen, K., Overall water splitting on (Ga1-xZnx)(N1-xOx) solid solution photocatalyst: Relationship between physical properties and photocatalytic activity. *J. Phys. Chem. B* **2005,** *109* (43), 20504-20510.

(31)    Maeda, K.; Teramura, K.; Masuda, H.; Takata, T.; Saito, N.; Inoue, Y.; Domen, K., Efficient overall water splitting under visible-light irradiation on $(Ga_{1-x}Zn_x)(N_{1-x}O_x)$ dispersed with Rh-Cr mixed-oxide nanoparticles: effect of reaction conditions on photocatalytic activity. *J. Phys. Chem. B* **2006,** *110* (26), 13107-13112.

(32)    Fox, M. A.; Dulay, M. T., Heterogeneous photocatalysis. *Chem. Rev.* **1993,** *93* (1), 341-357.

(33)    Ranjit, K. T.; Viswanathan, B., Photocatalytic reduction of nitrite and nitrate ions to ammonia on $M/TiO_2$ catalysts. *J. Photochem. Photobiol., A* **1997,** *108* (1), 73-78.

(34)    Choi, W.; Lee, J.; Kim, S.; Hwang, S.; Lee, M. C.; Lee, T. K., Nano Pt particles on $TiO_2$ and their effects on photocatalytic reactivity. *J. Ind. Eng. Chem.* **2003,** *9* (1), 96-101.

(35)    Hwang, S.; Lee, M. C.; Choi, W., Highly enhanced photocatalytic oxidation of CO on titania deposited with Pt nanoparticles: kinetics and mechanism. *Appl. Catal. B-Environ.* **2003,** *46* (1), 49-63.

(36)    Hufschmidt, D.; Bahnemann, D.; Testa, J. J.; Emilio, C. A.; Litter, M. I., Enhancement of the photocatalytic activity of various $TiO_2$ materials by platinisation. *J. Photochem. Photobiol., A* **2002,** *148* (1-3), 223-231.

(37)    Tung, R. T., Schottky-barrier formation at single-crystal metal-semiconductor interfaces. *Phys. Rev. Lett.* **1984,** *52* (6), 461-464.

(38)    Subramanian, V.; Wolf, E. E.; Kamat, P. V., Catalysis with $TiO_2$/Gold nanocomposites. Effect of metal particle size on the fermi level equilibration. *J. Am. Chem. Soc.* **2004,** *126* (15), 4943-4950.

(39)    Linsebigler, A. L.; Lu, G. Q.; Yates, J. T., Photocatalysis on $TiO_2$ surfaces - principles, mechanisms, and selected results. *Chem. Rev.* **1995,** *95* (3), 735-758.

(40)    Maeda, K.; Domen, K., Surface nanostructures in photocatalysts for visible-light-driven water splitting. In *Photocatalysis*, Bignozzi, C. A., Ed. 2011; Vol. 303, pp 95-119.

(41)    Litter, M. I., Heterogeneous photocatalysis: transition metal ions in photocatalytic systems. *Appl. Catal. B-Environ.* **1999,** *23*, 89-114.

(42)    Eastman, D. E., Photoelectric work functions of transition, rare-earth, and noble metals. *Phys. Rev. B* **1970,** *2* (1), 1-2.

(43)    Chiarello, G. L.; Aguirre, M. H.; Selli, E., Hydrogen production by photocatalytic steam reforming of methanol on noble metal-modified $TiO_2$. *J. Catal.* **2010,** *273* (2), 182-190.

(44)    Hara, M.; Nunoshige, J.; Takata, T.; Kondo, J. N.; Domen, K., Unusual enhancement of $H_2$ evolution by Ru on TaON photocatalyst under visible light irradiation. *Chem. Commun.* **2003,** *0* (24), 3000-3001.

(45)    Liu, M.; You, W.; Lei, Z.; Zhou, G.; Yang, J.; Wu, G.; Ma, G.; Luan, G.; Takata, T.; Hara, M., et al., Water reduction and oxidation on Pt-Ru/$Y_2Ta_2O_5N_2$ catalyst under visible light irradiation. *Chem. Commun.* **2004,** *0* (19), 2192-2193.

(46)    Mizukoshi, Y.; Sato, K.; Konno, T. J.; Masahashi, N., Dependence of photocatalytic activities upon the structures of Au/Pd bimetallic nanoparticles immobilized on $TiO_2$ surface. *Appl. Catal. B-Environ.* **2010,** *94* (3-4), 248-253.

(47)    Tominaga, A.; Mizukoshi, Y.; Nakagoe, O.; Tanabe, S., Preparation of hydrogen permeable membrane using nanoparticles electrophoresis technique. *Top. Catal.* **2009,** *52* (6-7), 860-864.

(48)    Fang, J.; Cao, S.-W.; Wang, Z.; Shahjamali, M. M.; Loo, S. C. J.; Barber, J.; Xue, C., Mesoporous plasmonic Au-$TiO_2$ nanocomposites for efficient visible-light-driven photocatalytic water reduction. *Int. J. Hydrogen Energ.* **2012,** *37* (23), 17853-17861.

(49)    Daniel, M.-C.; Astruc, D., Gold nanoparticles: assembly, supramolecular chemistry, quantum-size-related properties, and applications toward biology, catalysis, and nanotechnology. *Chem. Rev.* **2003,** *104* (1), 293-346.

(50)    Tian, Y.; Tatsuma, T., Mechanisms and applications of plasmon-induced charge separation at $TiO_2$ films loaded with Gold nanoparticles. *J. Am. Chem. Soc.* **2005,** *127* (20), 7632-7637.

(51)    Ikeda, S.; Hara, M.; Kondo, J. N.; Domen, K.; Takahashi, H.; Okubo, T.; Kakihana, M., Preparation of a high active photocatalyst, $K_2La_2Ti_3O_{10}$, by polymerized complex method and its photocatalytic activity of water splitting. *J. Mater. Res.* **1998,** *13* (4), 852-855.

(52)    Ingram, D. B.; Linic, S., Water splitting on composite plasmonic-metal/semiconductor photoelectrodes: evidence for selective plasmon-induced formation of charge carriers near the semiconductor surface. *J. Am. Chem. Soc.* **2011,** *133* (14), 5202-5205.

(53)    Korzhak, A. V.; Ermokhina, N. I.; Stroyuk, A. L.; Bukhtiyarov, V. K.; Raevskaya, A. E.; Litvin, V. I.; Kuchmiy, S. Y.; Ilyin, V. G.; Manorik, P. A., Photocatalytic hydrogen evolution over mesoporous $TiO_2$/metal nanocomposites. *J. Photochem. Photobiol., A* **2008,** *198* (2-3), 126-134.

(54)    Yamaguti, K.; Sato, S., Photolysis of water over metallized powdered titanium dioxide. *J. Chem. Soc., Faraday Trans.* **1985,** *81* (5), 1237-1246.

(55)    Domen, K.; Kudo, A.; Onishi, T.; Kosugi, N.; Kuroda, H., Photocatalytic decomposition of water into $H_2$ and $O_2$ over NiO-$SrTiO_3$ powder. 1. Structure of the catalyst. *J. Phys. Chem.* **1986,** *90* (2), 292-295.

(56)    Torres-Martinez, L. M.; Gomez, R.; Vazquez-Cuchillo, O.; Juarez-Ramirez, I.; Cruz-Lopez, A.; Alejandre-Sandoval, F. J., Enhanced photocatalytic water splitting hydrogen production on $RuO_2$/La $NaTaO_3$ prepared by sol-gel method. *Catal. Commun.* **2010,** *12* (4), 268-272.

(57)    Kato, H.; Kudo, A., New tantalate photocatalysts for water decomposition into $H_2$ and $O_2$. *Chem. Phys. Lett.* **1998,** *295*, 487-492.

(58)    Kudo, A.; Kato, H., Effect of lanthanide-doping into NaTaO$_3$ photocatalysts for efficient water splitting. *Chem. Phys. Lett.* **2000,** *331* (5-6), 373-377.

(59)    Kato, H.; Kobayashi, H.; Kudo, A., Role of Ag$^+$ in the band structures and photocatalytic properties of AgMO$_3$ (M: Ta and Nb) with the perovskite structure. *J. Phys. Chem. B* **2002,** *106* (48), 12441-12447.

(60)    Kato, H.; Kudo, A., Water splitting into H$_2$ and O$_2$ on alkali tantalate photocatalysts ATaO$_3$ (A = Li, Na, and K). *J. Phys. Chem. B* **2001,** *105* (19), 4285-4292.

(61)    Teramura, K.; Maeda, K.; Saito, T.; Takata, T.; Saito, N.; Inoue, Y.; Domen, K., Characterization of ruthenium oxide nanocluster as a cocatalyst with (Ga$_{1-x}$Zn$_x$)(N$_{1-x}$O$_x$) for photocatalytic overall water splitting. *J. Phys. Chem. B* **2005,** *109* (46), 21915-21921.

(62)    Young, E. R.; Costi, R.; Paydavosi, S.; Nocera, D. G.; Bulovic, V., Photo-assisted water oxidation with cobalt-based catalyst formed from thin-film cobalt metal on silicon photoanodes. *Energy Environ. Sci.* **2011,** *4* (6), 2058-2061.

(63)    Kanan, M. W.; Nocera, D. G., In situ formation of an oxygen-evolving catalyst in neutral water containing phosphate and Co($^{2+}$). *Science* **2008,** *321* (5892), 1072-1075.

(64)    Surendranath, Y.; Dinca, M.; Nocera, D. G., Electrolyte-dependent electrosynthesis and activity of cobalt-based water oxidation catalysts. *J. Am. Chem. Soc.* **2009,** *131* (7), 2615-2620.

(65)    Youngblood, W. J.; Lee, S. H. A.; Maeda, K.; Mallouk, T. E., Visible light water splitting using dye-sensitized oxide semiconductors. *Acc. Chem. Res.* **2009,** *42* (12), 1966-1973.

(66)    Abe, T.; Suzuki, E.; Nagoshi, K.; Miyashita, K.; Kaneko, M., Electron source in photoinduced hydrogen production on Pt-supported TiO$_2$ particles. *J. Phys. Chem. B* **1999,** *103* (7), 1119-1123.

(67)    Kanan, M. W.; Surendranath, Y.; Nocera, D. G., Cobalt-phosphate oxygen-evolving compound. *Chem. Soc. Rev.* **2009,** *38* (1), 109-114.

(68)    Zhong, D. K.; Sun, J. W.; Inumaru, H.; Gamelin, D. R., Solar water oxidation by composite catalyst/alpha-Fe$_2$O$_3$ photoanodes. *J. Am. Chem. Soc.* **2009,** *131* (17), 6086-6087.

(69)    Domen, K.; Kudo, A.; Onishi, T., Mechanism of photocatalytic decomposition of water into H$_2$ and O$_2$ over NiO - SrTiO$_3$. *J. Catal.* **1986,** *102* (1), 92-98.

(70)    Domen, K.; Naito, S.; Soma, M.; Onishi, T.; Tamaru, K., Photocatalytic decomposition of water-vapor on an NiO-SrTiO$_3$ catalyst. *J. Chem. Soc., Chem. Commun.* **1980,** (12), 543-544.

(71)    Iwase, A.; Kato, H.; Kudo, A., A novel photodeposition method in the presence of nitrate ions for loading of an iridium oxide cocatalyst for water splitting. *Chem. Lett.* **2005,** *34* (7), 946-947.

(72)    Le Gendre, L.; Marchand, R.; Laurent, Y., A new class of inorganic compounds containing dinitrogen-metal bonds. *J. Eur. Ceram. Soc.* **1997,** *17* (15-16), 1813-1818.

(73)    Maeda, K.; Teramura, K.; Lu, D. L.; Saito, N.; Inoue, Y.; Domen, K., Noble-metal/$Cr_2O_3$ core/shell nanoparticles as a cocatalyst for photocatalytic overall water splitting. *Angew. Chem. Int. Ed.* **2006,** *45* (46), 7806-7809.

(74)    Lugo, H. J.; Lunsford, J. H., The dehydrogenation of ethane over chromium catalysts. *J. Catal.* **1985,** *91* (1), 155-166.

(75)    Busca, G., Fourier-transform infrared spectroscopic study of the adsorption of hydrogen on chromia and on some metal chromites. *J. Catal.* **1989,** *120* (2), 303-313.

(76)    Yoshida, M.; Takanabe, K.; Maeda, K.; Ishikawa, A.; Kubota, J.; Sakata, Y.; Ikezawa, Y.; Domen, K., Role and function of noble-metal/Cr-layer core/shell structure cocatalysts for photocatalytic overall water splitting studied by model electrodes. *J. Phys. Chem. C* **2009,** *113* (23), 10151-10157.

(77)    Maeda, K.; Domen, K., Photocatalytic water splitting: recent progress and future challenges. *J. Phys, Chem. Lett.* **2010,** *1* (18), 2655-2661.

(78)    Jeon, M. K.; Park, J. W.; Kang, M., Hydrogen production from methanol/water decomposition in a liquid photosystem using the anatase and rutile forms of Cu-$TiO_2$. *J. Ind. Eng. Chem.* **2007,** *13* (1), 84-91.

(79)    Kawai, T.; Sakata, T., Photocatalytic hydrogen production from liquid methanol and water. *J. Chem. Soc., Chem. Commun.* **1980**, 694-695.

(80)    Chen, J.; Ollis, D. F.; Rulkens, W. H.; Bruning, H., Photocatalyzed oxidation of alcohols and organochlorides in the presence of native $TiO_2$ and metallized $TiO_2$ suspensions. Part (I): Photocatalytic activity and pH influence. *Water Res.* **1999,** *33* (3), 661-668.

(81)    Chen, J.; Ollis, D. F.; Rulkens, W. H.; Bruning, H., Photocatalyzed oxidation of alcohols and organochlorides in the presence of native $TiO_2$ and metallized $TiO_2$ suspensions. Part (II): Photocatalytic mechanisms. *Water Res.* **1999,** *33* (3), 669-676.

(82)    Jitputti, J.; Suzuki, Y.; Yoshikawa, S., Synthesis of $TiO_2$ nanowires and their photocatalytic activity for hydrogen evolution. *Catal. Commun.* **2008,** *9* (6), 1265-1271.

(83)    Ekambaram, S., Photoproduction of clean $H_2$ or $O_2$ from water using oxide semiconductors in presence of sacrificial reagent. *J. Alloys Compd.* **2008,** *448* (1-2), 238-245.

(84)    Rosseler, O.; Shankar, M. V.; Du, M. K.-L.; Schmidlin, L.; Keller, N.; Keller, V., Solar light photocatalytic hydrogen production from water over Pt and Au/$TiO_2$ (anatase/rutile) photocatalysts: influence of noble metal and porogen promotion. *J. Catal.* **2010,** *269* (1), 179-190.

(85)    Kandiel, T. A.; Dillert, R.; Robben, L.; Bahnemann, D. W., Photonic efficiency and mechanism of photocatalytic molecular hydrogen production over platinized titanium dioxide from aqueous methanol solutions. *Catal. Today* **2011,** *161* (1), 196-201.

(86)    Highfield, J. G.; Chen, M. H.; Nguyen, P. T.; Chen, Z., Mechanistic investigations of photo-driven processes over $TiO_2$ by in-situ DRIFTS-MS: part 1. platinization and methanol reforming. *Energy Environ. Sci.* **2009,** *2* (9), 991-1002.

(87)    Wang, C. Y.; Pagel, R.; Bahnemann, D. W.; Dohrmann, J. K., Quantum yield of formaldehyde formation in the presence of colloidal $TiO_2$-based photocatalysts: Effect of intermittent illumination, platinization, and deoxygenation. *J. Phys. Chem. B* **2004,** *108* (37), 14082-14092.

(88)    Tamaki, Y.; Furube, A.; Murai, M.; Hara, K.; Katoh, R.; Tachiya, M., Direct observation of reactive trapped holes in $TiO_2$ undergoing photocatalytic oxidation of adsorbed alcohols: Evaluation of the reaction rates and yields. *J. Am. Chem. Soc.* **2006,** *128* (2), 416-417.

(89)    Colombo, D. P.; Bowman, R. M., Does interfacial charge transfer compete with charge carrier recombination? A femtosecond diffuse reflectance investigation of $TiO_2$ nanoparticles. *J. Phys. Chem.* **1996,** *100* (47), 18445-18449.

(90)    Kandiel, T. A.; Ivanova, I.; Bahnemann, D. W., Long-term investigation of the photocatalytic hydrogen production on platinized $TiO_2$: an isotopic study. *Energy Environ. Sci.* **2014,** *7* (4), 1420-1425.

(91)    Kandiel, T. A.; Dillert, R.; Bahnemann, D. W., Enhanced photocatalytic production of molecular hydrogen on $TiO_2$ modified with Pt-polypyrrole nanocomposites. *Photochem. Photobiol. Sci.* **2009,** *8* (5), 683-690.

(92)    Wu, N. L.; Lee, M. S., Enhanced $TiO_2$ photocatalysis by Cu in hydrogen production from aqueous methanol solution. *Int. J. Hydrogen Energ.* **2004,** *29* (15), 1601-1605.

(93)    Hara, K.; Sayama, K.; Arakawa, H., Photocatalytic hydrogen and oxygen formation over $SiO_2$-supported $RuS_2$ in the presence of sacrificial donor and acceptor. *Appl. Catal., A* **1999,** *189* (1), 127-137.

(94)    Ishikawa, A.; Takata, T.; Kondo, J. N.; Hara, M.; Kobayashi, H.; Domen, K., Oxysulfide $Sm_2Ti_2S_2O_5$ as a stable photocatalyst for water oxidation and reduction under visible light irradiation (lambda <= 650 nm). *J. Am. Chem. Soc.* **2002,** *124* (45), 13547-13553.

(95)    Tang, J. W.; Ye, J. H., Correlation of crystal structures and electronic structures and photocatalytic properties of the W-containing oxides. *J. Mater. Chem.* **2005,** *15* (39), 4246-4251.

(96)    Schneider, J.; Bahnemann, D. W., Undesired role of sacrificial reagents in photocatalysis. *J. Phys, Chem. Lett.* **2013,** *4* (20), 3479-3483.

(97)    Hoffmann, M. R.; Martin, S. T.; Choi, W.; Bahnemann, D. W., Environmental applications of semiconductorphotocatalysis. *Chem. Rev.* **1995,** *95* (1), 69-96.

(98)     Bahnemann, D.; Henglein, A.; Lilie, J.; Spanhel, L., Flash-photolysis observation of the absorption-spectra of trapped positive holes and electrons in colloidal TiO$_2$. *J. Phys. Chem.* **1984,** *88* (4), 709-711.

(99)     Bahnemann, D.; Henglein, A.; Spanhel, L., Detection of the intermediates of the colloidal TiO$_2$-catalysed photoreactions. *Faraday Discuss.* **1984,** *78*, 151-163.

(100)   Kuznetsov, A. I.; Kameneva, O.; Alexandrov, A.; Bityurin, N.; Marteau, P.; Chhor, K.; Sanchez, C.; Kanaev, A., Light-induced charge separation and storage in titanium oxide gels. *Phys. Rev. E* **2005,** *71* (2), 021403.

(101)   Shen, Q.; Katayama, K.; Sawada, T.; Yamaguchi, M.; Kumagai, Y.; Toyoda, T., Photoexcited hole dynamics in TiO$_2$ nanocrystalline films characterized using a lens-free heterodyne detection transient grating technique. *Chem. Phys. Lett.* **2006,** *419* (4-6), 464-468.

(102)   Ikeda, S.; Sugiyama, N.; Murakami, S.-y.; Kominami, H.; Kera, Y.; Noguchi, H.; Uosaki, K.; Torimoto, T.; Ohtani, B., Quantitative analysis of defective sites in titanium(IV) oxide photocatalyst powders. *PCCP* **2003,** *5* (4), 778-783.

(103)   Serpone, N.; Lawless, D.; Khairutdinov, R.; Pelizzetti, E., Subnanosecond relaxation dynamics in TiO$_2$ colloidal sols (particle sizes R(p)=1.0-13.4 nm) - relevance to heterogeneous photocatalysis. *J. Phys. Chem.* **1995,** *99* (45), 16655-16661.

(104)   Bahnemann, D. W.; Hilgendorff, M.; Memming, R. d., Charge carrier dynamics at TiO$_2$ particles: Reactivity of free and trapped holes. *J. Phys. Chem. B* **1997,** *101* (21), 4265-4275.

(105)   Szczepankiewicz, S. H.; Moss, J. A.; Hoffmann, M. R., Slow surface charge trapping kinetics on irradiated TiO$_2$. *J. Phys. Chem. B* **2002,** *106* (11), 2922-2927.

(106)   Szczepankiewicz, S. H.; Moss, J. A.; Hoffmann, M. R., Electron traps and the stark effect on hydroxylated titania photocatalysts. *J. Phys. Chem. B* **2002,** *106* (31), 7654-7658.

(107)   Kumar, C. P.; Gopal, N. O.; Wang, T. C.; Wong, M.-S.; Ke, S. C., EPR investigation of TiO$_2$ nanoparticles with temperature-dependent properties. *J. Phys. Chem. B* **2006,** *110* (11), 5223-5229.

(108)   Lawless, D.; Serpone, N.; Meisel, D., Role of hydroxyl radicals and trapped holes in photocatalysis. A pulse radiolysis study. *J. Phys. Chem.* **1991,** *95* (13), 5166-5170.

(109)   Jaeger, C. D.; Bard, A. J., Spin trapping and electron spin resonance detection of radical intermediates in the photodecomposition of water at titanium dioxide particulate systems. *J. Phys. Chem.* **1979,** *83* (24), 3146-3152.

(110)   Howe, R. F.; Gratzel, M., EPR observation of trapped electrons in colloidal titanium dioxide. *J. Phys. Chem.* **1985,** *89* (21), 4495-4499.

(111)   Colombo, D. P.; Bowman, R. M., Femtosecond diffuse reflectance spectroscopy of TiO$_2$ powders. *J. Phys. Chem.* **1995,** *99* (30), 11752-11756.

(112)   Rothenberger, G.; Moser, J.; Graetzel, M.; Serpone, N.; Sharma, D. K., Charge carrier trapping and recombination dynamics in small semiconductor particles. *J. Am. Chem. Soc.* **1985,** *107* (26), 8054-8059.

(113)   Henderson, M. A., A surface science perspective on $TiO_2$ photocatalysis. *Surf. Sci. Rep.* **2011,** *66* (6-7), 185-297.

(114)   Feldhoff, A.; Mendive, C.; Bredow, T.; Bahnemann, D., Direct measurement of size, three-dimensional shape, and specific surface area of anatase nanocrystals. *Chemphyschem* **2007,** *8* (6), 805-809.

(115)   Brunauer, S.; Emmett, P. H.; Teller, E., Adsorption of gases in multimolecular layers. *J. Am. Chem. Soc.* **1938,** *60* (2), 309-319.

(116)   Guilbault, G. G.; Brignac, P. J.; Juneau, M., Substrates for the fluorometric determination of oxidative enzymes. *Anal. Chem.* **1968,** *40* (8), 1256-1263.

(117)   Kormann, C.; Bahnemann, D. W.; Hoffmann, M. R., Photocatalytic production of $H_2O_2$ and organic peroxides in aqueous suspensions of $TiO_2$, ZnO, and desert sand. *Environ. Sci. Technol.* **1988,** *22* (7), 798-806.

(118)   Kirk, A. D.; Namasivayam, C., Errors in ferrioxalate actinometry. *Anal. Chem.* **1983,** *55* (14), 2428-2429.

(119)   Hatchard, C. G.; Parker, C. A., A new sensitive chemical actinometer. II. potassium ferrioxalate as a standard chemical actinometer. *Proc. Phys. Soc., London, Sect. A* **1956,** *235* (1203), 518-536.

(120)   Lin, W. H.; Cheng, C.; Hu, C. C.; Teng, H., $NaTaO_3$ photocatalysts of different crystalline structures for water splitting into $H_2$ and $O_2$. *Appl. Phys. Lett.* **2006,** *89* (21).

(121)   Hu, C. C.; Teng, H., Influence of structural features on the photocatalytic activity of $NaTaO_3$ powders from different synthesis methods. *Appl. Catal., A* **2007,** *331*, 44-50.

(122)   Gong, X.-Q.; Selloni, A., Reactivity of anatase $TiO_2$ nanoparticles: The role of the minority (001) surface. *J. Phys. Chem. B* **2005,** *109* (42), 19560-19562.

(123)   Kung, H. H., *Transition Metal Oxides: Surface Chemistry and Catalysis*. Elsevier: Amsterdam, 1989.

(124)   Ivanova, I.; Kandiel, T. A.; Esch, T. E.; Vidic, J.; Haubrich, H.; Feldhoff, A.; Bredow, T.; Bahnemann, D. W., Structure and photocatalytic activity of pure and La-doped $NaTaO_3$: Experimental results vs. theoretical predictions. *J. Mater. Chem. A*, submitted.

(125)   Ni, M.; Leung, M. K. H.; Leung, D. Y. C.; Sumathy, K., A review and recent developments in photocatalytic water-splitting using for hydrogen production. *Renew. Sust. Energ. Rev.* **2007,** *11* (3), 401-425.

(126)   Chiarello, G. L.; Ferri, D.; Selli, E., Effect of the $CH_3OH/H_2O$ ratio on the mechanism of the gas-phase photocatalytic reforming of methanol on noble metal-modified $TiO_2$. *J. Catal.* **2011,** *280* (2), 168-177.

(127)   Mortimer, C. E.; Müller, U., *Chemie*. Thieme: Stuttgart, 2010.

(128) Kato, H.; Kudo, A., Visible-light-response and photocatalytic activities of $TiO_2$ and $SrTiO_3$ photocatalysts codoped with antimony and chromium. *J. Phys. Chem. B* **2002,** *106* (19), 5029-5034.

(129) Oosawa, Y.; Gratzel, M., Effect of surface hydroxyl density on photocatalytic oxygen generation in aqueous $TiO_2$ suspensions. *J. Chem. Soc. Faraday Trans. I* **1988,** *84* (1), 197-205.

(130) Niishiro, R.; Tanaka, S.; Kudo, A., Hydrothermal-synthesized $SrTiO_3$ photocatalyst codoped with rhodium and antimony with visible-light response for sacrificial $H_2$ and $O_2$ evolution and application to overall water splitting. *Appl. Catal. B-Environ.* **2014,** *150-151* (0), 187-196.

(131) Zhang, L. W.; Mohamed, H. H.; Dillert, R.; Bahnemann, D., Kinetics and mechanisms of charge transfer processes in photocatalytic systems: A review. *J. Photochem. Photobiol., C- Photochem. Rev.* **2012,** *13* (4), 263-276.

(132) Ohtani, B., Photocatalysis A to Z-What we know and what we do not know in a scientific sense. *J. Photochem. Photobiol., C- Photochem. Rev.* **2010,** *11* (4), 157-178.

(133) Li, Z. H.; Chen, G.; Liu, J. W., Electron structure and optical absorption properties of cubic and orthorhombic $NaTaO_3$ by density functional theory. *Solid State Commun.* **2007,** *143*, 295-299.

(134) Hu, C. C.; Tsai, C. C.; Teng, H., Structure characterization and tuning of perovskite-like NaTaO3 for applications in photoluminescence and photocatalysis. *J. Am. Ceram. Soc.* **2009,** *92* (2), 460-466.

(135) Domen, K.; Naito, S.; Onishi, T.; Tamaru, K., Photocatalytic hydrogen-production from a mixture of water and 2-propanol on some semiconductors. *Chem. Lett.* **1982,** (4), 555-558.

(136) Kanhere, P.; Nisar, J.; Tang, Y. X.; Pathak, B.; Ahuja, R.; Zheng, J. W.; Chen, Z., Electronic Structure, Optical Properties, and Photocatalytic Activities of $LaFeO_3$-$NaTaO_3$ Solid Solution. *J. Phys. Chem. C* **2012,** *116* (43), 22767-22773.

(137) Kato, H.; Kudo, A., Photocatalytic water splitting into $H_2$ and $O_2$ over various tantalate photocatalysts. *Catal. Today* **2003,** *78* (1-4), 561-569.

(138) Li, X.; Zang, J. L., Hydrothermal synthesis and characterization of Lanthanum-doped $NaTaO_3$ with high photocatalytic activity. *Catal. Commun.* **2011,** *12* (14), 1380-1383.

(139) Pan, J.; Liu, G.; Lu, G. Q.; Cheng, H.-M., On the true photoreactivity order of {001}, {010}, and {101} facets of anatase $TiO_2$ crystals. *Angew. Chem. Int. Ed.* **2011,** *50* (9), 2133-2137.

(140) Diebold, U., The surface science of titanium dioxide. *Surf. Sci. Rep.* **2003,** *48* (5-8), 53-229.

(141) Lazzeri, M.; Vittadini, A.; Selloni, A., Structure and energetics of stoichiometric $TiO_2$ anatase surfaces. *Phys. Rev. B* **2001,** *63* (15), 155409.

(142)   Kato, H.; Kudo, A., Highly efficient decomposition of pure water into $H_2$ and $O_2$ over $NaTaO_3$ photocatalysts. *Catal. Lett.* **1999,** *58* (2-3), 153-155.

(143)   Carneiro, J. T.; Savenije, T. J.; Moulijn, J. A.; Mul, G., Toward a Physically Sound Structure-Activity Relationship of $TiO_2$-Based Photocatalysts. *J. Phys. Chem. C* **2010,** *114* (1), 327-332.

(144)   Bloh, J. Z.; Dillert, R.; Bahnemann, D. W., Designing Optimal Metal-Doped Photocatalysts: Correlation between Photocatalytic Activity, Doping Ratio, and Particle Size. *J. Phys. Chem. C* **2012,** *116* (48), 25558-25562.

(145)   Tamaki, Y.; Furube, A.; Murai, M.; Hara, K.; Katoh, R.; Tachiya, M., Direct observation of reactive trapped holes in $TiO_2$ undergoing photocatalytic oxidation of adsorbed alcohols: Evaluation of the reaction rates and yields. *J. Am. Chem. Soc.* **2005,** *128* (2), 416-417.

(146)   Lin, W.-C.; Yang, W.-D.; Huang, I. L.; Wu, T.-S.; Chung, Z.-J., Hydrogen production from methanol/water photocatalytic decomposition using $Pt/TiO_{2-x}N_x$ catalyst. *Energy Fuels* **2009,** *23*, 2192-2196.

(147)   Zalas, M.; Laniecki, M., Photocatalytic hydrogen generation over lanthanides-doped titania. *Sol. Energy Mater. Sol. Cells* **2005,** *89* (2-3), 287-296.

(148)   Zielinska, B.; Borowiak-Palen, E.; Kalenczuk, R. J., Photocatalytic hydrogen generation over alkaline-earth titanates in the presence of electron donors. *Int. J. Hydrogen Energ.* **2008,** *33* (7), 1797-1802.

(149)   Patsoura, A.; Kondarides, D. I.; Verykios, X. E., Photocatalytic degradation of organic pollutants with simultaneous production of hydrogen. *Catal. Today* **2007,** *124* (3-4), 94-102.

(150)   Munuera, G.; Carrizos.I, Adsorption of alcohols on anatase. *Acta Cient Venez* **1973,** *24*, 226-231.

(151)   Lilie, J.; Beck, G.; Henglein, A., Pulse radiolysis and polagraphie - half-wave potentials for oxidation and reduction of short-lived organic radicals on Hg electrode. *Ber. Bunsenges. Phys. Chem.* **1971,** *75* (5), 458-465.

(152)   Wardmann, P., Reduction potentials of one-electron couples involving free radicals in aqueous solution. *J. Phys. Chem. Ref. Data* **1989,** *18* (4), 1637-1989.

(153)   Ohtani, B.; Nishimoto, S., Effect of surface adsorptions of aliphatic alcohols and silver ion on the photocatalytic activity of titania suspended in aqueous solutions. *J. Phys. Chem.* **1993,** *97* (4), 920-926.

(154)   Bahruji, H.; Bowker, M.; Davies, P. R.; Pedrono, F., New insights into the mechanism of photocatalytic reforming on $Pd/TiO_2$. *Appl. Catal., B* **2011,** *107*, 205-209.

(155)   Bahruji, H.; Bowker, M.; Davies, P. R.; Al-Mazroai, L. S.; Dickinson, A.; Greaves, J.; James, D.; Millard, L.; Pedrono, F., Sustainable $H_2$ gas production by photocatalysis. *J. Photochem. Photobiol., A* **2010,** *216* (2-3), 115-118.

(156)   Hussein, F. H.; Rudham, R., Photocatalytic dehydrogenation of liquid alcohols by platinized anatase. *J. Chem. Soc., Faraday Trans.* **1987,** *83*, 1631-1639.

(157)   Anpo, M.; Takeuchi, M., The design and development of highly reactive titanium oxide photocatalysts operating under visible light irradiation. *J. Catal.* **2003,** *216*, 505-516.

(158)   T. Erdey-Gruz, M. V., *Z. Phys. Chem.* **1930,** *150*, 203-2013.

(159)   Tavares, M. C.; Machado, S. A. S.; Mazo, L. H., Study of hydrogen evolution reaction in acid medium on Pt micro electrodes. *Electrochim. Acta* **2001,** *46* (28), 4359-4369.

(160)   Scharlin, P.; Battino, R.; Silla, E.; Tunon, I.; Pascual-Ahuir, J. L., Solubility of gases in water: Correlation between solubility and the number of water molecules in the first solvation shell. *Pure Appl. Chem.* **1998,** *70* (10), 1895-1904.

(161)   Fenby, D. V., Deuterium exchange in water-methanol systems: calculation of equilibrium constants. *Aust. J. Chem.* **1977,** *30* (11), 2371-2375.

(162)   Martin, S. T.; Herrmann, H.; Choi, W.; Hoffmann, M. R., Time-resolved microwave conductivity. Part 1.-$TiO_2$ photoreactivity and size quantization. *J. Chem. Soc., Faraday Trans.* **1994,** *90* (21), 3315-3322.

(163)   Henderson, M. A.; White, J. M.; Uetsuka, H.; Onishi, H., Photochemical charge transfer and trapping at the interface between an organic adlayer and an oxide semiconductor. *J. Am. Chem. Soc.* **2003,** *125* (49), 14974-14975.

(164)   Wang, C.-y.; Böttcher, C.; Bahnemann, D. W.; Dohrmann, J. K., In situ electron microscopy investigation of Fe(III)-doped $TiO_2$ nanoparticles in an aqueous environment. *J. Nanopart. Res.* **2004,** *6* (1), 119-122.

(165)   Friedmann, D.; Hansing, H.; Bahnemann, D., Primary processes during the photodeposition of Ag clusters on $TiO_2$ nanoparticles. *Z. Phys. Chem.* **2007,** *221* (3), 329-348.

(166)   Ismail, A. A.; Bahnemann, D. W.; Bannat, I.; Wark, M., Gold nanoparticles on mesoporous interparticle networks of titanium dioxide nanocrystals for enhanced photonic efficiencies. *J. Phys. Chem. C* **2009,** *113* (17), 7429-7435.
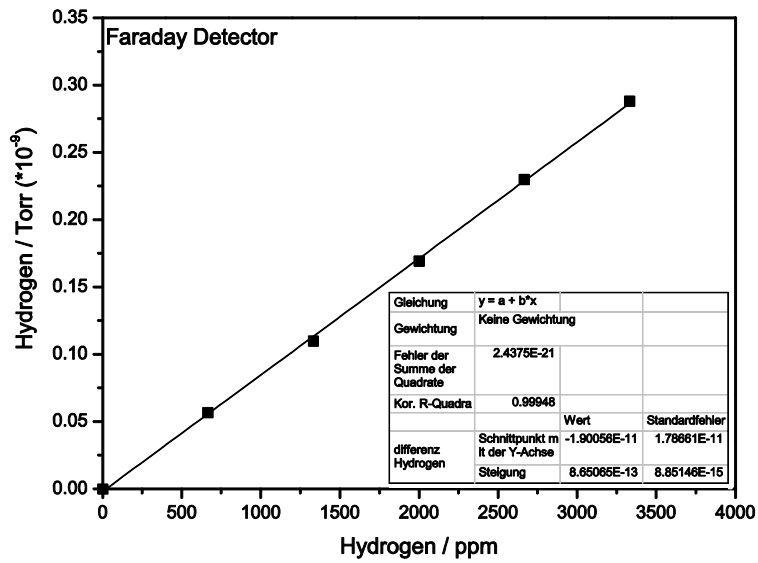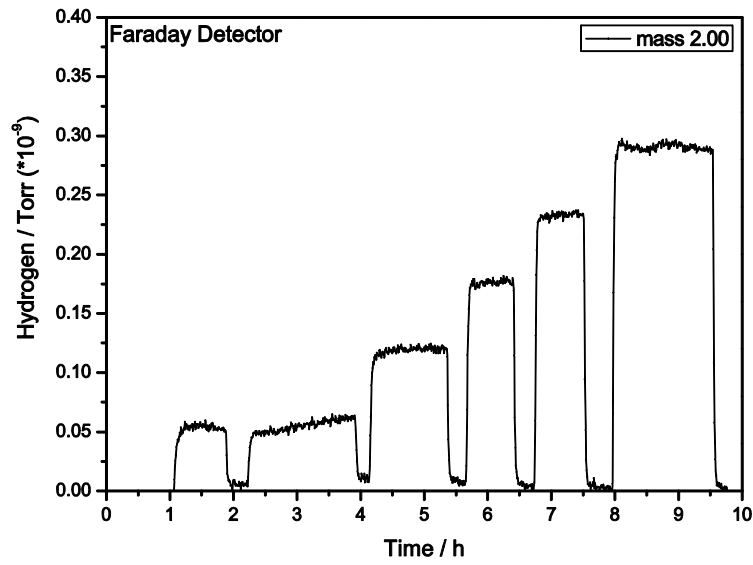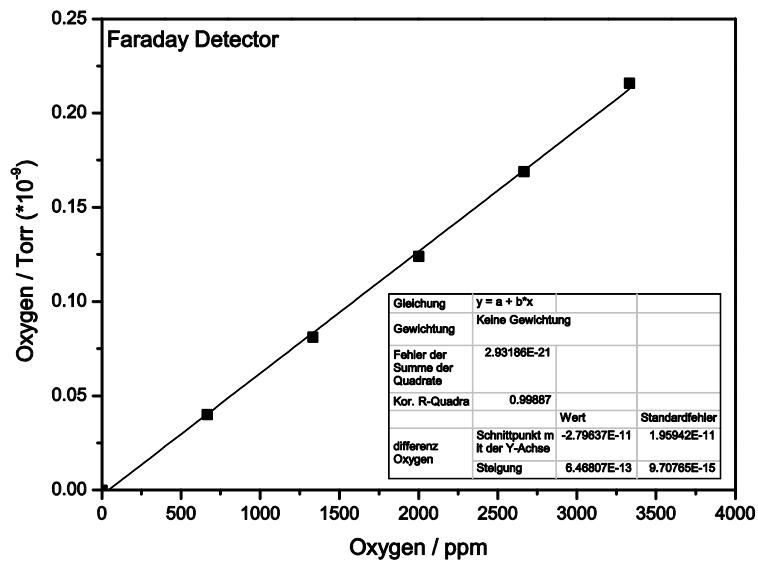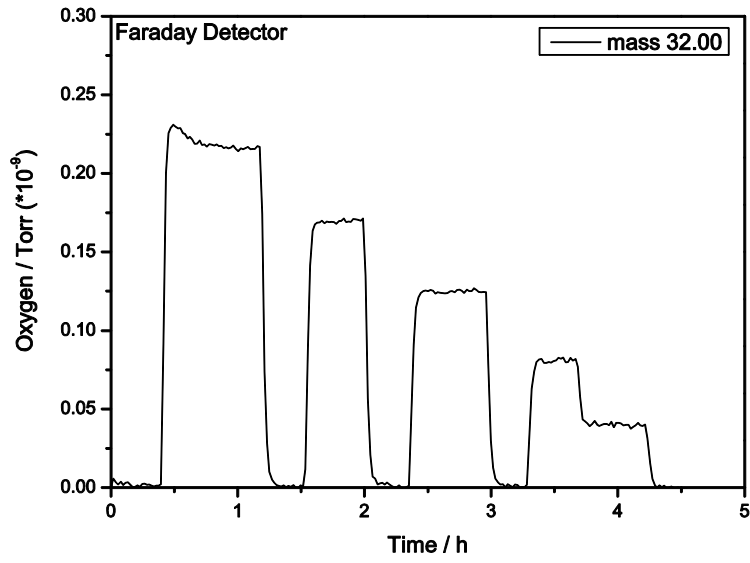
# 8. Appendix

## 8.1 Additional information

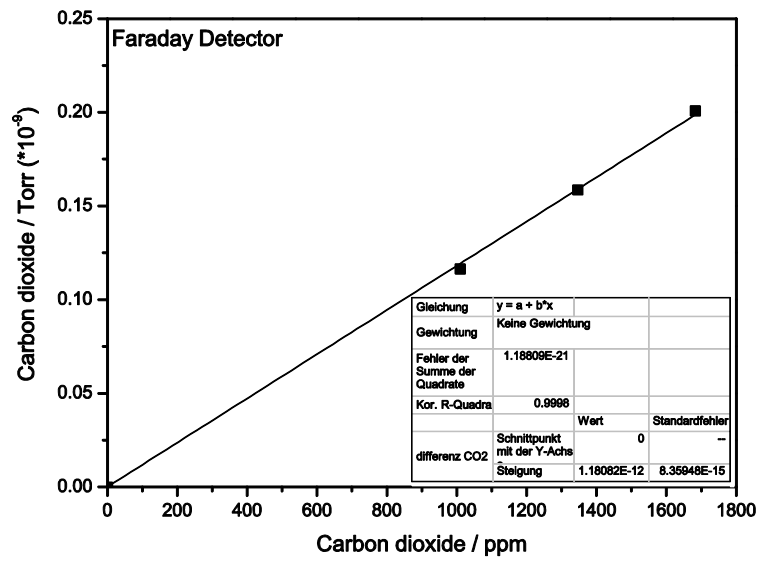TEM bright-field and HTEM micrographs of La-doped $NaTaO_3$ loaded with cocatalysts investigated in this work:
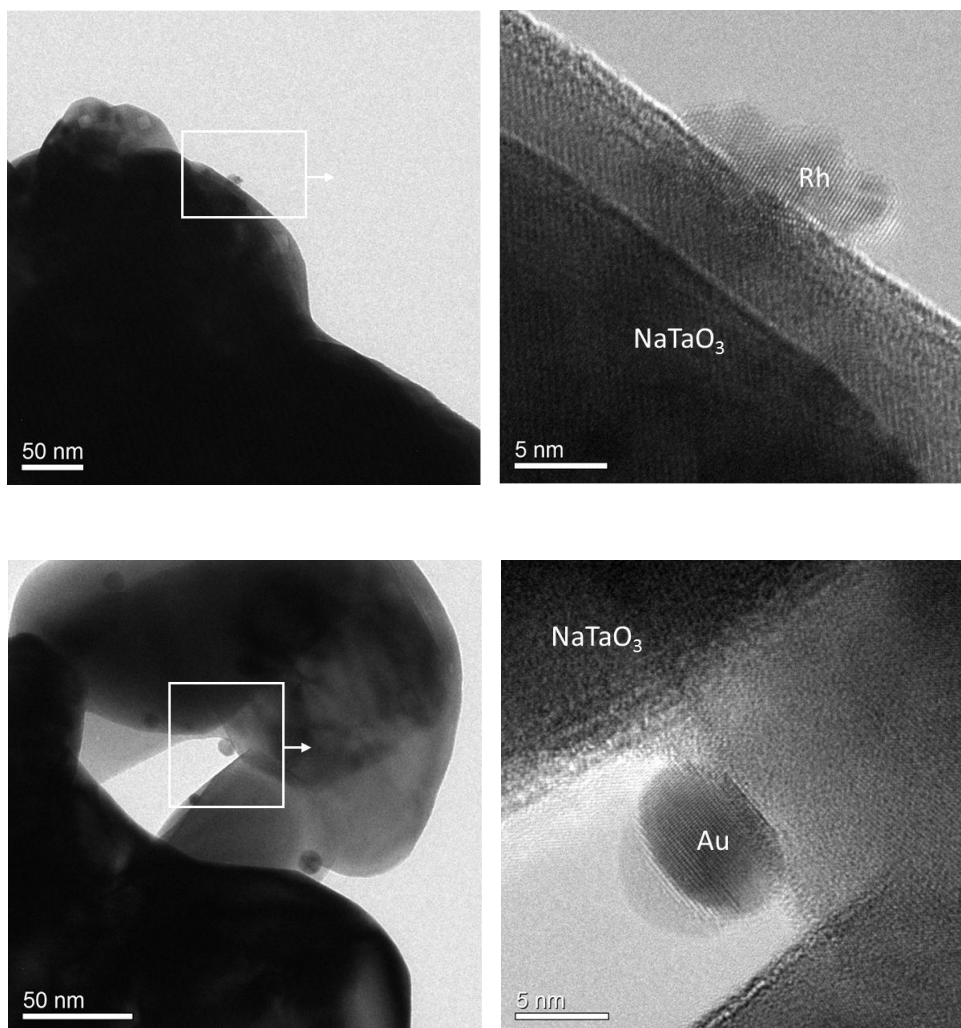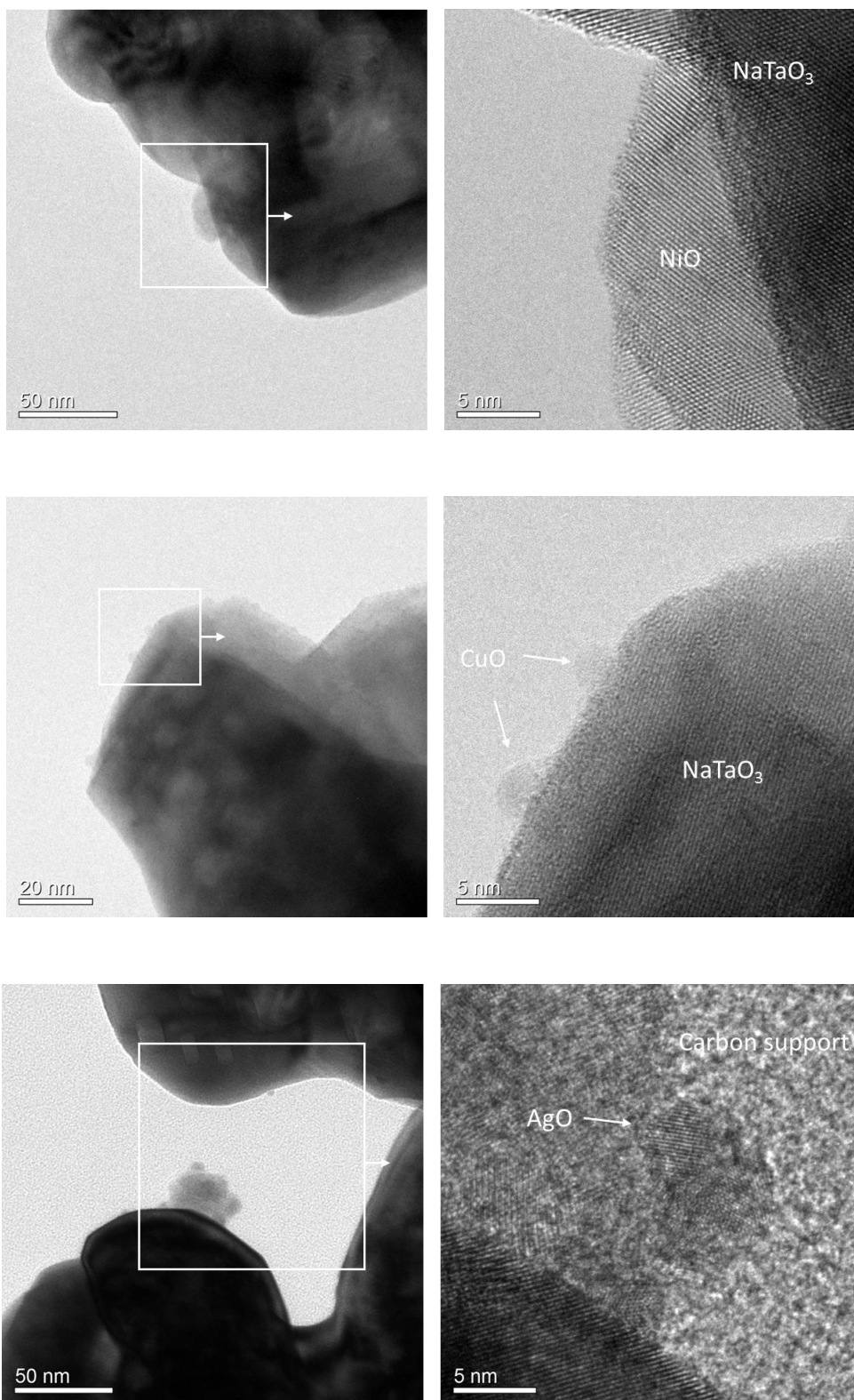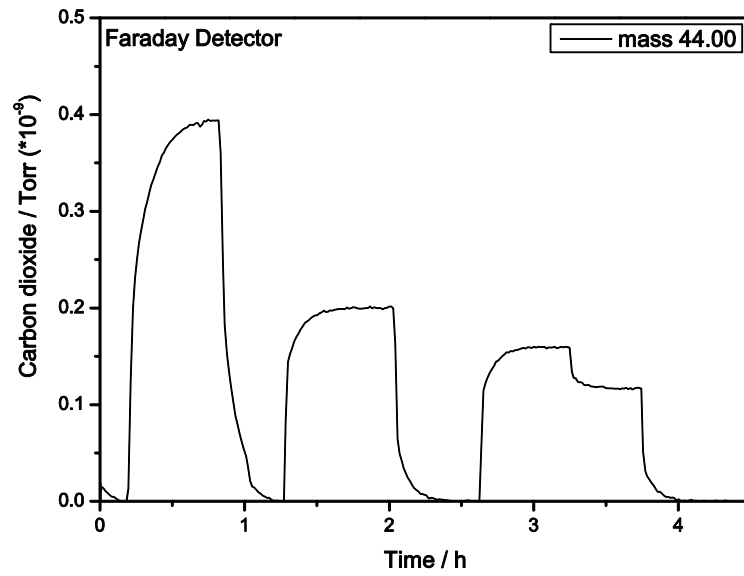
Typical calibration curves for hydrogen ($H_2$), oxygen ($O_2$), and carbon dioxide ($CO_2$) measured by means of QMS:

CXXX

## 8.2 Publications

**Journal publications:**

Ivanova, I.; Kandiel, T.; Hakki, A.; Dillert, R.; and Bahnemann, D. W.
„Photocatalytic evolution of molecular hydrogen and oxygen over La-doped $NaTaO_3$ particles: Effect of different cocatalysts"
To be submitted to *ACS Catalysis*

Ivanova, I.; Kandiel, T. A.; Esch, T. E.; Vidic, J.; Haubrich, H.; Feldhoff, A.; Bredow, T.; and Bahnemann, D. W.
"Structure and photocatalytic activity of pure and La-doped $NaTaO_3$: Experimental results vs. theoretical predictions.
*Journal of Materials Chemistry A* **2014**, submitted

Ivanova, I.; Bahnemann, D. W.; and Mendive, C. B.
"New insights into the photocatalytic transformation of oxalic acid on titania"
*Langmuir*, **2014**, submitted

Ivanova, I.; Schneider, J.; Gutzman, H.; Kliemann, J.-O.; Gärtner, F.; Klassen, T.; Bahnemann, D.W.; and Mendive, C. B.
"Photocatalytic degradation of oxalic and dichloroacetic acid on $TiO_2$ coated metal substrates"
*Catalysis Today* **2013,** 209, 84-90

Ivanova, I.; Freitag, J.; Schneider, J.; and Bahnemann, D. W.
"Nanoparticulate photocatalysts for water splitting: Mechanistic, thermodynamic and kinetic aspects"
Contribution to the book chapter in Wiley-VCH Series on "Nanotechnology", Volume 7 on Nanomaterials for light energy conversion and storage", submitted

Montoya, J. F.; Ivanova, I.; Dillert, R.; Bahnemann, D. W.; Salvador, P.; Peral, J.
"Catalytic Role of Surface Oxygens in $TiO_2$ Photooxidation Reactions: Aqueous Benzene Photooxidation with $(TiO_2)$-O-18 under Anaerobic Conditions"
*Journal of Physical Chemistry Letters* **2013,** *4* (9), 1415-1422

Kandiel, T. A.; Ivanova, I.; and Bahnemann, D. W.
„Long-term investigation of the photocatalytic hydrogen production on platinized $TiO_2$: an isotopic study"
*Energy & Environmental Science* **2014,** *7* (4), 1420-1425

Ahmed, L. M.; Ivanova, I.; Hussein, F. H.; and Bahnemann, D. W.
„Role of platinum deposited on $TiO_2$ in photocatalytic methanol oxidation and dehydrogenation reactions"
*International Journal of Photoenergy* **2014,** *2014*, 9

Kandiel, T.A.; Ahmed, A.; Ivanova, I.; and Bahnemann, D. W.
"Photocatalytic and Photoelectrochemical Oxidation Mechanisms of Methanol on $TiO_2$ in Aqueous Solution"
*Applied Surface Science*, 2014, accepted

## Oral Presentations:

Ivanova, I.; Esteban, P.; Schneider, J.; Kandiel, T.; Dillert, R.; and Bahnemann, D.W.
„Photokatalytische Wasserspaltung an Mischoxidkatalysatoren"
NanoDay, Laboratorium für Nano- und Quantenengineering (LNQE), Leibniz Universität Hannover, September 17, 2012, Hannover, Germany.

Ivanova, I.; Kandiel, T.; Dillert, R.; and Bahnemann, D.W.
„ La-Doped $NaTaO_3$ Particles: Effect of Different Cocatalysts on Photocatalytic Hydrogen and Oxygen Evolution Activities"
245th ACS National Meeting & Exposition, April 7-11, 2013, New Orleans, Louisiana.

Ivanova, I.; Esteban, P.; Kandiel, T.; Dillert, R.; and Bahnemann, D.W.
„Photocatalytic and Electrochemical Investigations of La-Doped $NaTaO_3$ Particles for Hydrogen and Oxygen Evolution"
2nd International Conference on Materials for Energy, May 12-16, 2013, Karlsruhe, Germany.

Ivanova, I.; Kandiel, T.; and Bahnemann, D.W.
Photocatalytic Hydrogen Evolution over La-doped $NaTaO_3$ Particles: An Isotopic Study"
20th International Conference on Conversion and Storage of Solar Energy, 27 July-1 August, Berlin, Germany.

## Poster Presentations:

Ivanova, I.; Mendive C.B.; and Bahnemann, D.W.
"Is oxalic acid a good adsorbate to study surface reactions on $TiO_2$ under UVA illumination?"
NanoDay, Laboratorium für Nano- und Quantenengineering (LNQE), Leibniz Universität Hannover, September 30, 2010, Hannover, Germany.

Ivanova, I.; Schneider, J.; Mendive, C.B.; and Bahnemann, D.W.
"Photocatalytic degradation of oxalic and dichloroacetic acid on $TiO_2$ coated metal substrates"
7th European Meeting on Solar Chemistry and Photocatalysis: Enviromental Applications - SPEA7, June 17-20, Oporto, Portugal.

## 8.3 Curriculum vitae

### Personal data

| | |
|---|---|
| Name, Forename: | Ivanova, Irina |
| Date of birth: | 03.06.1984 |
| Place of Birth: | Taschkent (Usbekistan) |

### Education

| | |
|---|---|
| 08/2002 - 07/2005 | Abitur at Helene-Lange-School Hannover (Grammar School) |
| 10/2005 - 03/2010 | Chemistry Study (diploma) at the Leibniz University of Hannover |
| 03/2010 - 09/2010 | Diploma Thesis at the Institute of Technical Chemistry, Leibniz University of Hannover: "Die Rolle der Adsorption von Oxalat und Dichloracetat für deren photokatalytische Oxidation an der Titandioxid-Oberfläche" |
| 10/2010 - 09/2014 | PhD Student at the Institute of Technical Chemistry, Leibniz University of Hannover: "Photocatalytic Water Splitting in Sodium Tantalate Suspensions" |